University of California

Los Angeles

Multisensory Representations of Space in Hippocampal CA1

A dissertation submitted in partial satisfaction

of the requirements for the degree

Doctor of Philosophy in Biomedical Engineering

by

Lavanya Acharya

2015

Abstract of the Dissertation

Multisensory Representations of Space in Hippocampal CA1

by

Lavanya Acharya

Doctor of Philosophy in Biomedical Engineering

University of California, Los Angeles, 2015

Professor Mayank R Mehta, Co-Chair

Professor Mark S Cohen, Co-Chair

How the brain represents space is a long-standing question, whose answer is most likely to be found within the hippocampal formation. There, spatially selective neurons called place cells provide strong evidence that they are able to form relations between elements of the environment and map the position of the animal with respect to them. These cells are modulated by multiple inputs, and their activity patterns both at the neuronal and population change appropriate to the available sensory and motor information. However, the degree of their contributions and the mechanism behind their integration are unclear.

The goal of this thesis is to determine the contribution of these different afferent signals by manipulating the spatial information provided by them in order to shed light on the mechanisms of multisensory integration in the hippocampus. This is difficult, if not impossible, to realize in real world (RW) experiments but virtual reality (VR) has become a popular tool that can be used to achieve this dissociation. In this thesis VR environments are used to manipulate the spatially relevant information provided by visual and locomotion cues and hence determine their contributions to the hippocampal spatial map.

The results described show that distal visual cues alone are insufficient to generate spatially selective activity, but are sufficient to generate activity that is selective to the head-direction of the animal. Additionally, traditionally described spatially selective activity in the form of place fields is not necessary in order to perform a spatial navigation task.

The dissertation of Lavanya Acharya is approved.

Dario Ringach

James Bisley

Mark S Cohen, Committee Co-Chair

Mayank R Mehta, Committee Co-Chair

University of California, Los Angeles

2015

To my mother . . .

who taught me how to question

To my father . . .

who taught me how to dream

To my sister . . .

who taught me how to love

To my husband . . .

who is my strength and anchor

Table of Contents

List of Figures

List of Tables

Acknowledgments

I would first like to thank my advisor ***Dr. Mayank Mehta*** for introducing me to and guiding me through the fascinating study of the hippocampus and for teaching me to have pride in my work. Without him I would never have found myself where I am today.

I would also like to thank my committee members ***Dr. Mark Cohen***, ***Dr. James Bisley*** and ***Dr. Dario Ringach*** who have not only taken the time to discuss and critique my ideas but have given me much needed encouragement by expressing excitement at the prospect of my proposed projects at every committee meeting.

I would also like to thank my mentors ***Dr. Pascal Ravassard*** and ***Dr. Ashley Kees*** who taught me everything I know about research and who have guided, supported and protected me through many difficult times.

My fellow authors, labmates and friends, ***Dr. Zahra M.Aghajan***,***Jason Moore***, ***Briana Popeney***, ***Jesse Cushman***, ***Cliff Vuong***, I thank for their invaluable help, support and love.

I would like to thank my wonderful undergradute students, ***Neha Agarwal*** and ***Freesia Quezada*** who I had the honor to mentor and who have taught me more about science and teaching than I could ever have managed by myself.

My parents, ***P.H.V Acharya*** and ***Rajeswari Acharya*** have been wonderful in supporting my ambitions my entire life and I would never have been able to build up the courage to take on this enormous task if not for their support, encouragement and confidence in my abilities. They share this achievement with me.

I thank my sister, ***Lalitha Acharya***, who has never ceased to look after me and who cannot get enough credit for the person I am today.

My husband, ***Murtaza Bhaimia*** has been my rock through my difficult journey these past five years and continues to support and encourage my dreams. I would not have been able to graduate without him by my side.

I'd like to thank my wonderful grandfather ***N. V Krishnamurty*** for passing on his wonderful sense of curiosity.

I'd also like to thank ***Dr. Shonali Dhingra***, and ***Dr. Roman Sandler*** for helping me with LaTeX

Thank you to my wonderful friends ***Sneha Mohan***, ***Rashmi Canchi*** ***Aviral Srivastava***, ***Dr. Sonia Guha***, ***Dr. Neha Shah*** and ***Dr. Niyati Mehta*** for their support and love.

Lastly, I would like to acknowledge and thank my rats for their lives: ***Jackson***, ***Farnsworth***, ***Queue***, ***Spock***, ***Ili***, ***Merry***, ***Pippin*** and ***Hobbes***.

Chapter 2 is a version of the published work Aghajan, Z. M., Acharya, L., Moore, J. J., Cushman, J. D., Vuong, C., & Mehta, M. R. (2014). Impaired spatial selectivity and intact phase precession in two-dimensional virtual reality. Nature neuroscience. LA, JC, ZMA and MM designed the experiments; LA, CV and JC performed the experiments; ZMA and JM performed analyses with input from MM;ZMA, LA,JM and MM wrote the manuscript with other authors.

Chapter 3 is a version of a manuscript in press at Cell and has been published on the pre-print server bioRvix. Acharya, L., Aghajan, Z. M., Vuong, C., Moore, J., & Mehta, M. (2015). Visual cues determine hippocampal directional selectivity (in press) Cell. LA and MM designed the experiments; LA and CV performed the experiments; ZMA and JM performed analyses with input from MM;ZMA, LA,JM and MM wrote the manuscript with other authors.

Chapter 4 is unpublished data and I would like to credit Dr. Jesse Cushman and Cliff Vuong for help with data collection, and Jason Moore for analysis of the data. Dr. Mayank Mehta was principal investigator on the project.

Vita

Education

2010–2015

Candidate, Doctor of Philosophy in Biomedical Engineering,

University of California, Los Angeles

2010–2011

Masters in Biomedical Engineering,

University of California, Los Angeles

2006–2010

Bachelor of Engineering in Medical Electronics,

Visvesvaraya Technological University, Bangalore, India

Publications

Z. M.Aghajan, L. Acharya*, J. M. Moore, J. D. Cushman, C. Vuong, M. R. Mehta*, ***Impaired spatial selectivity and intact phase precession in two-dimensional virtual reality***, Nature Neuroscience 2014

L. Acharya, Z. M.Aghajan*, C. Vuong, J. M. Moore, M. R. Mehta*, ***Visual cues determine hippocampal directional selectivity***, (in press) Cell

Presentations *Presenter*, ***Impaired spatial selectivity in two-dimensional virtual reality***, Society for Neuroscience annual conference poster session, November 15, 2014.

Presenter, ***Distal visual cues are insufficient for the generation of spatial selectivity***, UCLA Brain Research Institute, 26th annual 2014 neuroscience poster session

Presenter, ***Causal role of visual cues in determining hippocampal directional responses at single neuron and ensemble level***, UCLA Brain Research Institute, 27th annual 2015 neuroscience poster session

Skills ***Experimentation*** In-Vivo Electrophysiology, Multi-unit extracellular tetrode recording, Rodent Behavior and Training, Experimental Design, Surgery (hyperdrive implantation), Rat Perfusion, Brain Extraction, Tetrode and Hyperdrive construction

Tools and Software MATLAB, Neuralynx Digitalynx, Neuralynx Cheetah program, Spike sorting (clustering)

Others Histology, C, C++, VHDL, Verilog, MEMS Fabrication

Awards ***Dissertation Year Fellowship***, UCLA 2015

Neuroscience Graduate Travel Award, UCLA 2015

Work Experience

Teaching TA for two lower division life sciences and two upper division neuroscience courses.

Mentoring Mentored three undergraduate students; designed undergraduate thesis projects.

CHAPTER 1

A brief introduction: constructing spaces

1.1 Introduction

Imagine: you are entering the parking lot of a mall and heading towards your car. You remember where you parked it and you have a vague, but sufficient, idea which direction you need to go to get there. How do you know where you are with respect to the structure? Parking lots can be notoriously confusing, some with no markings to indicate different locations. Imagine this is one of the those. You can find your car, however, despite this visually poor environment, and despite the almost symmetrical and repeating patterns that make its structure.

How does your brain know where you are with respect to the larger space you are in? How does it construct the space within which the two locations are? How does it, then, construct a pathway from point A to point B?

You could invoke any number of brain areas as candidates for solving this problem of representing space. What makes it interesting is the frame of reference with respect to which your brain needs to represent the space around you in order to find the solution. There are very few brain regions that can do this appropriately, which narrows down our question considerably. One of them is the hippocampal formation, a medial temporal brain area, that has exhibited the ability to represent space in what is known as an allocentric frame of reference.

1.2 Reference Frames

Movement through and interaction with space can be mapped onto two frames of reference: the egocentric frame and the allocentric frame [1].

In *the egocenteric reference frame* the body is the reference point. For example, cells in the posterior parietal cortex of the rat fire only when the animal is turning right, but not left or vice versa [2]. Here, it does not matter whether the animal is in the northeast corner of the environment and heading south or facing south and turning west somewhere else entirely (Figure 1.1).

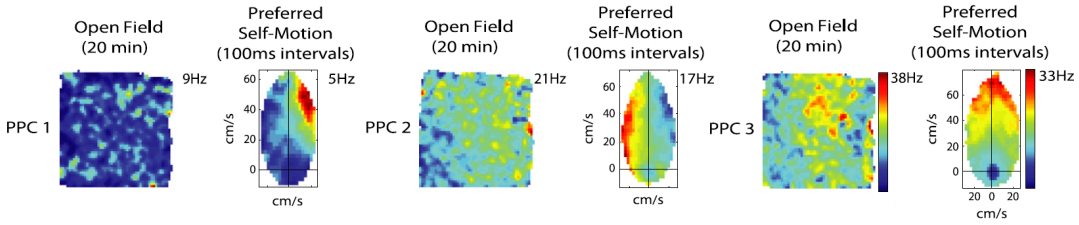

Figure 1.1: Neurons showing egocentric coding. The left panels show the firing rate map of neurons from the rodent posterior parietal cortex (PPC) when the animal is allowed to freely explore an open arena. Colors indicate the firing rate of the neuron as indicated by the color bar. Note that PPC neurons do not exhibit any selectivity to position but fire action potentials depending on the movement of the rat, i.e, when the rat is only turning right, left, or running straight. Modified from Whitlock et.al, 2006.

In *the allocentric frame of reference* space is mapped with respect to the environment surrounding the body. For example, some cells in the thalamus encode which direction the animal is facing [3] with respect to the environment. That is, one cell might increase its rate of firing when the animal is facing north but no other direction, but irrespective of its position in the space. Another neuron might increase its firing rate only when the animal is facing south.

In the hippocampus, which is the focus of this thesis, there exist excitatory neurons that encode the animal's location in space with respect to the environment around it. These neurons were discovered in 1971 [4] and are called ***place cells*** and their receptive fields are known as ***place fields***. The activity pattern of these neurons constitutes an allocentric representation because their frame of reference is outside the body.

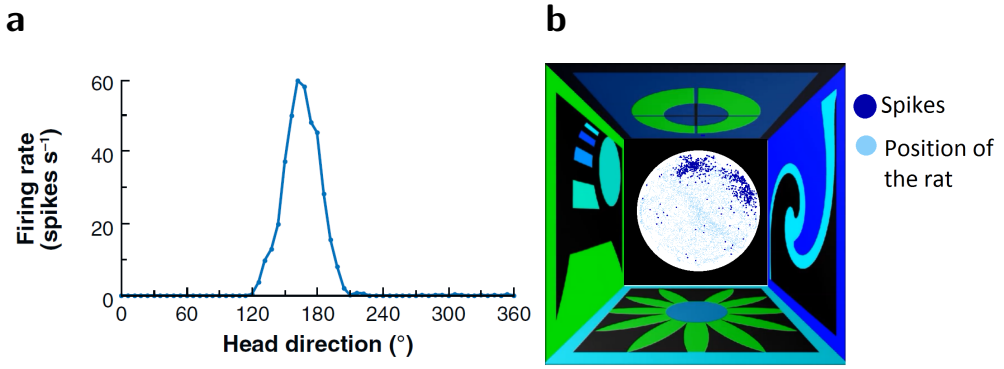

Figure 1.2: Neurons showing allocentric coding. (a) These neurons are selective to the allocentric direction of the head of the subject. Note the firing rate of the neuron depicted in the figure increases when the animal is facing 120°–210°. Modified from Taube, 2007. **(b)** Neurons in dorsal CA1 of the hippocampus are selective to position. The figure dipicts a $300 \times 300cm$ room with patterns on the walls. The rat is allowed to forage for rewards on a platform. Note how the neuron fires spikes only on the north side of the table and is silent everywhere else. The region where the place cell fires is designated its place field.

If, for example, you were in a room with a window on the west wall, a desk by the east wall and a couch in the middle (Figure 1.3) **neuron A** may fire action potentials when you are in the area near the window, **neuron B** when you are by the desk, **neuron C** near the couch, **neuron D** by the north wall and **neuron E** by the south wall.

This representation is such that together, the five neurons encode all areas of

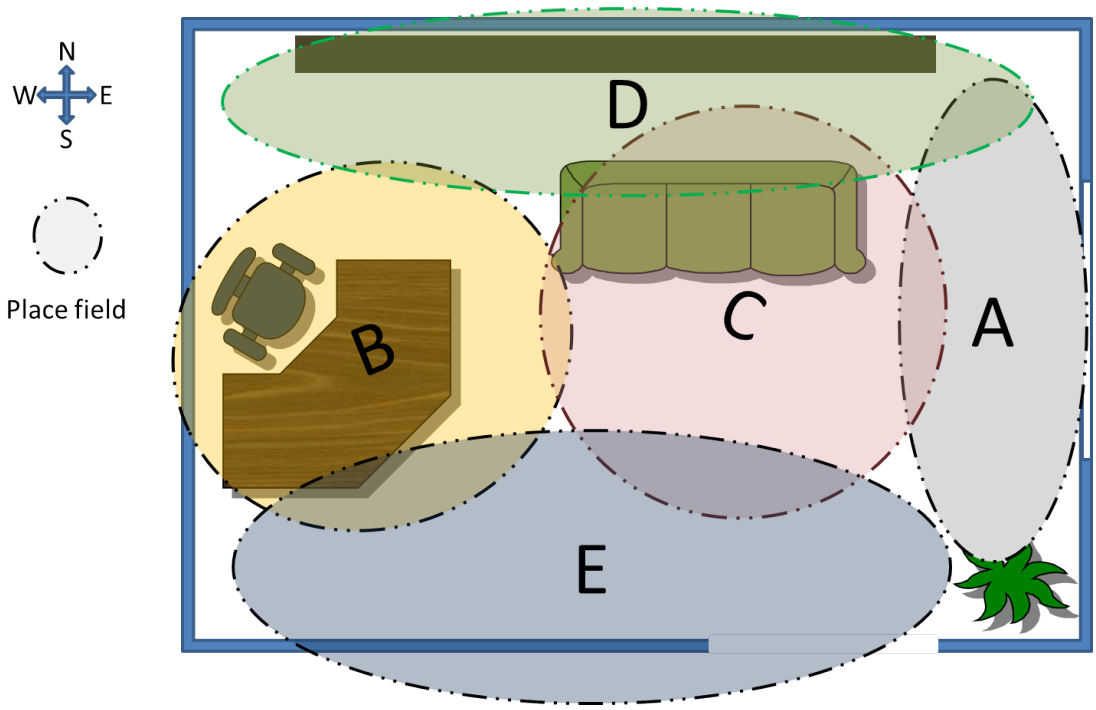

Figure 1.3: Representation of a neuronal map of a room. Each place cell fires action potentials when the subject is in a specific region of space known as the place field of the neuron. Note how the population of five neurons depicted together map the entire room.

the room. This allows one to determine with some degree of accuracy where in the room you might be at any given time depending on which neuron is firing action potentials.

1.3 The hippocampal formation

The hippocampus, where place cells are found, is part of a larger structure known as the ***hippocampal formation*** (the hippocampus is therefore also referred to as the *hippocampus proper* to distinguish it from the hippocampal formation). The hippocampal formation (Figure 1.4a)is a temporal brain area that consists of

- the dentate gyrus
- ***the hippocampus proper*** which is further subdivided into three areas

a

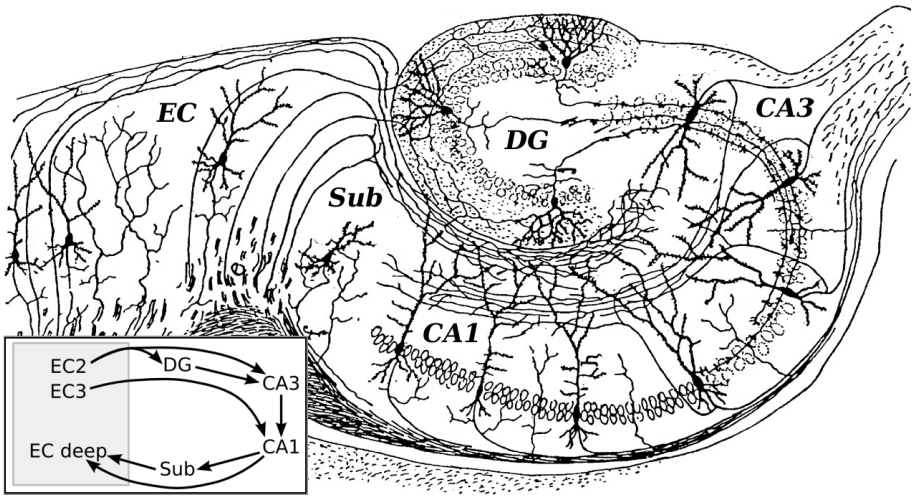

b

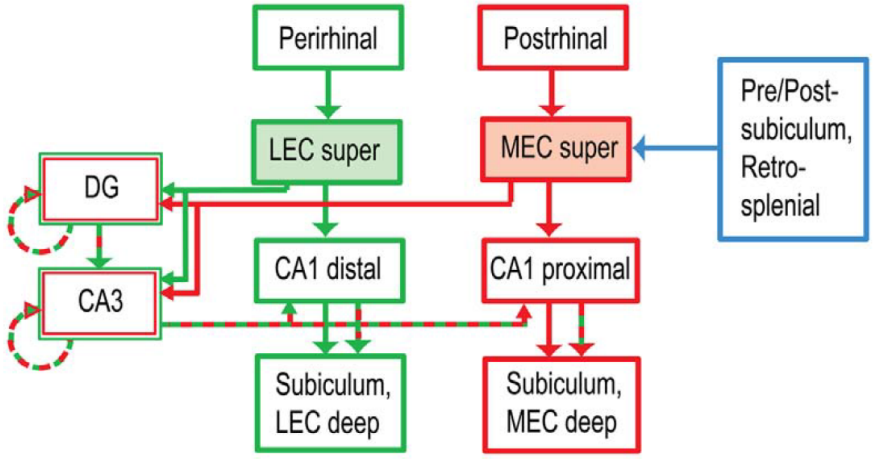

Figure 1.4: The hippocampal formation. (a) A drawing of the hippocampal formation with all of its parts by Santiago Ramon y Cajal. Reproduced from Wikipedia. **(b)** A representation of the connections and direction of information flow between the different subdivisions of the hippocampal formation. Reproduced from Deshmukh and Knierim, 2011.

known as the areas *cornu ammonis* or *CA1, 2* and *3*. These regions consist of excitatory neurons known as pyramidal neurons due to their triangular shape which, in CA1 and CA3, behave as place cells.

- ***the entorhinal cortex*** which is further divided into two functionally distinct regions: the *lateral entorhinal cortex (LEC)* and *medial entorhinal cortex (MEC)*. The LEC has neurons that have been shown to be selective to objects, and odors [5] and it has been proposed that the LEC receives information from the ***what*** stream of visual processing. The MEC, on the other hand, has spatially selective neurons [6] which, unlike place cells in the hippocampus, have a firing fields that are arranged in a triangular lattice.

- the subiculum, presubiculum and parasubiculum

The flow of information through this brain structure is largely unidirectional (Figure 1.4b). In brief, the hippocampus proper lies at the heart of the brain region with all information from the neocortex necessarily having to pass through the entorhinal cortex to reach the hippocampus. Information from the *what* and *where* pathways arrive at the lateral and medial entorhinal cortices from the perirhinal and postrhinal cortices respectively. The medial entorhinal cortex also receives information about self-motion from the retrosplenial cortex and about head-direction from the thalamus through the pre- and post-subicular cortices. The entorhinal cortex then sends projections to the dentate gyrus from layer II through the perforant pathway and from layer III to CA1 through the perforant and alvear pathways. The dentate gyrus projects to the pyramidal neurons in CA3 through mossy fibers. CA3 had recurrent connections within it where it projects back to its own neurons, and in addition, projects to CA1 through its shaffer collaterals. CA1 then projects back to the deeper layer V of the entorhinal cortex directly and through the subiculum to complete the loop.

1.4 Multisensory integration in the hippocampal formation

Studying the mechanisms of multisensory integration that results in a coherent allocentric representation of space is not trivial since the hippocampus is part of a complex loop receiving signals from both the *what* and *where* streams of visual processing, and areas encoding self-motion information [7] (Figure 1.4b). Most likely due to this, place cells are able to respond dynamically to the environment, as evidenced by studies showing that their activity is modulated by sensory and motor inputs, as well as behavioral variables [8–12]. However, distal visual cues, which are visual cues that are in the distance, such as the skyline of a city, or the mountains, or the walls of a room, have traditionally been considered the primary inputs that generate the spatial map since rotating these cues cause place cells to change the location of their firing fields [9]. Additionally, while place fields can form in the dark, they remap with the availability of distal visual cues on turning on the lights [13]. Apart from visual and olfactory cues, CA1 neurons have also been shown to be able to encode distance [14] and time [15, 16]. Not only this, hippocampal place cells are also capable of changing their activity patterns to account for changes in the environment, a phenomenon known as remapping. If only certain cues or configuration of cues change but others remain the same, then as expected, some neurons maintain their firing patterns while others remap to account for the changes in the environment [12].

Additionally, hippocampal place cells exhibit another kind of coding which is known as phase precession. Hippocampal LFP exhibits a charactristic oscillation between $4Hz$ and $12Hz$ known as theta. The firing pattern of place cells within their place fields is strongly modulated by this oscillation such that the phase of the oscillation at which the neuron spikes shifts backwards as the animal moves through the place field.

Most importantly, while all of the above mentioned observations are at the neuronal level, i.e activity patterns that can be observed in a single neuron, hippocampal neurons have also been shown to exhibit coding at the population level. For example, the disto-code [14] has been observed both in single neurons and in the ensemble of recorded neurons when the animal is running on a linear track. Additionally, as described in Chapter 2 we have shown this to be true in two-dimensional environments as well.

Hence, *selectivity to space* is a simplistic description of the activity of hippocampal neurons. The activity of these neurons has been shown to not only be able to encode for the position of the animal in a given environment but also the configuration of sensory cues, time and distance. In addition, phase precession, also called a *temporal code* as opposed to *rate code* (spatial selectivity, for example) allows one to pinpoint exactly where within the place field the animal might be depending on what phase of theta the neurons is firing action potentials. Phase precession is also considered to be important for synaptic plasticity given that it occurs within the appropriate time-scale of 10s of milliseconds.

Given the complex nature of both the anatomical and functional structure of the hippocampal formation and the behavioral correlates of the activity of hippocampal neurons, it is especially difficult to tease apart not only the different levels and kinds of neural codes, but also what environmental cues are the most relevant. Various experimental and computational tools have been developed over the years in order to control for these innumerable variables. This thesis depends heavily on one particular experimental tool: the virtual reality.

1.5 Hippocampal activity in virtual reality

Virtual reality is an especially useful tool when studying brain areas that have such multisensory responses. Depending on the design of the system virtual re-

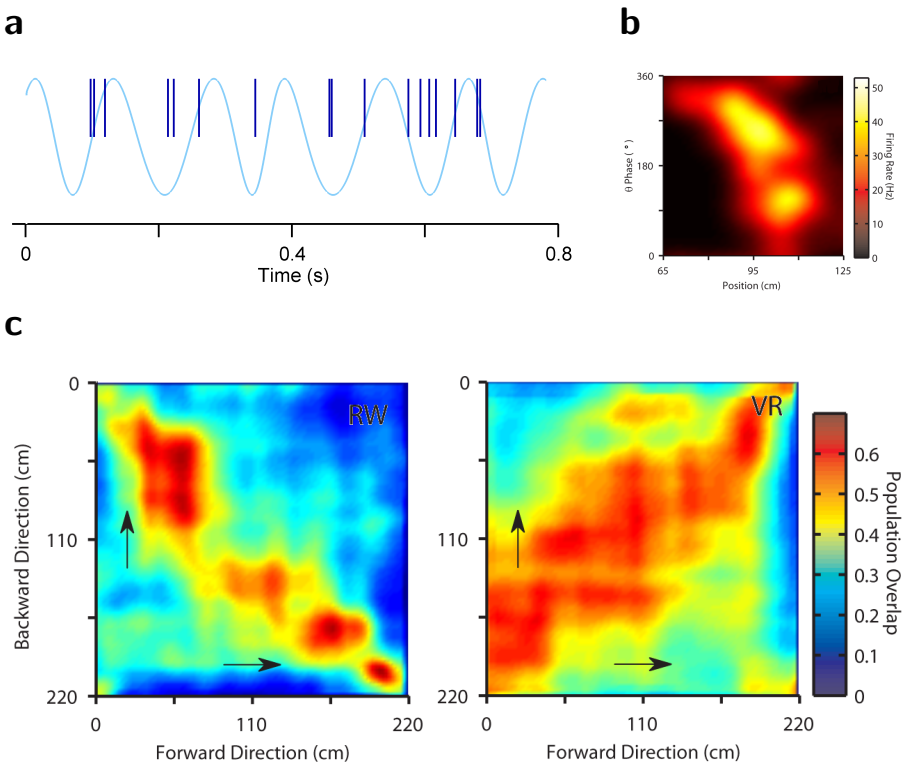

Figure 1.5: Hippocampal phase precession. (a) The figure depicts phase precession of a recorded neuron with respect to the LFP theta oscillation recorded from the same electrode. The LFP theta trace filtered in theta band $(4 - 12Hz)$ is shown by the light blue trace and spikes from the place cell by the vertical dark blue lines. Note how the spikes occur at earlier phases on subsequent theta cycles. **(b)** This figure shows another common depiction of phase precession. The color of the heat map indicates the firing rate of spikes as indicated by the color bar. Note how, as time passes, the phase at which the neurons fires the maximum spikes reduces. Figure modified from Ravassard et al, 2013. **(c)** shows the *population vector overlap* of a population of neurons under two different conditions. The data were collected from animals running back and forth along a linear track. This depiction shows the similarity in the activity of the population in one direction versus the other. In the figure on the left, the data were collected in a real world setup and activity patterns show highest correlation (indicated by the population overlap value) at the same positions along the track. However, in contrast, the data on the right, collected in a virtual environment where the sensory cues available are dramatically, shows a selectivity to distance as indicated by the high correlation values at similar distances along the track. Modified from Ravassard et al, 2013.

ality allows one to precisely control the amount of information provided by a particular sensory input. In order to fully understand the implications of using a virtual reality system it is important to think about the sensory inputs that are providing the relevant information to the brain area of interest. In the context of the hippocampus, we will be focusing on spatial information.

1.5.1 Multisensory cues

Multisensory information is broadly classfied into three categories: proximal cues, distal cues and internal or self-motion cues. ***Proximal cues*** are defined as those sensory cues that are close to the animal and which the animal can interact with. These can belong to

- the olfactory modality, such as smells on the ground or on an object,
- the tactile modality, such as different textures,
- or the auditory modality, such as a source of sound that can be clearly pinpointed, for example a chirping cricket.

Distal cues are those that are far away and can be

- visual, such as the skyline of a city, or auditory such as a distant sound coming from a particular direction,
- or olfactory, such as the smells from the kitchen in a different room of the house.

Self-motion cues are those that are generated by the body of the animal. These cues are subdivided into proprioceptive cues, motor efference copy, vestibular cues, and optic flow.

1.5.2 Real world versus virtual reality

The term ***real world*** refers to any experimental setup that is physically constructed and is in contrast to a virtual reality environment which is generally a projection on a screen in front of the animal. In the real world, or ***RW*** as it will be referred to throughout this thesis, the brain receives information from all of the sensory modalities. However, these can be manipulated to some extent by either constructing the experiment such that specific cues are modified to either provide no useful information or conflicting information, or by making lesions in the sensory organ itself or some brain region downstream of the sensory organ. For example, if one would like to test the importance of proximal olfactory cues to hippocampal spatial selectivity, one could, as has already been done [13], wipe the floor of the open arena to remove odors. Or, one could create conflict between proximal and distal cues [12] to test the significance of one or the other to hippocampal place cells. Self-motion cues can be tested by forcing the behavior of the animal to be one way or the other [11] such as comparing neural activity when the animal is performing a random foraging task to when he is doing a goal directed task and walking repeatedly along the same path between two or more fixed locations. As another example, vestibular cues can be manipulated by either spinning the animal to disorient him and render vestibular information useless for a short period of time, or by lesioning the vestibular apparatus itself.

However, ***virtual reality*** or ***VR***, provides additional flexibility in that it allows us to manipulate cues very precisely, such as control with minute precision when, where and how much of an odor is released, or a reward is dispensed. It also allows us to create environments that would not be possible to do in the real world. For example, one could switch distal visual cues instantaneously so as to create the illusion of being *teleported* to a different room entirely, or make it so that the subject has to run twice as fast to cover the same distance in virtual space. These manipulations allow us to test sensory inputs and behavioral variables in ways

that are not possible to achieve in the real world.

The VR setup used in this thesis, described in detail in Section 2.3.2, is constructed specifically for rats and to achieve the following:

- to render proximal cues completely unreliable in that neither proximal olfactory, tactile or visual cues (such as textures, odors or patterns on the virtual floor) provide any spatially informative information. This means that the rat cannot utilize any of these cues to determine where in the virtual environment he is.

- to make vestibular cues unreliable. The VR is constructed such that while the rat is free to move his head as he wishes, he is body-fixed using a harness that wraps around his torso which is in turn fixed to the frame of the setup causing him to be unable to turn his body. The implication of this restriction is that while his vestibular apparatus generates normal amounts of rotational acceleration signal when he moves his head, it will not be able to generate an appropriate rotational acceleration signal when he turns around in the virtual space since he is not physically turning himself. Additionally, he moves forward in the virtual space by running on a spherical treadmill. This means, while he runs forward, his vestibular apparatus generates no linear acceleration signal.

- to allow for precise control of visual cues. The system is such that we can precisely control the information visual cues provide, allowing us to test the influence of these cues in different configurations on hippocampal activity.

- to allow for testing of behavioral vairables. By manipulating rewards and training the animal to behave a certain way, such as running in straight lines or performing a random foraging task, we can test the influence of behavior on the activity of hippocampal neurons.

- to allow for manipulation of optic flow information by changing the pattern of the visual cue, or the gain of the sensors that detect motion of the spherical treadmill.

There are other VR setups that are constructed differently. For example, some VR setups consist of a head-fixed mouse on a treadmill viewing the virtual scene on two large monitors placed in front of it [17]. These setups are especially useful when one wants to record from neurons by either patch clamping them or use optogenetics. Other setups allow the animal to turn himself around [18].

1.5.3 Conclusion

The goal of this thesis is to determine the contribution of multisensory inputs to the generation of the hippocampal spatial map, and to also determine how these multisensory inputs are integrated. The virtual reality proves a very useful tool to achieve this goal as it allows for the unraveling of these numerous inputs.

The following chapters describe the following main results:

- multiple spatially informative inputs are necessary in order to generate spatially selective activity in the hippocampus, and visual cues alone are insufficient.
- the hippocampus is capable of encoding the direction the animal is facing without vestibular cues.
- spatial selectivity in the hippocampus is not necessary at the behavioral level to solve a spatial navigation task.

CHAPTER 2

Hippocampal activity in two-dimensional virtual reality

2.1 Abstract

During real world (RW) exploration rodent hippocampal activity shows robust spatial selectivity, hypothesized to be largely governed by distal visual cues. However, primate and human hippocampal studies, done with only visual cues, find only weak spatial selectivity. This discrepancy could arise because multiple sensory and motor cues influence rodent hippocampal spatial selectivity in RW. To resolve these issues and determine the contribution of solely distal visual cues, we measured hippocampal activity for the first time from body-fixed rodents exploring a two-dimensional virtual reality (VR) and compared it to a visually similar RW. Spatial selectivity was dramatically reduced in VR. Instead, small but significant selectivity to distance traveled was found. Despite the impaired spatial selectivity, most spikes in VR occurred within $\sim 2s$ long, phase-precessing ***hippocampal motifs***, with similar structure in RW and VR. Selectivity to space and to distance traveled were greatly enhanced in VR tasks with stereotypical trajectories. Thus, distal visual cues alone are insufficient to generate robust hippocampal spatial selectivity, and temporal selectivity can exist without spatial selectivity. These results have important implications for VR experiments and elucidate the mechanisms of hippocampal spatio-temporal selectivity.

2.2 Introduction

Dorsal hippocampal neurons fire at elevated rates in restricted regions of space [4,19] when subjects randomly forage in a two-dimensional space, termed a spatial rate code. Distal visual cues are thought to reliably determine this spatial selectivity because changing or rotating them causes corresponding large changes in place cells' spatial tuning [9, 19]. However, place cells' activity is also influenced by other sensory and motor cues including: specific and nonspecific proximal cues, such as olfactory and somatosensory cues [20], [21], [8, 10, 12, 13, 22]; and locomotion cues such as optic flow and proprioception, which together with vestibular cues are thought to provide self-motion information for path integration [11,23,24]. Consistently, lesions of vestibular nuclei disrupt angular tuning of head-direction cells [25] and spatial tuning of hippocampal place cells [26], although lesions of the head-direction cell network, which is thought to provide vestibular input to hippocampus, do not significantly alter hippocampal spatial selectivity [27]. Additionally, the output of vestibular nuclei suppresses self-motion signals and depends on multisensory stimuli [28]. Indeed, in all the above experiments it is difficult to dissociate the contribution of distal visual cues from other cues. Thus, the contribution of distal visual cues alone—which are the only spatially informative stimuli in typical human and primate studies of hippocampal activity [29–31]—to the spatial selectivity of place cells in normal rats remains to be fully explained.

Neural activity is also modulated jointly by theta rhythm and the rat's position within the place field, called theta-phase precession or a temporal code [14,32–34], which is thought to be closely linked to hippocampal spatial selectivity [34]. Nevertheless, phase precession is also seen when rats run in a running-wheel without any systematic change in visual cues [16]. Hence, to understand the mechanisms of the hippocampal spatial rate and temporal codes, it is important to determine if the two can be dissociated during spatial exploration. Finally, dorsal hippocam-

pal neurons are typically active for sustained periods lasting more than one second [4, 19], even under a variety of conditions [15, 16, 35, 36], and this sustained nature of activity has received little attention.

These questions are particularly important to address since neural mechanisms of navigation in humans and non-human primates are mostly studied in stationary subjects, often in VR [29–31], with only distal visual cues and no vestibular or proximal cues. Here, hippocampal neurons show only weak spatial selectivity [29, 30, 37] at apparent odds with high spatial selectivity seen in studies in freely behaving rodents. Further, an increasing number of functional imaging studies in rodents are done in head-fixed animals in VR [38].

VR allows one to eliminate spatially informative multisensory, non-specific cues and minimize vestibular cues, leaving only distal visual cues to provide reliable spatial information [14, 17, 39, 40]. All previous neurophysiological studies in rodents in VR have been done in one-dimensional mazes, and have found largely intact spatial selectivity. In these environments visual cues are repeatedly paired with the same set of locomotion cues, such as speed of optic flow and proprioception, which have been hypothesized to play a major role in driving neural responses [11, 14, 23, 24, 41], as evidenced by disto-coding in one-dimensional VR paths [14]. This consistency is removed in random foraging in two-dimensional VR environments where the same physical location in space can be approached from multiple different directions at different speeds. We thus investigated the contribution of only distal visual cues in determining selectivity in such an experimental set-up.

2.3 Methods

Methods Summary

Four adult male Long-Evans rats were trained to on a variety of tasks in RW

and VR. All rats foraged for randomly scattered rewards in two-dimensional RW and VR environments. Additionally, three of these rats were trained to follow a goal-directed strategy by running towards randomly located reward-indicating pillars in VR. Further, the same three rats were trained to run towards consistently positioned reward locations in VR. There were either two or three fixed reward locations. The environments had identical dimensions ($200cm$ diameter circular platform at the center of a $300 \times 300cm$ room) and distal visual cues. Electrophysiological data from dorsal CA1 were obtained using hyperdrives with approximately 22 independently adjustable tetrodes [14]. Spike extraction and sorting were done offline using custom software. Spatial selectivity and phase precession were quantified using measures previously described [14] and are described in detail in 2.3.8 and 2.3.13. Motifs were detected using custom analyses described in the main text. Only data measured during locomotion (speed $> 5cm/s$) were used for all analyses to ensure consistent hippocampal state [42].

2.3.1 Subjects

Data were collected from four adult male Long-Evans rats (approximately 3.5 months old at the start of training), individually housed on a 12 hour light/dark cycle and food restricted (minimum $15g$ of food per day) to maintain body weight. They were allowed an unrestricted number of sugar water rewards in VR but the total amount of water available for them to drink was restricted to approximately $40ml$ per day to maintain motivation, but no less than $30ml$ per day. All experiments and data collection were performed during the light cycle. All experimental procedures were approved by the UCLA Chancellor's Animal Research Committee and were conducted in accordance with USA federal guidelines.

2.3.2 Virtual Reality environment

The virtual reality setup (Figure 2.1a) consists of a 360° cylindrical screen on which the virtual scene is projected. A spherical treadmill constructed from a styrofoam ball forms the middle section of the base of the screen. The projection on the screen is the reflection of a pre-distorted image, generated using a micro-projector, from a spherical mirror. The reflected image is projected on all surfaces within the screen including the base. The rat is positioned on the ball, directly underneath the projector and secured by a harness attached to the frame of the setup by means of a hinge-mechanism that allows the animal to rear or lay down on the ball freely, but restricts full body rotations. The harness is structured to wrap around the torso of the rat to allow movements of the head while restricting the body.

The styrofoam ball is positioned over a hover-craft that generates a thin layer of air allowing for free, and low-friction rotation of the ball in all directions. The ball is stabilized by means of three ball-bearings and its movements in all three axes sensed using optical sensors akin to those used in optical computer mice. As the animal moves the ball by running or walking, the movements sensed by the sensors are used to update the visual scene appropriately at 60 fps to generate the illusion of movement through the virtual space. The animal is motivated to navigate through the virtual environment by dispensing sugar water rewards through a tube fixed to the base of the screen directly in front of the rat. A computer-controlled valve is used to dispense rewards in a controlled manner when the animal enters pre-determined regions within the virtual space designated as reward zones. Any reward that is not consumed is then collected in a waste beaker to allow for accurate measurement of the amount of reward consumed by the animal, which can be used as a measure of the animal's performance on the task.

2.3.3 Behavioral Tasks

Both RW and VR setups were inside an acoustically and EMF-shielded experiment room measuring $400 \times 400 \times 250cm$.

2.3.3.1 Random foraging in RW and VR

The RW environment, positioned in the southwest corner of the experiment room consisted of a $300 \times 300 \times 250cm$ room that had distinct visual cues on each wall. The walls were constructed from curtains suspended from the ceiling and a $200cm$ diameter, $50cm$ high platform was placed at the center the room (Figure 2.1b). Rats were trained to forage for pellets of frootloop cereal randomly scattered on the platform by the experimenter. Each session lasted about 30 minutes and the experimenter remained in one fixed location for the duration of the session. At any given time, there were between one and three reward pellets on the table.

The VR room had identical size and distal visual cues (Figure 2.1b), and rats were trained to foraged for randomly located rewards on a platform of the same size as in the RW room. Rewards in VR were in the form of sugar water dispensed through a reward tubes placed directly in front of the rats. The reward locations were hidden unmarked and 40–$60cm$ in diameter, depending on the ability of the rat to find the reward zone. In any given session, the reward zones were all of the same size. Entry into the reward locations triggered the appearance of a white dot of the same size as the reward zone on the platform in addition to a reward tone and sugar water delivery. At each reward location, the rat could receive a maximum of five sugar water rewards dispensed by means of opening a valve connected to the reward reservoir. Rewards were dispensed as long as the rat was within the reward zone and would cease the moment he exited. However, he would receive at least one reward at each reward zone. Motion parallax between

the virtual elevated table and the virtual floor underneath indicated the virtual edge of the platform. Movement beyond the platform edge resulted in no change in visual scene. Rats quickly learned to avoid or turn away from the virtual edges (Figure 2.1d). It took about three weeks of handling and pre-training and two weeks of VR training for rats to learn to do the random foraging task efficiently.

Rats were trained on the RW task after implantation. Three rats were run in both RW and VR every day. To verify that exposure to both worlds on the same day was not playing a role in neural responses a fourth rat never ran in both RW and VR on the same day. Further, the order of running on VR and RW on the same days was randomized. No qualitative differences were found between these conditions and hence all data were combined.

2.3.3.2 Goal directed tasks in VR

We trained three rats to run in three different goal-directed tasks: random-pillar, two-pillar and three-pillar. In all of these tasks the reward zone in VR space was indicated by a pillar with black and white stripes suspended $50cm$ above the table and a white dot directly underneath it on the table (Figure 2.1c). All other variables, including the VR room, were identical to the one used for the random foraging tasks. When rats reached the reward zone, five rewards were dispensed, the pillar disappeared and another pillar appeared elsewhere in the maze. Rats readily learned this task and reliably ran towards the pillars [43].

In the random-pillar task a pillar appeared at a pseudorandom positions in the two VR worlds. No qualitative differences were found between neural activity patterns in the random-pillar task and the random foraging task and hence these data were combined for subsequent analyses.

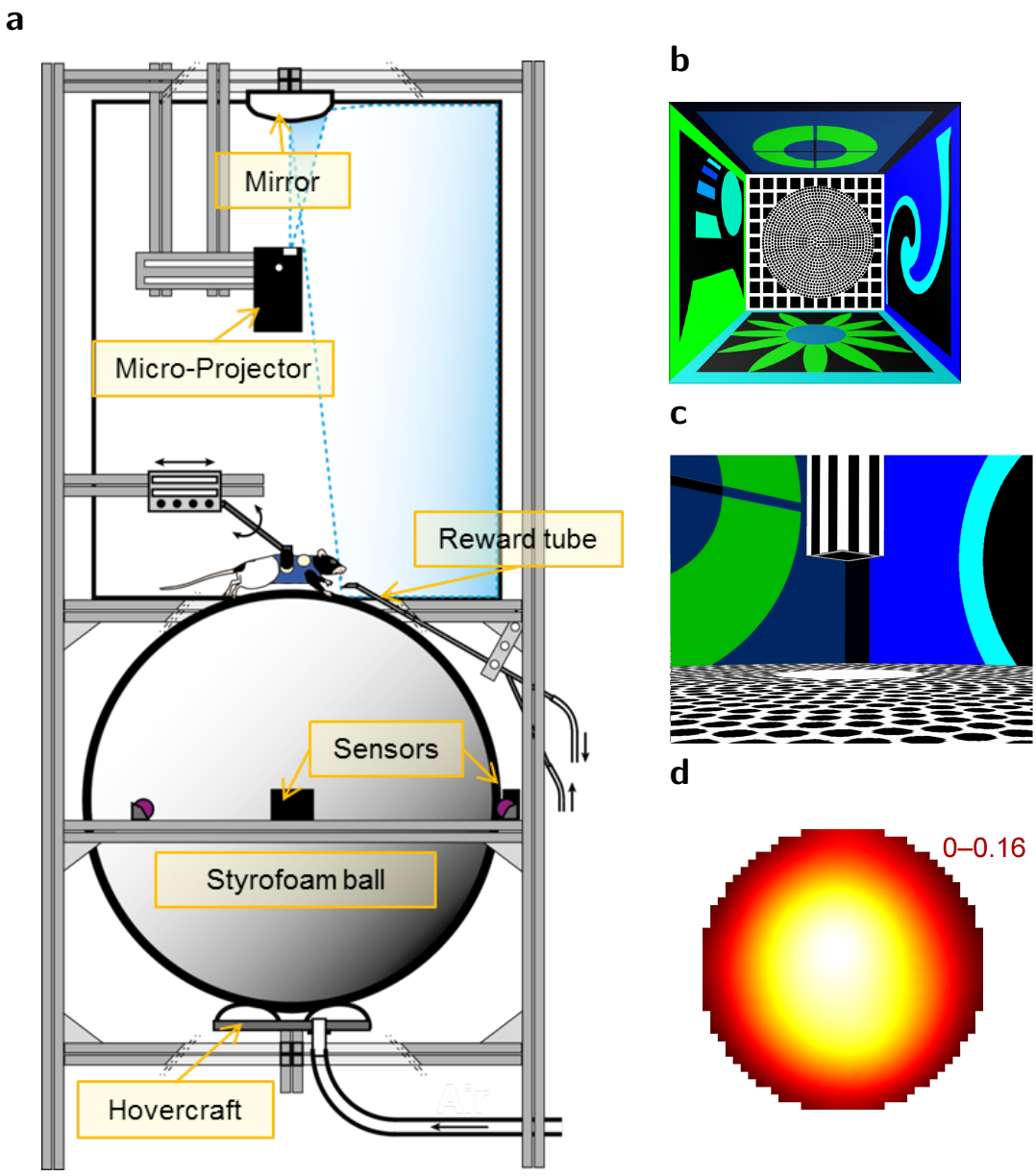

Figure 2.1: Description of the Virtual Reality (VR) system. (a) shows a schematic of the virtual reality setup, **(b)** is a top-view schematic of the virtual environment, which was identical to the RW room. **(c)** is a rat's-eye view schematic of the pillar in the goal-directed tasks. **(d)** shows the percentage of time spent in all parts of the maze, averaged across all rats showing that rats learned to avoid the edges in VR. Lighter colors indicate higher values raging from 0–0.16%.

In the two-pillar task a pillar appeared alternately at one of two fixed places positions in the middle of the VR table, and 160cm apart.

In the three-pillar task the reward the indicating pillar appeared sequentially at the vertices of an equilateral triangle with 138cm long sides centered on the VR platform.

2.3.4 Surgery

Rats that reached performance criterion were implanted with custom-made hyperdrives that contained 22 to 24 tetrodes whose dorsal-ventral position in the brain could be independently adjusted. For the implantation, the rat was anesthetized using isoflurane and positioned in a stereotax using ear bars. An incision was made that exposed the skull from the frontal plate to the occipital plate in the anterior-posterior direction and up to the bony ridge mediolaterally. The skull was thoroughly cleaned and nine screw holes drilled along the periphery of the exposed skull. One craniotomy was made over CA1 in each hemisphere at coordinates 4.0 AP, 2.4 ML with respect to bregma. Craniotomies of shape and size closely matching those of the cannulae were made using a drill mounted on a CNC machine that provided 10 micron precision in all three planes. After careful removal of the dura, screws were inserted and the hyperdrive was positioned over the craniotomies and the cannulae lowered into the craniotomies using the CNC machine until they were about 100 to 200 microns below the surface of the skull. The suspended hyperdrive was then held in place by embedding the cannulae and the bottom of the hyperdrive in dental cement. Rats, on average, took about ten days to fully recover from the surgery, during which time they were not run on any tasks, but tetrodes were gradually lowered into the brain in steps of $70 - 310\mu m$ per day.

2.3.5 Electrophysiology

Recordings were made using tetrodes which consisted of four wires twisted around eachother. Each wire was 13 microns in diameter and had 6.5 microns of polyimide insulation. Heat was used to cause the polymer to reflow and fuse the four wires together after twisting. These tetrodes were then loaded into the hyperdrive prior to surgery and the tips of carefully cut and plated with a 3:1 mixture of gold solution and carbon nanotubes. Twenty-four such tetrodes resulted in ninety-six recording channels.

Each tetrode could be moved by a screw that was accessible to the experimenter by means of a turning tool. Each turn of the screw moved the tetrode by approximately $310\mu m$ and tetrodes could be moved by a minimum distance of $20\mu m$ (1/16th of one full turn). Tetrodes were adjusted everyday by a distance between 1 and 1/4 turns for the first seven to ten days. At the end of this period, most tetrodes were deep in the neocortex and adjusting steps were made significantly smaller (1/4 to 1/16 turns each day) till they reached CA1. Tetrodes were advanced to CA1 in groups of four or five. CA1 was identified by the presence of sharpwave-ripple complexes and strong theta oscillation.

Once the animal had recovered sufficiently to be able to perform the behavioral task and at least one tetrode was in CA1 and pyramidal neurons could be identified, recording would commence. Task sessions were flanked by one hour baseline sessions during which the animal was allowed to sleep in a box placed within the experiment room. Red, green and blue LEDs on the head cap allowed for monitoring the position of the rat in both baseline and task sessions. For the rats that were run on both RW and VR tasks on the same day, the two tasks were run in one block with the baselines before and after the task block.

Recordings were made at a sampling rate of $40kHz$ and bandpass filtered between $0.9Hz$ and $9kHz$ using a Neuralynx Digital Lynx SX system. The recording

system was interfaced with the tetrodes through an electrode interface board with three headstages, each with 24 acquisition channels. The user interface allowed the experimenter to observe the continuous traces and spike clusters online during adjusting and recording.

2.3.6 Spike detection and sorting

Spikes extraction and detection was done offline. To detect spikes, the continuous traces were bandpass filtered between $600Hz$ and $6kHz$ and a nonlinear energy operator threshold applied. $1ms$ spikes were extracted, upsampled fourfold, aligned with respect to their peaks and downsampled to 32 data points. These were sorted into individual units using custom software—a modified version of the MClust software package (MClust-3.5, A.D. Redish).

Classification of single unit cell type was performed using the same methods as previously described [14]. For each clustered unit, the energy normalized waveforms were computed and the peak to trough fall times determined. Units were classified as interneurons if their fall times were less than $0.4ms$ and had firing rates of at least $5Hz$ during periods of running. Units with fall times more than $0.4ms$ and firing rates less than $5Hz$ during periods of run were classified as pyramidal units. Principal component analysis of the average waveforms was used to verify classification.

In addition to classification, neurons were identified across two sessions as the same cell by comparing cluster boundaries in multiple projections and waveform shapes from both sessions. If the identity of a cluster from the two sessions was even slightly different due to electrode drift, and could not be conclusively classified as the same unit, they were discarded from same cell analysis.

2.3.7 Statistics

Offline analyses were performed using custom MATLAB codes. Tests of significance between linear variables (circular variables) were done using the two-sided nonparametric Wilcoxon rank-sum test (Kuiper test). Tests of significance for the mean values of distributions being different from zero were performed using the two-sided nonparametric Wilcoxon signed-rank test. To compute circular statistics, CircStat toolbox was used [44]. Tests of significance of correlation between two variables were done using a t-test for correlation coefficients. All ensemble averages are in the form $mean \pm s.e.m$ unless otherwise stated. All correlation values are reported as the linear correlation coefficient r. Two different sessions had a small number of single units, which could potentially inflate our estimate of the number of independent samples, thus altering the significance level of the statistical tests. Hence, as a conservative estimate, we did all tests of significance using only half as many cells in VR and RW. All significant results were still highly significant. No statistical methods were used to predetermine sample sizes, but our sample sizes are similar to those generally employed in the field. Data collection and analysis were not performed blind to the conditions of the experiments.

2.3.8 Quantification of ratemaps

Theta rhythm is interrupted [42] and behavior is uncontrolled when rats pause to consume rewards or to groom. Hence these periods were excluded and only data recorded during periods of active locomotion ($runningspeed > 5cm/s$) were used. The duration of recording sessions were matched between RW and VR to remove possible sources of variability. A cell was considered active if its mean firing rate exceeded $0.2Hz$ and fired at least 100 spikes during locomotion and was thus included in the analysis. Spatial firing rates were computed using occupancy

and spike histograms with $5 \times 5cm$ bins smoothed with a $7.5cm$ two-dimensional Gaussian smoothing kernel. Bins with very low occupancy relative to the experimental session were excluded to avoid artificially high firing rates. The spatial information content, sparsity and coherence of the ratemaps were computed using methods described previously [14]. To determine the stability of ratemaps, firing rates were computed in the first and second halves of the session separately. The bin-by-bin correlation between the ratemaps in the two halves provided a measure of ratemap stability. To obtain the similarity of ratemaps of the same cell in RW and VR we computed the correlation of firing rates and computed statistical significance by comparing it against correlations when cell identities were shuffled.

2.3.9 Computation of coactivation of cell pairs

To determine the degree of coactivity of pairs of cells active in a session, we first constructed the firing rate of neurons as a function of both time elapsed and distance traveled ($200ms(5cm)$ time(distance) bins, smoothed with $400ms(10cm)$ Gaussian smoothing kernel). We then computed the cross-covariance of firing rates for pairs of active cells within a session. To obtain an estimate of chance level, we generated control data by time-reversing the spike train of one of the cells in the cell pair and time shifting both of them by random amounts between 10–$100s$. This procedure was repeated 10 times. We detected the peak value in the cross-covariance of the original cell pairs and the control data in both distance and time domains.

The dynamic ratemap for a pair of coactive cells was constructed as follows: for each spike from the first cell, the rat trajectory and spikes from the second cell within the next $200cm$ traveled were aggregated relative to the spike positions from the first cell. We used $15 \times 15cm$ spatial bins and computed the occupancy time and number of spikes in each bin. Dividing the number of spikes by the occupancy time in each spatial bin provided the dynamic ratemap. Information

content and sparsity of these ratemaps were quantified as described previously.

$$peak_{actual}^{distance} \geq mean(peaks_{control}^{distance}) + 2 \times standarddeviation(peaks_{control}^{distance}) \quad (2.1)$$

$$peak_{actual}^{time} \geq mean(peaks_{control}^{time}) + 2 \times standarddeviation(peaks_{control}^{time}) \quad (2.2)$$

We then calculated the fraction of cell pairs whose firing rate cross-covariance had a significant peak.

2.3.10 Goal-Directed Tasks

2.3.10.1 Quantification of degree of goal-directedness

In all three tasks, the degree of goal-directed behavior was quantified by calculating the median excess path length. We defined the difference between the shortest distance between two consecutive reward locations and the actual path length traveled by the rat as the excess path length. We then calculated the median value of this excess path length over an entire session to obtain the excess path length for the session.

2.3.10.2 Characterizing Selectivity to Distances Traveled in VR Goal-Directed Tasks

To investigate the degree of selectivity to distance traveled in the goal-directed tasks (VR systematic-pillar and VR random-pillar), we linearized the paths by measuring the distance traveled between two consecutive reward and normalizing them to unity. To control for the variability in the path lengths, we only considered trials for which the distance traveled was around the median path length ($median \pm 0.4 \times median$). This threshold value of 0.4 ensured that the number of trials and path-length variability were similar in random-pillar and systematic-pillar tasks. The following analysis was also repeated when considering all trials

regardless of the path lengths and the results were qualitatively similar. For each cell, we constructed a linearized ratemap as a function of the normalized distance traveled. For cells with mean firing rate above $0.5Hz$, we then computed the information content, sparsity and peak value of the ratemaps to quantify this selectivity. To examine the nature of this selectivity on an ensemble level, for each cell we partitioned the selected trials into two random groups. We computed the firing rate for each partition separately. The population vector overlap for the two partitions was calculated and the significance values were obtained using previously described methods [14].

2.3.10.3 Computation of Disto-code in VR Three-Pillar Task

Here, a one-dimensional linearized ratemap was constructed (distances were normalized to unity) for each arm separately. A given arm pair was used for analysis if the mean firing rate was higher than $0.5Hz$ on at least one arm. We then computed the arm selectivity index for each two-arm combination as:

$$D_{ij} = |\frac{\Sigma_l^L(\lambda_l^i - \lambda_l^j)}{\Sigma_l^L(\lambda_l^i + \lambda_l^j)}| \tag{2.3}$$

Where λ_l^i and λ_l^j are the rates in the l^{th} bin along arms i and j. For the arm pairs with $D < 0.5$ (pairs with firing along both arms) we computed the population vector overlap, its significance level and disto-coding index similar to the methods described previously [14].

2.3.11 Detection of Motifs

To detect motifs a method similar to the one used for detecting place fields on a one-dimensional track was used. We constructed a spike train, a vector of data whose length spanned the period of experimental session, by binning the spikes for which the running speed was greater than $5cm/s$. This spike train was

smoothed using a $200ms$ Gaussian smoothing kernel and transformed to firing rate by dividing by the bin duration. Peaks where firing rate exceeded $5Hz$ were detected and marked as candidate motifs. The boundaries of a motif were defined as the points where the firing rate first dropped below 10% of the peak rate (within the motif) for at least $250ms$ (two theta cycles). If the time-lag between the first and last spike in the putative motif, called the duration of the motif, exceeded $300ms$, this sequence was considered a valid motif and was included in the analysis.

For each cell we computed the mean firing rate within individual motifs and calculated the mean of those values to obtain a single number for individual cells.

2.3.12 Construction of Motif-fields

The center of a motif was defined as the center of mass of the firing rate as a function of time within the motif. This value was subtracted from the spike times within the motif to center them around zero. This procedure was repeated for all motifs and the centered motifs were aligned to obtain a motif-field for a given neuron. The firing rate as a function of time within the motif-field was calculated as the number of spikes within each temporal bin divided by the total amount of time in that bin, smoothed by a $200ms$ Gaussian smoothing kernel. Motif-field duration was defined as twice the weighted standard deviation of the motif firing rate, i.e. the width of the distribution.

2.3.13 Theta Period and Phase Precession

Similar to the methods described previously [14], each LFP was filtered between 4 and $12Hz$ using a 4th order Butterworth filter. Theta period was computed by detecting the peak between 50 and $200ms$ in the filtered LFP autocorrelation for epochs when the running speed was above $5cm/s$. Spiking theta period was

calculated by computing the spike train autocorrelation, smoothing by a $15ms$ wide Gaussian kernel, and detecting the peak. Quality of phase precession within a motif-field was defined as the circular linear correlation coefficient (CLCC) [14] between spike phases and latency of spike timing with respect to the motif center.

To further examine the dynamics of LFP theta, we investigated the LFPs recorded from the same electrode on the same day in both worlds without any electrode movement between the two sessions. Analysis was further restricted only to data when rats ran at speeds greater than $5cm/s$ to eliminate contamination by variable periods of stopping when theta is reduced. In order to compare data from different sessions, the power spectrum from each electrode was normalized by the mean power on that electrode in RW and VR over the frequency range $1 - 100Hz$.

2.3.14 Control Analysis for Motifs

To estimate which motif properties can arise purely by chance, surrogate motifs for each neuron were generated as follows. The mean firing rate during locomotion and the depth of theta modulation were computed for each neuron. Surrogate activity was generated using a Poisson distributed and theta modulated spike train with the same mean firing rate and depth of theta modulation as the experimentally measured neuron. Motifs, motif-fields, and their properties were computed using procedures described above. This procedure was repeated 50 times for each neuron to generate a null distribution. Mean value and standard deviation of this null distribution were used to compute the z-scored values for each cell.

2.3.15 Control Analysis for Spatial Selectivity

To determine the statistical significance of spatial selectivity we generated control data by shifting the experimentally observed spike train with respect to behavioral

data by random amounts between $10100s$. All of the measures used to quantify the spatial selectivity were expressed in the units of z-score or standard deviations around the control data.

2.4 Results

2.4.1 Nature of spatial selectivity of hippocampal responses

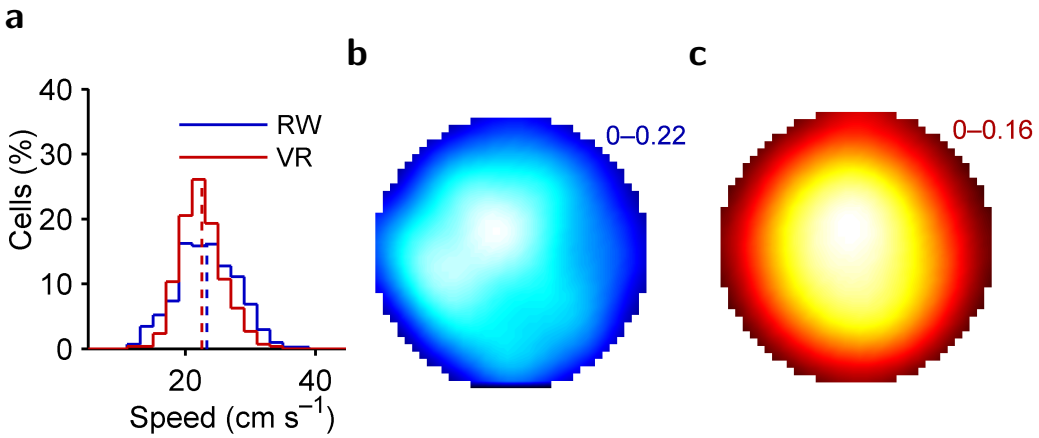

Figure 2.2: Similar rat behavior in RW and VR. (a) Mean running speed at the time of occurrence of spikes (excluding speeds $< 5cm/s$) was slightly reduced ($3\%, p = 0.0005$) in VR ($22.40 \pm 0.13cm/s$, red) compared to RW ($23.27 \pm 0.16cm/s$, blue). Colored, dashed vertical lines indicate the mean values of the corresponding distributions, here and subsequently. **(b)**, **(c)** Percentage of time spent in all parts of the maze, averaged across all rats showing that rats spent comparable time away from edges in RW and VR. Numbers indicate range; lighter shades indicate higher values. These color conventions (RW, blue shades; VR, red shades; lighter shades, higher values) apply to all subsequent figures.

We measured hippocampal activity during a random foraging task in RW and VR [18, 43] with similar distal visual cues (Figure 2.1b). In VR rats were body-

fixed with a harness on a floating ball, allowing head movements but precluding full body-turns, thus minimizing vestibular cues (Figure 2.1a)(see Methods) [14, 43]. Rats quickly learned to avoid the virtual edges based entirely on visual cues [43] and spent a similar amount of time away from the edges and in the center of the platform (Figure 2.2b,2.2c) compared to RW.

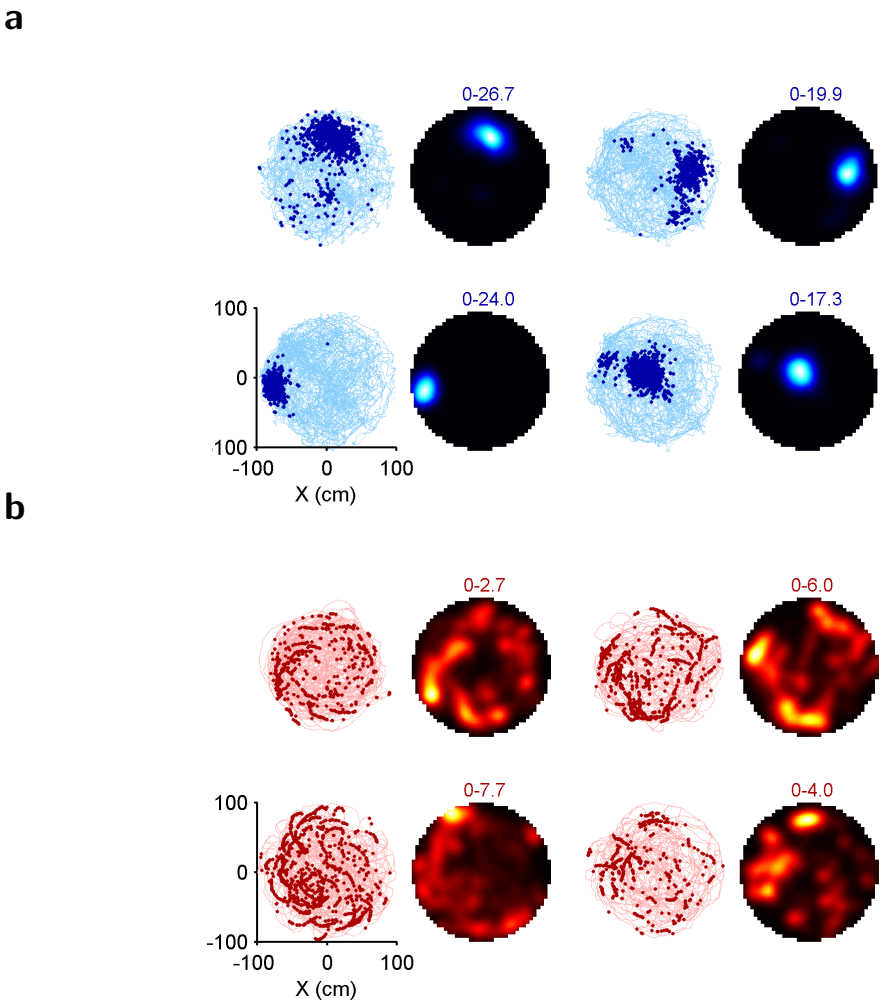

Figure 2.3: Different neural ratemaps in RW and VR. a), b) Rat trajectory and spike positions for different neurons and corresponding firing ratemaps in RW and VR.

From the dorsal CA1 of four rats we measured the activity of 1066 and 1238 principal neurons in RW and VR respectively, under a variety of conditions (see

Methods). Neurons fired vigorously in restricted regions of space in RW as expected (Figure 2.3a, Supplementary Video 1). In contrast, they showed little spatial selectivity in VR during random foraging (Figure 2.3b, Supplemnetary Video 2).

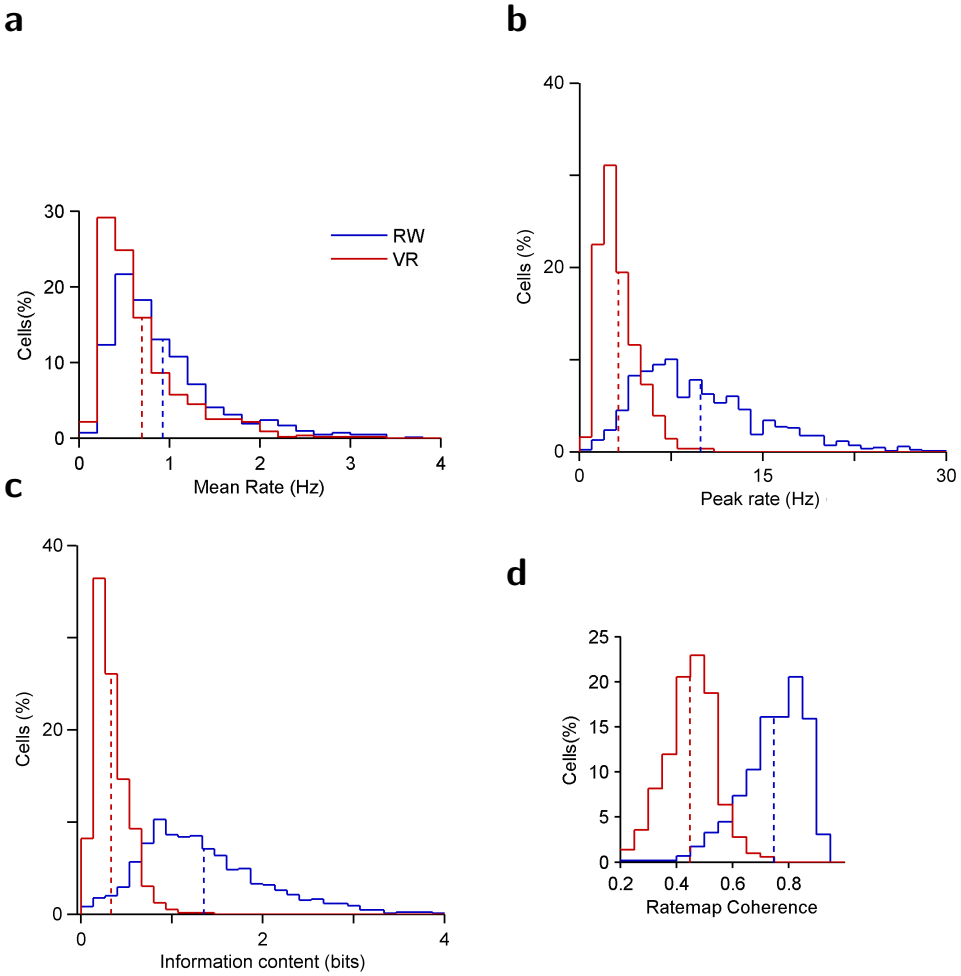

Figure 2.4: Reduced activity and spatial selectivity in VR (a) Mean firing rates were 25% ($p = 7.6 \times 10^{20}$) lower in VR ($0.70 \pm 0.02Hz$) than in RW ($0.93 \pm 0.02Hz$). **(b)** Peak firing rates of neurons were 68% ($p = 1.1x10^{161}$) smaller in VR ($3.19 \pm 0.07Hz$, n=719 cells from 4 rats) compared to RW ($9.90 \pm 0.18Hz$, n=1066 cells from 4 rats). **(c)** Spatial information content in VR ($0.33 \pm 0.01bits$) was 75% ($p = 1.1 \times 10^{183}$) lower than in RW ($1.35 \pm 0.02bits$) **(d)** Ratemap coherence computed using $10 \times 10cm$ bins, was 40% ($p = 2.3 \times 10^{-157}$) reduced in VR (0.45 ± 0.01) compared to RW (0.75 ± 0.01).

Across the ensemble, neurons had moderately reduced (25%) mean firing rates but greatly reduced (68%) peak firing rates in VR (Figure 2.4a, 2.4b). Neurons in VR also had greatly reduced spatial information content (75%) (Figure 2.4c), stability (59%) (Figure 2.5a, 2.5b), coherence (40%) (Figure 2.4d) and sparsity (42%) (Figure 2.5c) compared to spatially localized, stable, and sparse RW ratemaps.

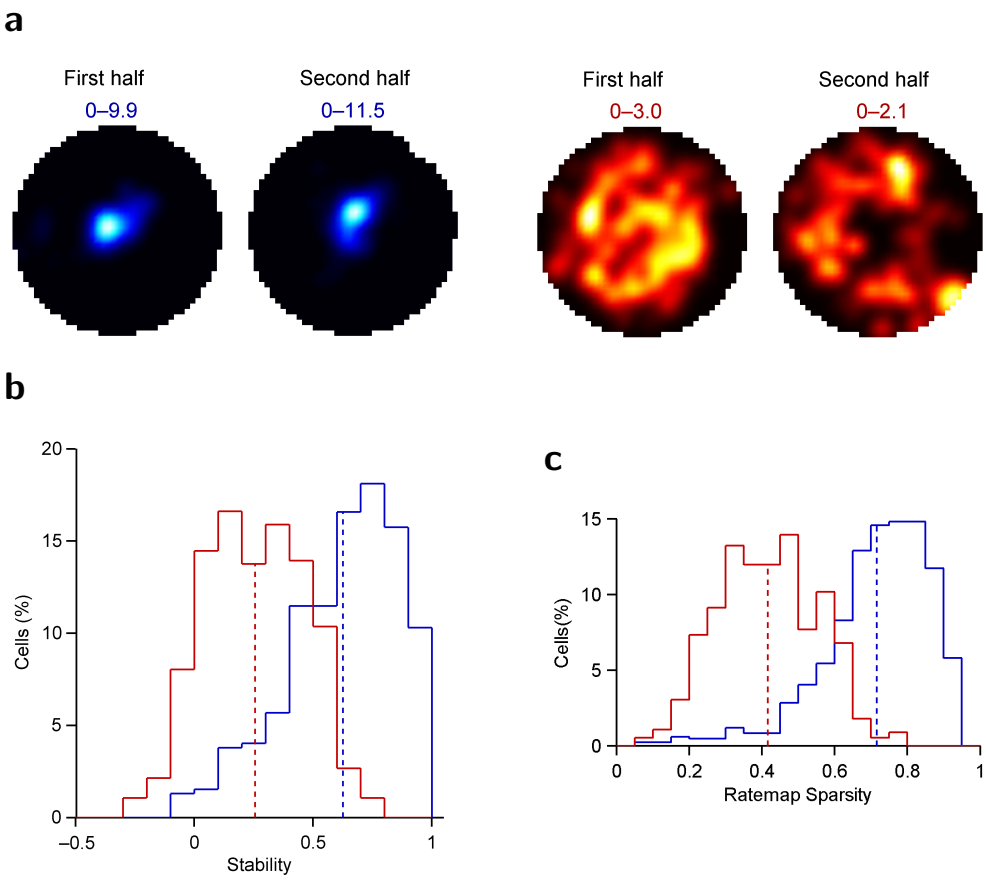

Figure 2.5: Reduced activity and spatial selectivity in VR (a) Ratemaps of a neuron during the first and second halves of a session in RW and VR. **(b)** Stability of ratemaps in VR (0.26 ± 0.01) was significantly reduced ($difference = 0.37, p = 1.2 \times 10^{124}$) compared to RW ($0.63 \pm 0.01$). **(c)** , Ratemap sparsity, a measure of spatial selectivity, was also greatly ($42\%, p = 2.3 \times 10^{-162}$) reduced in VR ($0.42 \pm 0.01$) compared to RW ($0.72 \pm 0.01$).

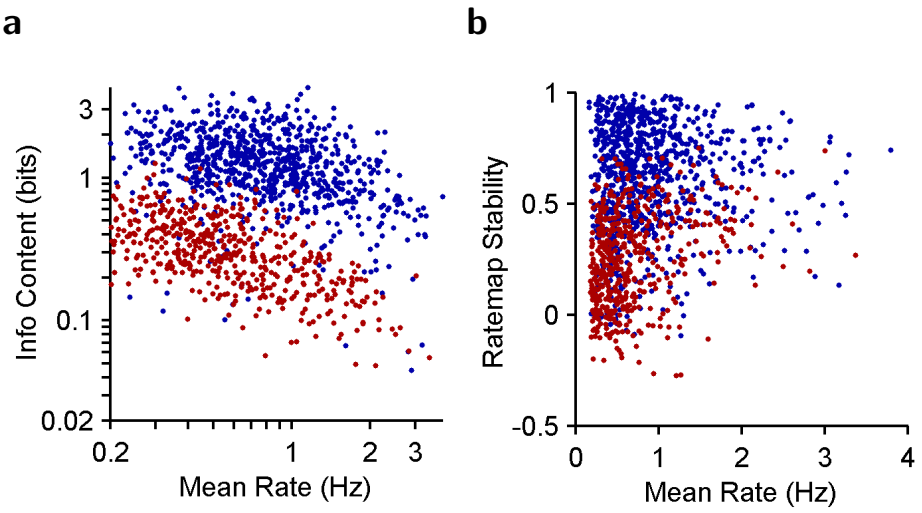

Figure 2.6: Information content and stability were higher in RW than in VR at mean rate values. (a) At all mean rates, spatial information content was negatively correlated with the mean firing rate of a cell in both worlds (RW $r = -0.36, p = 1.6 \times 10^{27}$; VR $r = -0.48, p = 3.2 \times 10^{-33}$). **(b)** Spatial stability was lower in VR compared to RW. Stability was not correlated with mean firing rate in RW ($r = 0.02, p = 0.54$) and weakly positively correlated in VR ($r = 0.28, p = 1.1 \times 10^{-11}$).

Though mean firing rate was inversely correlated with information content (Figure 2.6a), this large reduction in spatial selectivity cannot be accounted for by the differences in mean firing rates in VR and RW since neurons with similar firing rates had significantly lower spatial selectivity (Figure 2.6a) and stability in VR (Figure 2.6b).

Analysis of relative spatial dynamics [45] between simultaneously measured cells showed that neurons did not maintain consistent spatial relationships with each other in VR in contrast to RW (Figure 2.8). This was further confirmed by the analysis of cross-covariance of firing rates in time and in distance (see Methods) showing little evidence of coactivation or reliable pairing of groups of neurons in VR, in contrast to RW (Figure 2.8).

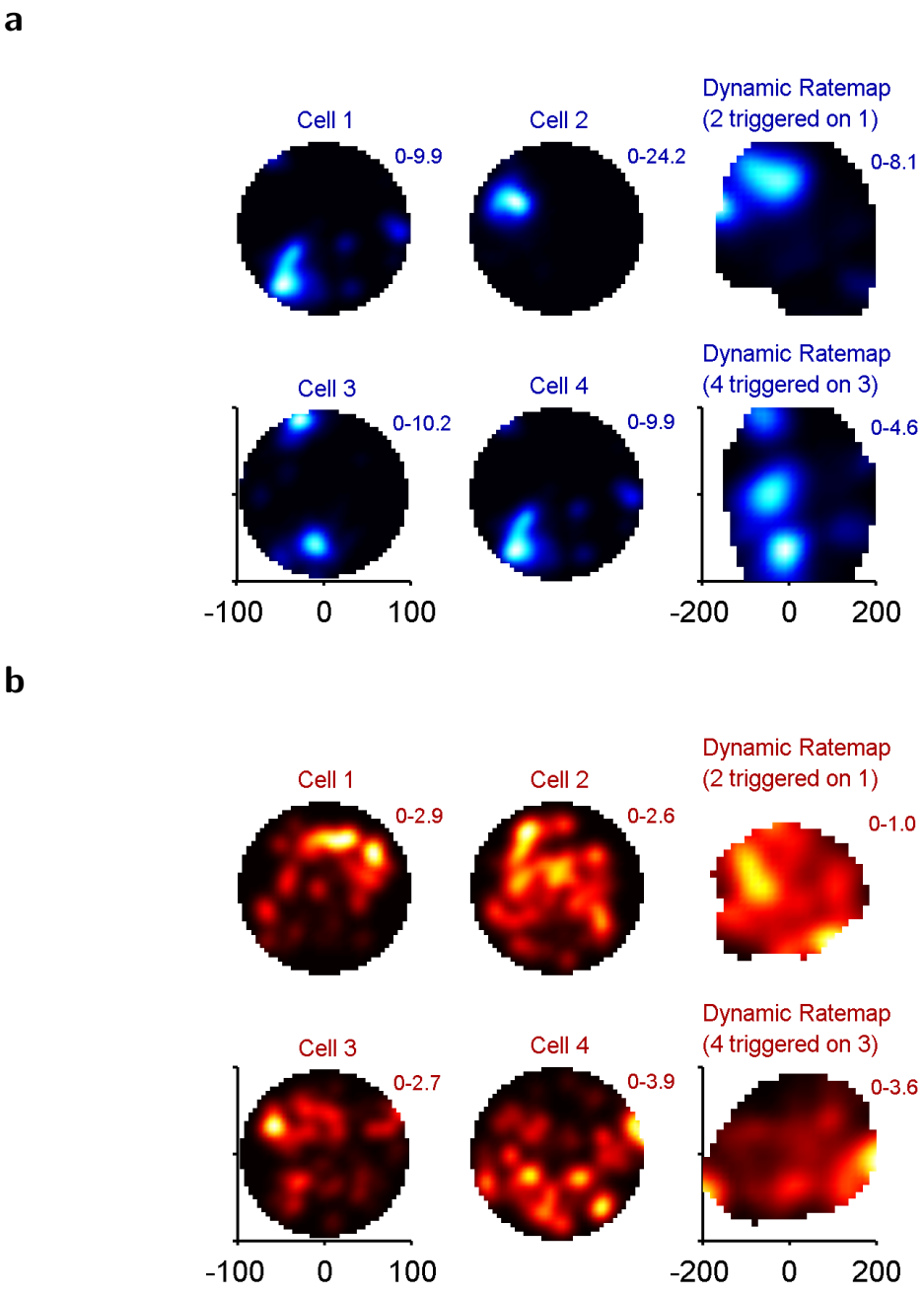

Figure 2.7: Loss of spatial selectivity in dynamic ratemaps in VR. (a) Spatial ratemaps of two pairs of neurons in RW (left) and their dynamic ratemap (right) showing spatially localized activity. **(b)**Same as (a) but for two pairs of neurons in VR showing no spatial selectivity.

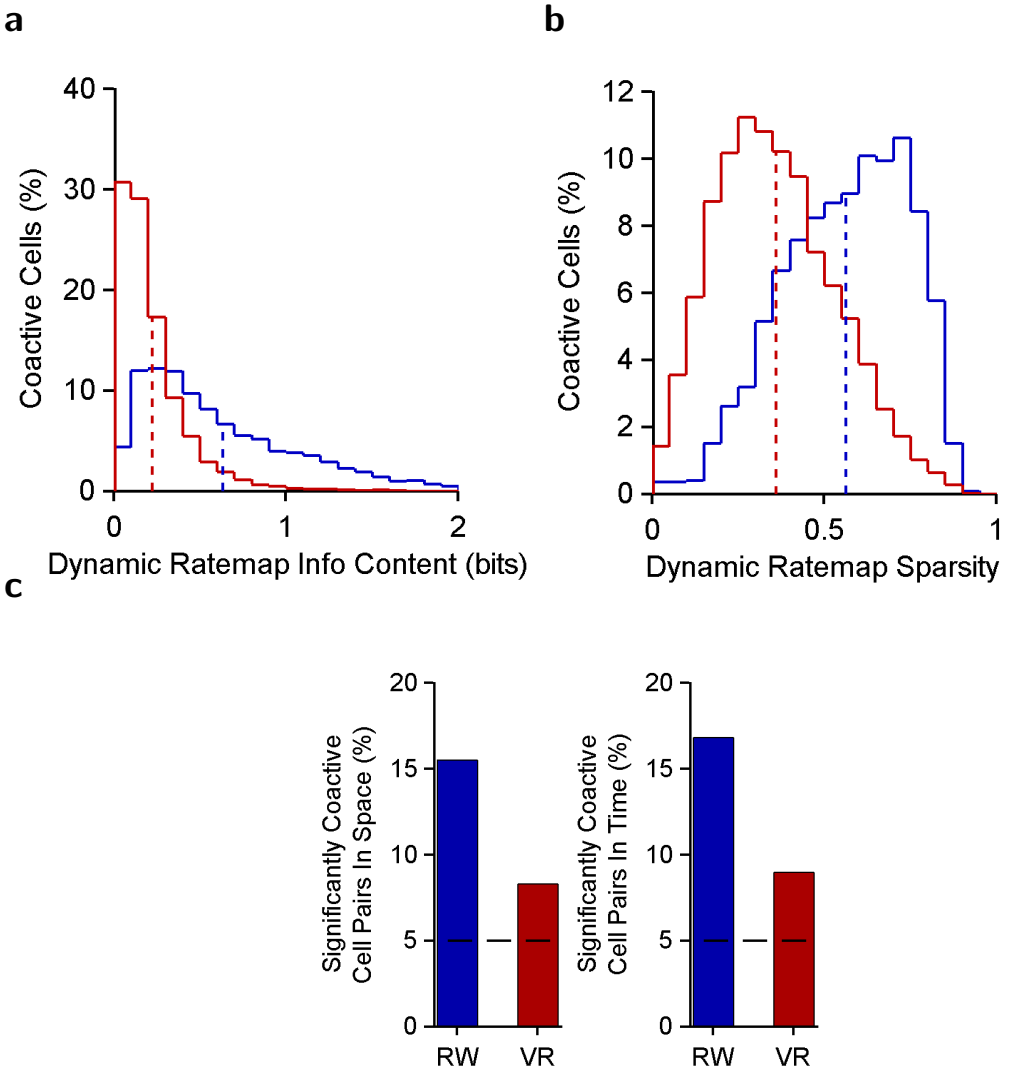

Figure 2.8: Reduction in neuronal coactivation in VR. (a) Dynamic ratemap information content in RW ($0.63 \pm 0.01\ bits, n = 10831\ pairs$) was 65% greater ($p < 10^{-100}$) than in VR ($0.22 \pm 0.00\ bits, n = 8202\ pairs$). **(b)** Dynamic ratemap sparsity in RW (0.56 ± 0.002) was also greater (36%, $p < 10^{-100}$) than in VR (0.36 ± 0.002). The relative spiking of coactive neurons was spatially informative in RW but not in VR. **(c)** In order to investigate coactivity of cell pairs (including sequential activity on intermediate time- and length scales) we computed cross-covariances between the firing rates of pairs of active cells in a session as a function of time elapsed or distance traveled (see Methods). The fraction of coactive cells in RW (15.5(16.8)% in distance(time) domain) was far greater than that in VR (8.3(8.9)% in distance(time) domain).

These results demonstrate that, in VR, neurons did not have place fields that were drifting together, nor were they activated in a sequential fashion, in some unknown reference frame.

We also characterized activity of 258 neurons recorded in both worlds on the same day (See Methods). Of these, only 109 (42%) had a mean firing rate above a minimal activity threshold of $0.2Hz$ in both worlds.

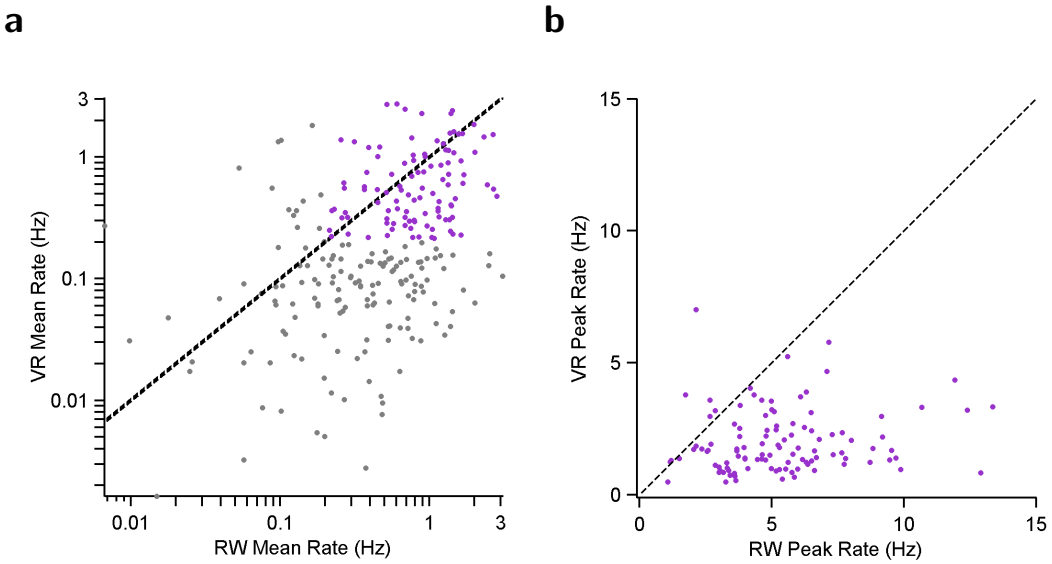

Figure 2.9: Comparison of activities of cells active in both RW and VR on the same day. (a) For cells recorded in both worlds on the same day mean firing rate was correlated regardless of minimum firing rate (grey, $r = 0.32, p = 1.7 \times 10^{-7}, n = 258$). This was also true for the subset of cells active at high rates in both worlds (purple, $r = 0.21, p = 0.03, n = 109$), used for all subsequent same-cell analyses. **(b)** The peak firing rate of the same cell was reduced in VR compared to RW and the two were not significantly correlated ($r = 0.12, p = 0.23$), despite their correlated mean rates, due to lack of spatial selectivity in VR.

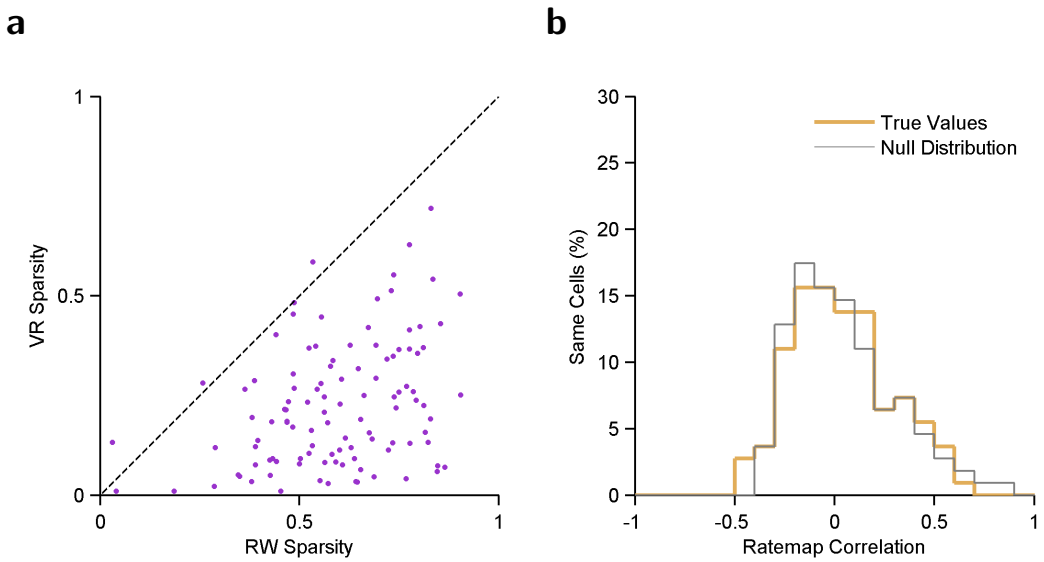

Figure 2.10: Comparison of activities of cells active in both RW and VR on the same day. (a) Spatial ratemap sparsity of the same cell was also reduced in VR but correlated with RW ($r = 0.36, p = 0.0001$), which could be partially explained by correlated mean firing rates. **(b)** Despite positive correlations in mean rate and sparsity, the distribution of correlation of ratemaps of the same cells between RW and VR was not significantly different from zero ($p = 0.39$) and not different from the ratemap correlations obtained by shuffling the cell identities ($p = 0.97$).

For these neurons, the mean firing rates, but not peak firing rates, were significantly correlated between RW and VR (Figure 2.9a, 2.9b), although they showed spatial selectivity in RW but not in VR and had uncorrelated ratemaps (Figure 2.10a, 2.10b).

2.4.2 Contribution of task type and locomotion cues

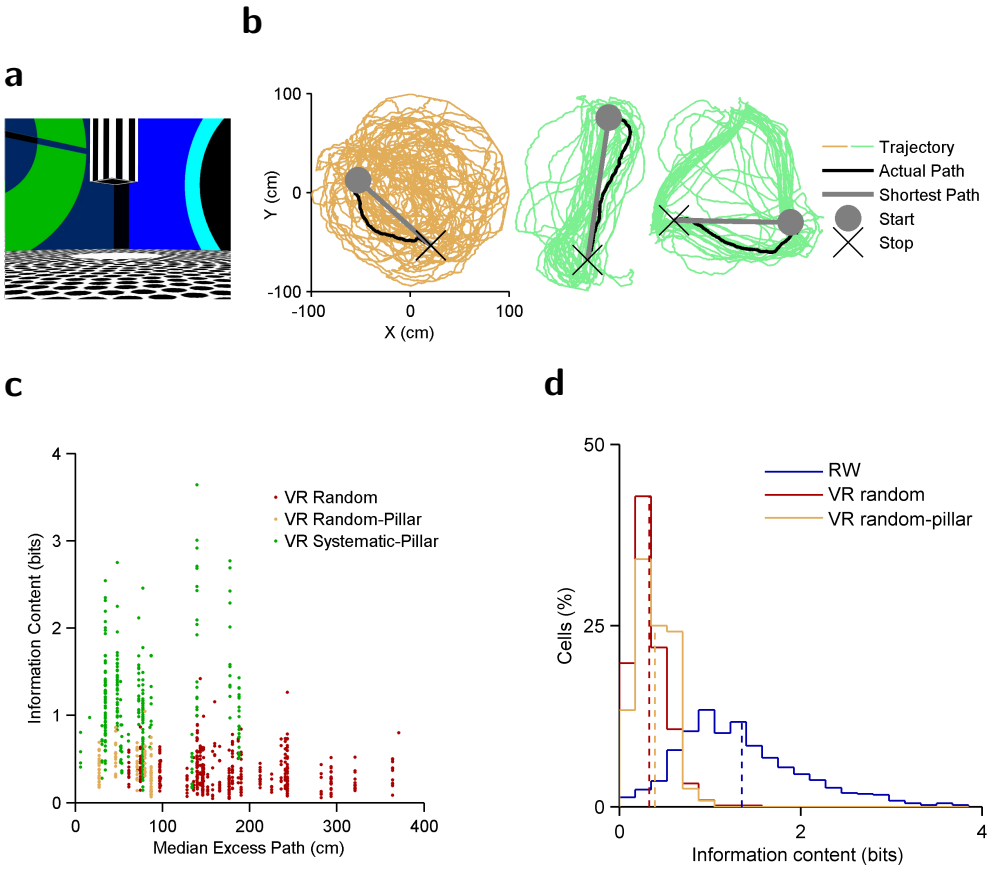

Figure 2.11: Quantification of behavior and neural responses during goal-directed VR tasks. (a) Schematic showing a pillar suspended in VR. **(b)** Sample trajectories between two reward locations and the corresponding shortest path between them in the random-pillar task (left) and systematic-pillar tasks (center, right). **(c)** Behavior was significantly more goal-directed during the pillar tasks (median excess path length: random pillar $56.3 \pm 10.8cm, p = 6.1 \times 10^{-4}$; systematic pillar $77.3 \pm 12.2cm, p = 1.4 \times 10^{-5}$) than during random foraging (median excess path length: $178.2 \pm 13.9cm$, see Methods. VR random-pillar and VR systematic-pillar were equally goal-oriented($p = 0.44$). **(d)** Spatial information content in VR Random-Pillar ($0.39 \pm 0.02bits, n = 195$cells from 3 rats) was only slightly ($16\%, p = 1.6 \times 10^4$) larger than in VR random ($0.33 \pm 0.01bits$), and still substantially smaller ($71\%, p = 1.1 \times 10^{55}$) than in RW ($1.35 \pm 0.02bits$).

In RW, rats might use a goal-directed strategy to navigate to a food pellet, whereas in VR, there were no reward-predicting cues; such a difference in task type could influence hippocampal activity [11]. To control for this, we did a separate experiment where we measured the activity of 195 neurons from three rats while they ran towards a reward-indicating suspended pillar appearing at random locations in VR (Figure 2.11a, see Methods) [43]. The excess path length of the rats'trajectory between rewards was significantly shorter during this random-pillar task (69%) than the random foraging task, indicative of a goal-directed strategy (Figure 2.11b, 2.11c). There was no substantial difference in spatial selectivity between the two task types in VR (Figure 2.11d, Supplementary Video 2), which argues that the loss of spatial selectivity was not due to differences in task type. Hence, for subsequent comparisons between RW and VR, data from random foraging and random-pillar tasks were combined.

The loss of spatial selectivity in two-dimensional VR is in stark contrast to not only two-dimensional RW, but also to previous studies in one-dimensional VR [14, 17, 39, 40] where clear spatial selectivity was found. To test whether spatial selectivity could exist in the same two-dimensional VR environment without the vestibular cues present in RW, we did another experiment in which the task type was similar to the random-pillar task, but the reward-indicating pillars appeared systematically at fixed locations (see Methods). In the first variant, pillars appeared at two fixed but alternating positions in VR (Figure 2.12a). Because rats ran in more stereotyped trajectories, locomotion cues—such as step counting from the previous reward and speed of optic flow—were made spatially informative because the same cues occurred repeatedly at the same positions across the task. Consequently, unique locomotion cues were repeatedly paired with distinct distal visual cues at each position. Spatially selective neural responses appeared in this systematic-pillar task with significantly enhanced spatial information content and ratemap sparsity compared to VR random foraging (Figure 2.13a, 2.13b).

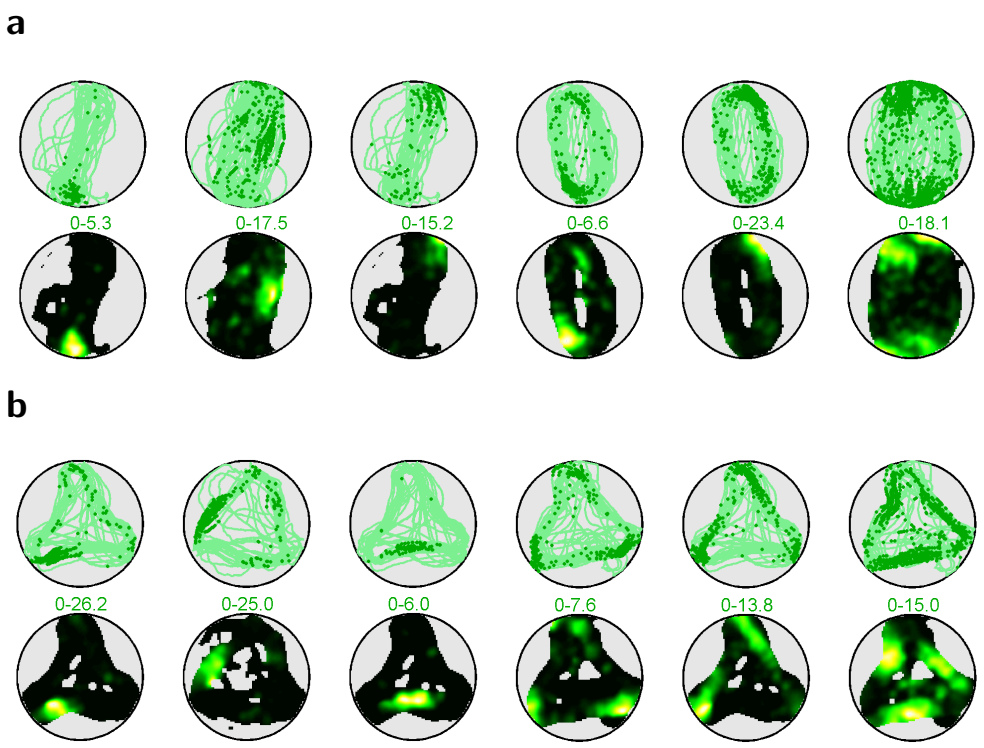

Figure 2.12: Dependence of spatial selectivity on task type and locomotion cues. **(a)**, **(b)** Top) Trajectory of the rat (light green trace) and position of the rat at the time of occurrence of spikes (darker dots) for example neurons during the systematic path tasks. Bottom) Ratemaps corresponding to the above neurons.

While some neurons had a focused place field in only one movement direction, or arm, similar to place cells in RW, others spiked on both arms (Figure 2.12a), which we investigate in detail below.

To rule out the possibility that spatial selectivity arose simply due to alternating contexts in two movement directions, or that the rat did not traverse a large portion of the maze, we did another variant of the systematic-pillar task in which the reward-indicating pillars appeared sequentially at the vertices of an equilateral triangle (see Methods). Here the rats walked repeatedly along the same paths while covering a greater fraction of the two-dimensional maze and, because adjacent arms were rotated 120° with respect to each other rather than 180°, the visual scene was more similar along different arms than in the two-pillar

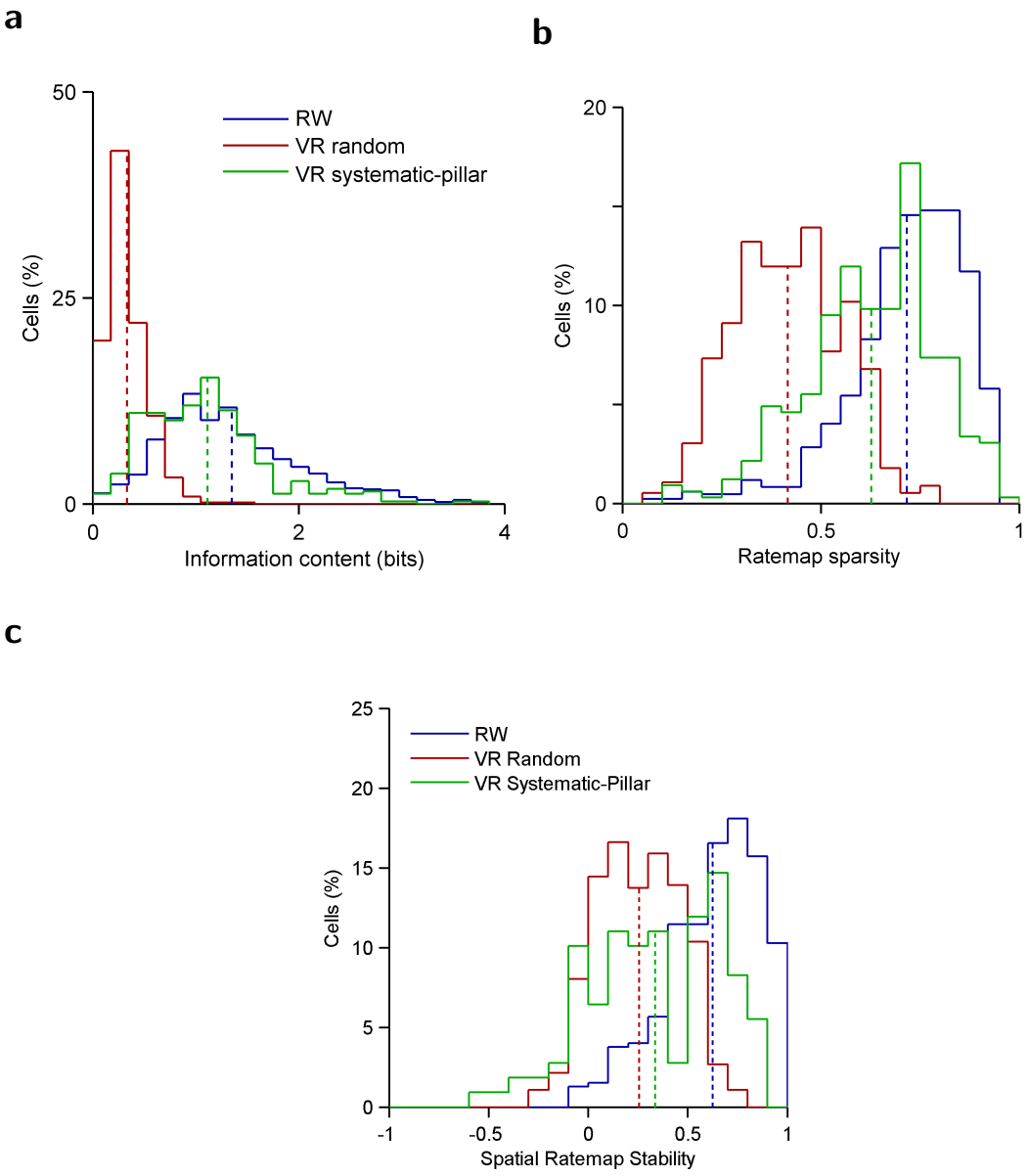

Figure 2.13: Dependence of spatial selectivity on task type and locomotion cues. **(a)** Spatial information content in VR with systematic pillars ($1.11 \pm 0.03 bits, n = 324$ cells from 3 rats) was significantly larger than in VR random ($70\%, p = 1.0 \times 10^{101}$) and only slightly smaller than in RW ($17\%, p = 5.3 \times 10^{8}$). **(b)**Spatial sparsity in VR systematic-pillar (0.63 ± 0.01) was significantly greater ($34\%, p = 4.7 \times 10^{63}$) than in VR random ($0.42 \pm 0.01$), and close ($12\% less, p = 4.6 \times 10^{20}$) to that in RW ($0.72 \pm 0.01$) **(c)** Ratemap stability in the VR systematic-pillar task ($0.34 \pm 0.03, n = 282$ cells with at least 100 spikes in each session half) is greater than VR random foraging ($p = 2.4 \pm 10^{-3}$) and smaller than RW random foraging ($p = 1.8 \times 10^{-18}$).

task (Figure 2.12b). Spatially selective, stable responses also appeared in this task, significantly greater than in the two-dimensional random foraging tasks in VR, but comparable to that in two-dimensional random foraging in RW (Figure 2.12b, 2.13a, 2.13b). Here too, some neurons spiked on only one arm of the triangle (Supplementary Video 3), similar to RW place cells, while others spiked along multiple arms (Supplementary Video 4).

In both of the systematic-pillar experiments, vestibular cues remained minimal and spatially uninformative during turns, yet spatial selectivity was comparable to that in RW random foraging. Further, in systematic-pillar tasks and the random-pillar task, the path between two successive reward locations was not always direct, but often deviated from the optimal, straight-line path (Figure 2.11b). This departure, or excess-path length, was comparable in both systematic- and random-pillar tasks (Figure 2.11c), indicating similar levels of goal-directed behavior and demonstrating that differences in the departure from the shortest paths do not underlie the observed differences in spatial selectivity. Thus, the task type cannot explain the observed differences in spatial selectivity under different conditions in RW and VR.

The presence of firing on multiple arms in the systematic-pillar tasks (Figure 2.12a, 2.12b) suggests that neurons might be coding for the distance traveled along the paths. If so, this raises the possibility that neurons in the random-pillar task might also exhibit similar coding despite their lack of two-dimensional spatial selectivity. The fact that the beginning and end of a trial were clearly delineated by the visible pillars in all goal-directed tasks allowed us to test these possibilities by quantifying neurons's activity as a function of normalized distance traveled along each path, subsequently referred to as distance (see Methods).

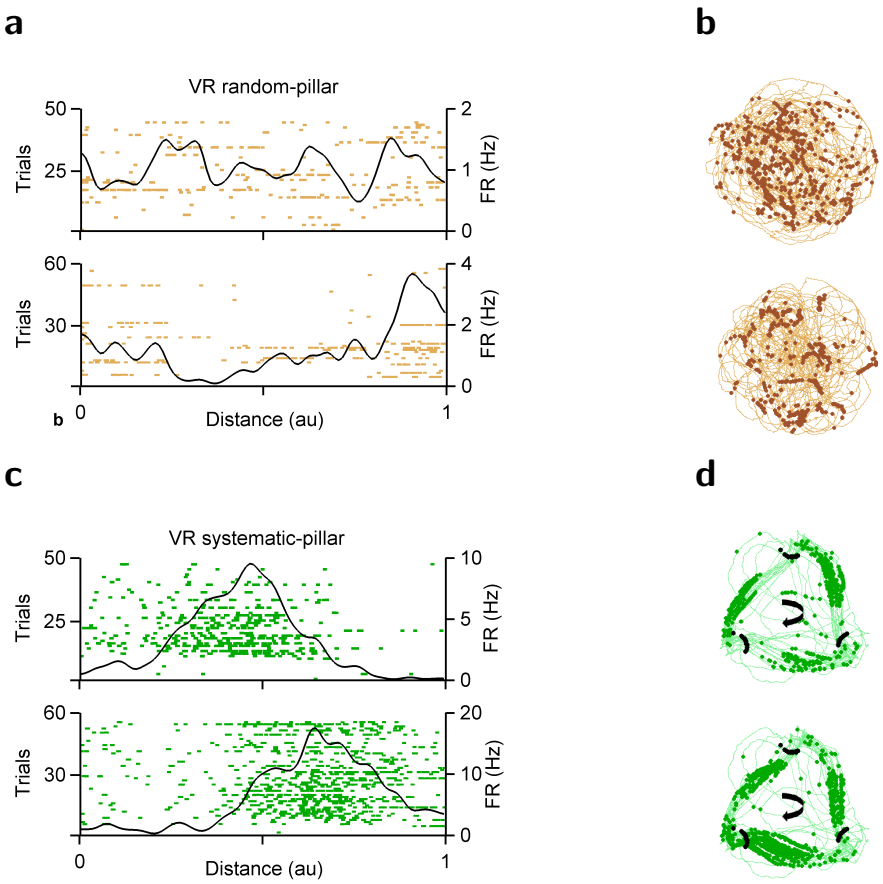

Figure 2.14: Selectivity to distance traveled in the VR goal-directed tasks at the neuronal level. (a), **(c)** Firing rate of cells as a function of normalized distance traveled across trials. **(b)**, **(d)** Trajectory of the rat (light brown,green) and spike positions (dark brown,green) during the VR random- and systematic- pillar tasks for the same cells shown in Figure 2.14a). The black dots indicate the reward locations and the arrows correspond to running direction.

In the random-pillar task many, but not all, neurons exhibited random firing both on linearized paths and in the two-dimensional space (Figure 2.14a, 2.14b). In contrast, a majority of neurons in the systematic-pillar tasks often fired at the same distance (Figure 2.14c, 2.14d). Linearized ratemaps in the random-pillar tasks had lower information content(49%, Figure 2.15a), sparsity(36%, Figure

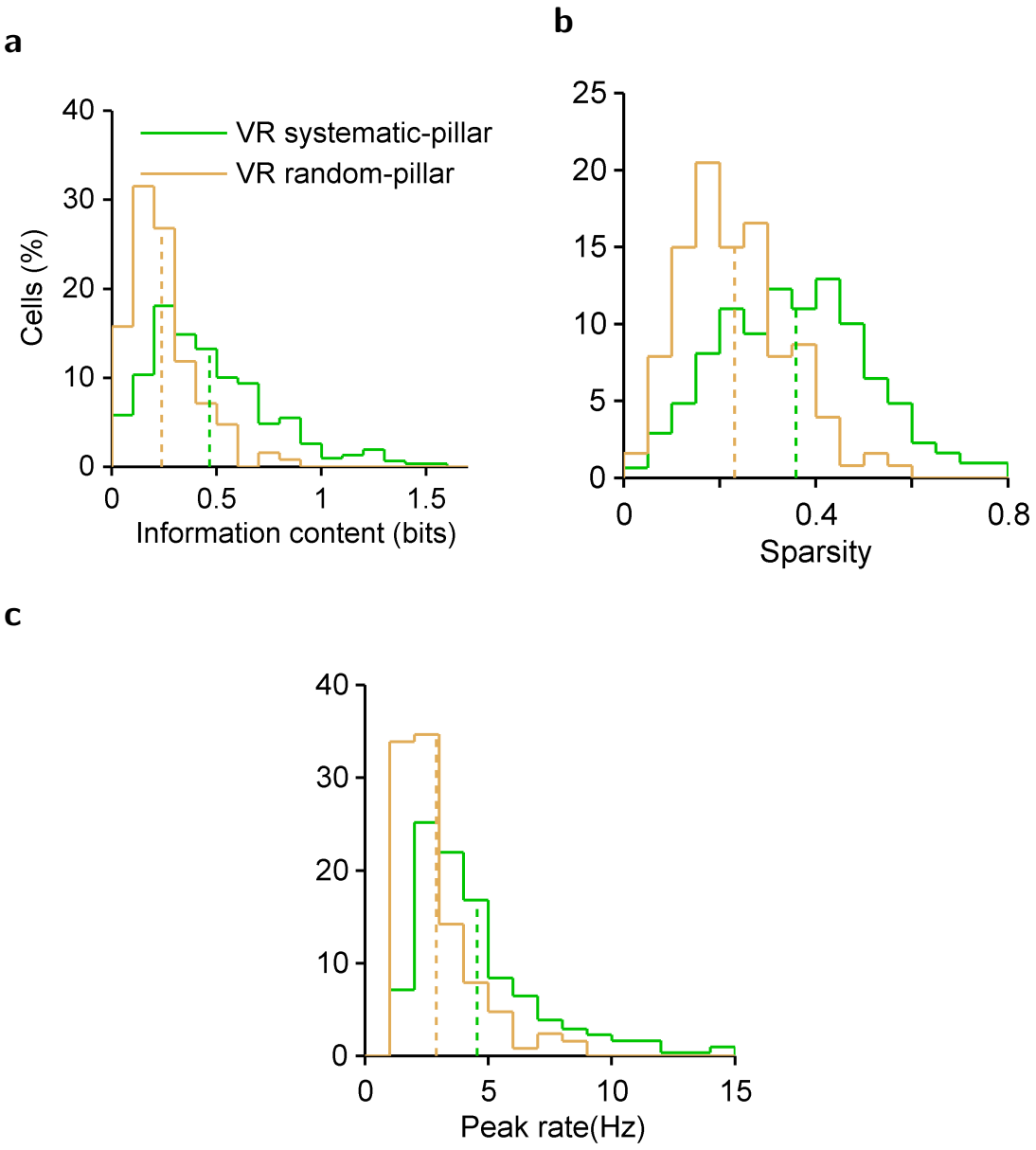

Figure 2.15: Firing properties of neurons with distance selectivity. (a) Information content in linearized paths in VR random-pillar task ($0.24 \pm 0.01 bits, n = 127$ cells from 3 rats) was significantly lower ($49\%, p = 1.2 \pm 10^{17}$) than in VR systematic-pillar ($0.47 \pm 0.02 bits, n = 310$ cells from 3 rats). **(b)** Sparsity of the linearized firing ratemaps in VR random-pillar (0.23 ± 0.01) was significantly reduced ($36\%, p = 5.9 \times 10^{16}$) compared to VR systematic-pillar (0.36 ± 0.01). **(c)** Peak firing rates were 36% ($p = 3.1 \times 10^{15}$) smaller in VR random-pillar ($2.89 \pm 0.14 Hz$) compared to VR systematic-pillar ($4.55 \pm 0.15 Hz$).

2.15b), and peak rate (36%, Figure 2.15c) compared to the systematic-pillar task, though a small number of neurons in the random-pillar task had measures comparable to those in the systematic-pillar task. We further characterized this selectivity on a population level by computing the population vector overlap (PVO) between the firing rates of two groups of randomly selected paths for each cell (see Methods). While the significant overlap in the random-pillar task was limited to regions near the beginning and end of trials, it was present at all distances in the systematic-pillar tasks (Figure 2.16).

Additionally, we tested if the neurons spiked at the same distance on two different arms of the triangle, located in different parts of the maze. We quantified the number of cells that fired on multiple arms by calculating the arm selectivity index (Figure 2.17a, see Methods). For cells that were active on multiple arms ($index < 0.5$), which constituted a majority, PVO analysis between the two arms' ratemaps revealed significant overlap at all distances indicative of a robust disto-code, notably on non-overlapping paths (Figure 2.17a, 2.17b). These results, together with the differences in two-dimensional spatial selectivity presented above, suggest that repeated traversals along the same path, such as in the systematic-pillar task, are crucial for generating robust spatial selectivity and selectivity to distance, a generalization of the disto-code.

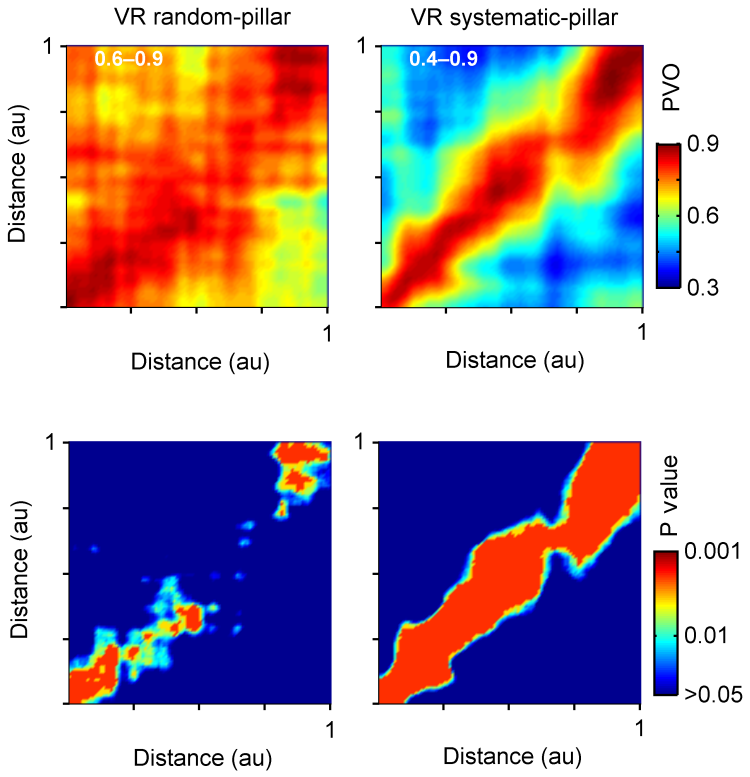

Figure 2.16: Selectivity to distance traveled in the VR goal-directed tasks at the neuronal level. PVO in VR random-pillar (top left) and VR systematic-pillar (top right). The range of overlap is indicated by the numbers at the top left corners. The bottom row depicts the significance levels for the corresponding PVO presented in the top row. The significant diagonal indicates selectivity to distance on an ensemble level.

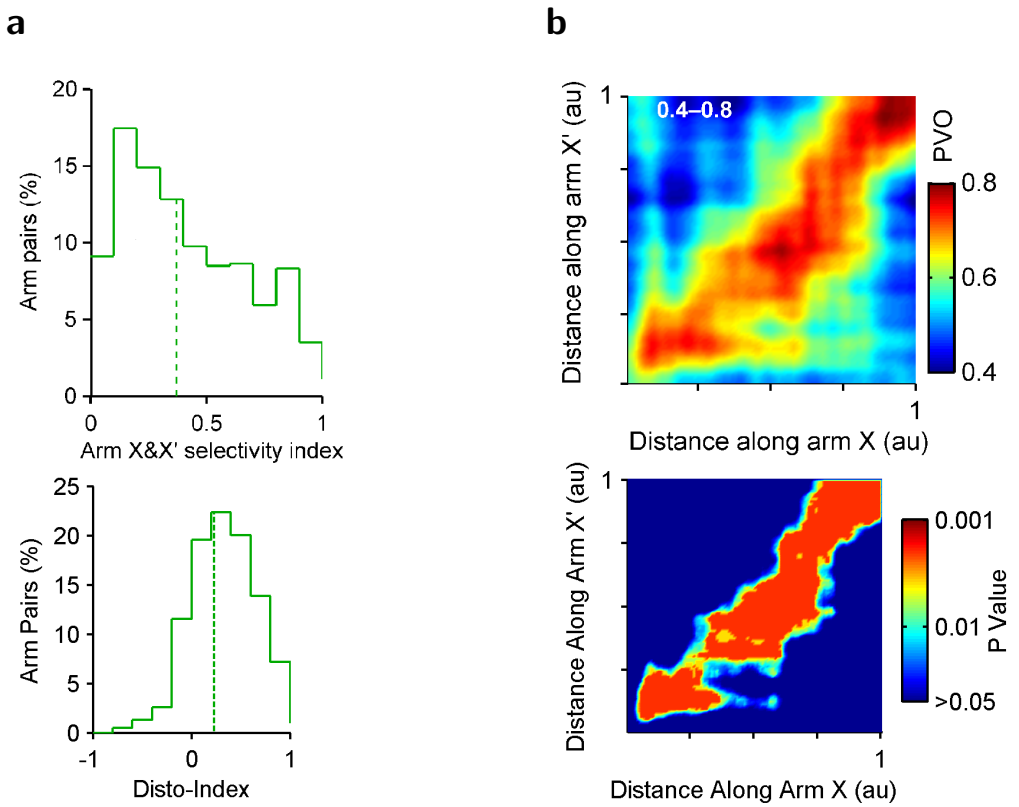

Figure 2.17: Selectivity to distance traveled in the VR goal-directed tasks at the neuronal level. (a) Top) For different arm pairs with minimal activity on at least one arm ($meanrate > 0.5Hz, n = 625$ from 3 rats), the arm selectivity index (0.37 ± 0.01) quantifies the likelihood of firing on one arm ($index > 0.5$) versus on multiple arms ($index \leq 0.5$). Bottom) Disto-coding index (see Methods) for the population of multi-arm selective arm pairs (n = 431) in the three-pillar task was also significantly positive ($0.23 \pm 0.02, p = 1.5 \times 10^{-31}$), further supportive of a disto-code. **(b)** PVO for arm pairs with arm selectivity index below 0.5 (top, n=431 from 3 rats) and the significance levels (bottom).

2.4.3 Hippocampal motifs and phase precession

In RW, neurons generated long spike-sequences lasting about two seconds as rats traversed through well-defined place fields (Figure 2.18a,2.3a).

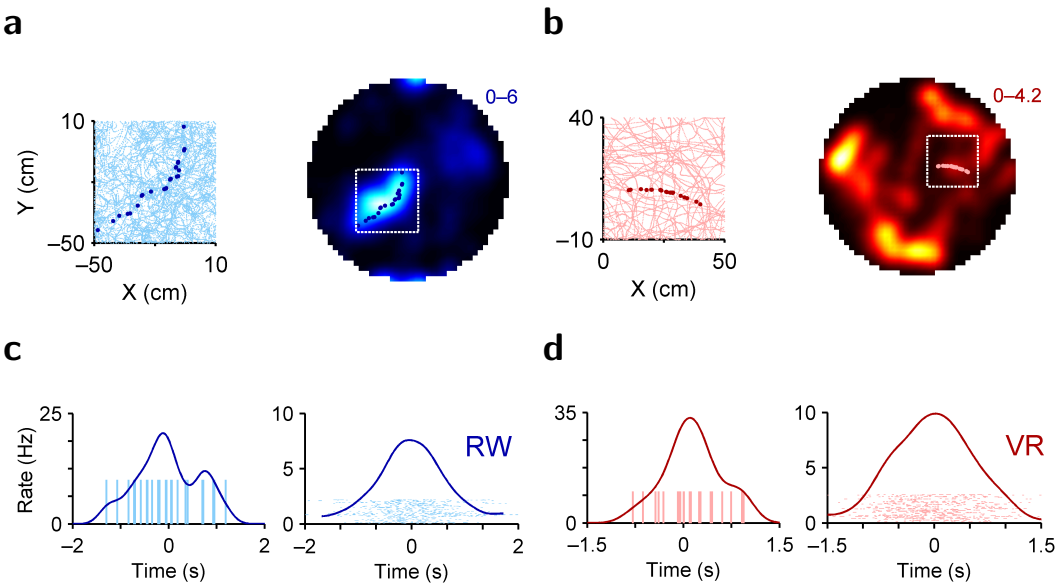

Figure 2.18: Hippocampal motifs and motif-fields. (a), **(b)** Spike positions of an example motif from a cell overlaid on a segment of the rats trajectory (left) and firing ratemap (right) in RW and VR. **(c)**, **(d)** Left) Motif firing rate as a function of time and individual spike times (vertical lines) for the same motifs as in 2.18a and 2.18b respectively. Right: Motif-field firing rate as a function of time. Spikes from individual motifs are depicted in the raster plot, aligned around motifs centers of mass to form the motif-field. In other words, each row represents an individual pass through the motif-field.

Surprisingly, despite having no clearly defined place fields, neurons in VR also fired similarly long spike-sequences, appearing as streaks of spikes (Figure 2.18b,2.3b). We term these long spike- sequences ***hippocampal motifs*** identified as time periods in which a neuron achieved a peak firing rate of at least $5Hz$ and maintained a firing rate above 10% of that peak for at least $300ms$. All individual motifs from a cell were aligned around their center of mass and aggregated together to obtain the cell's ***motif-field*** (Figure 2.18c, see Methods).

Motif properties, including mean motif duration, fraction of spikes contained

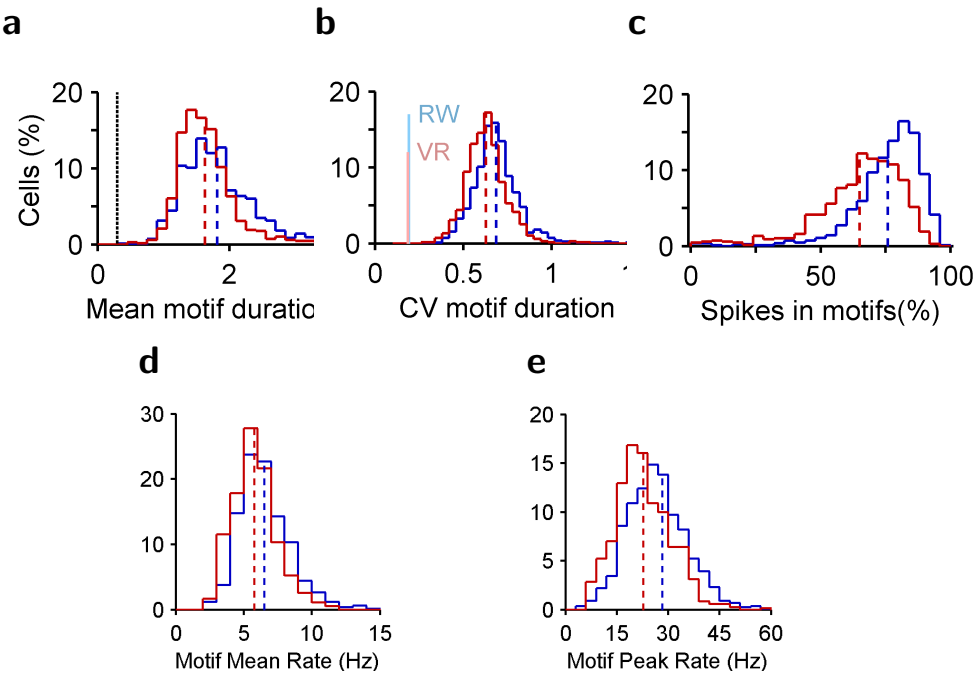

Figure 2.19: Similar hippocampal motifs in RW and VR (a) Mean motif durations of cells with at least five motifs (RW: 1064/1066 cells; VR: 911/914 cells = 719 cells (4 rats, VR random) + 195 cells (3 rats, VR random-pillar)) were comparable in RW ($1.82 \pm 0.02s$) and VR ($1.63 \pm 0.02s$) but slightly smaller in VR ($7\%, p = 2.2 \times 10^{12}$). The shortest allowed motif duration (dotted line) was much smaller than the ensemble average. **(b)** The coefficients of variation (CV) of motif durations within each cell were comparable in RW (0.69 ± 0.00) and VR (0.63 ± 0.01), but slightly lower in VR ($8\%, p = 5.7 \times 10^{20}$). Both were much greater than the CV of the distributions in the left panel (solid vertical lines). **(c)** Majority of spikes were contained within motifs (RW $75.90 \pm 0.47\%$; VR $64.99 \pm 0.63\%$) but there was a small reduction in VR ($14\%, p = 1.2 \times 10^{51}$). **(d)**, **(e)** Motif mean rates and peak rates in VR (mean $5.92 \pm 0.06Hz$; peak $23.39 \pm 0.24Hz$) were slightly smaller (mean $10\%, p = 7.7 \times 10^{-10}$; peak $21\%, p = 6.1 \times 10^{-21}$) than in RW (mean $6.52 \pm 0.06Hz$; peak $28.32 \pm 0.69Hz$).

in motifs, mean firing rate, and peak firing rate, were comparable in the two worlds (Figure 2.19a, 2.19c, 2.19d, 2.19e), and far greater than expected by chance, particularly when accounting for the lower mean rates in VR (Figure 2.20a, 2.20c,

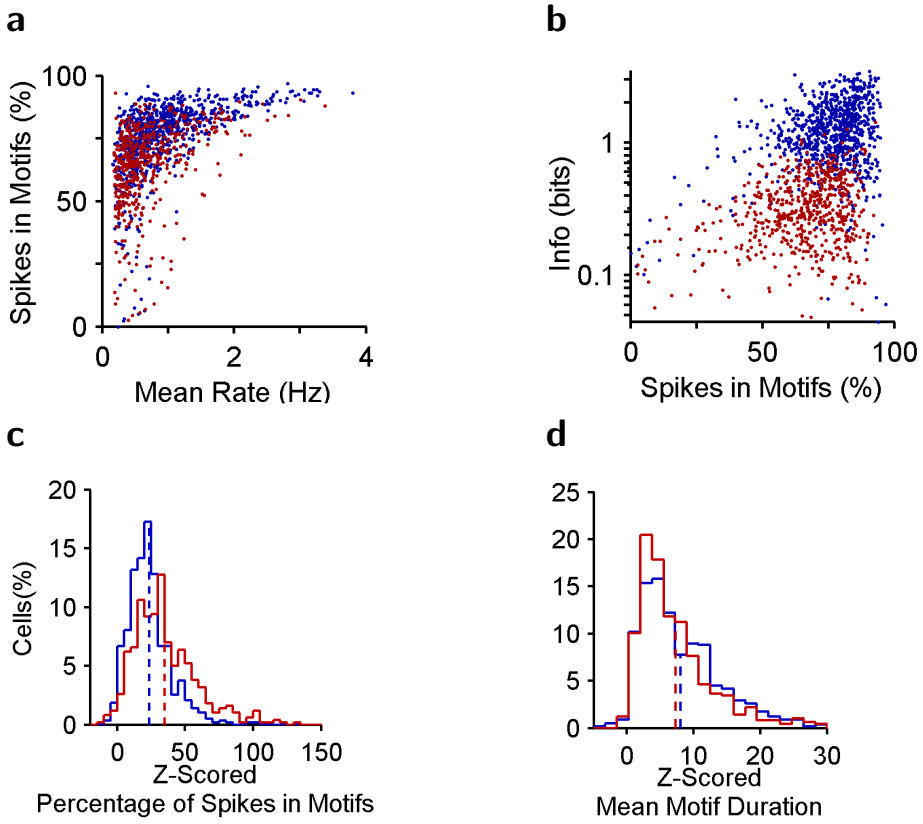

Figure 2.20: Relationship between mean firing rate, percentage of spikes within motifs and information content of a neuron. (a) Mean rate and percentage of spikes within motifs were significantly correlated (RW $r = 0.54, p = 4.1 \times 10^{-65}$; VR $r = 0.41, p = 1.2 \times 10^{-28}$). **(b)** The percentage of spikes in motifs was significantly correlated with spatial information content. (RW $r = 0.28, p = 4.2 \times 10^{-17}$; VR $r = 0.26, p = 6.5 \times 10^{-12}$) **(b)** Z-scored percentage of spikes in motifs was significantly above zero in VR ($35.15 \pm 1.06, p = 3.9 \times 10^{-83}$) and RW ($23.52 \pm 0.64, p = 1.0 \times 10^{-26}$) **(b)** Z-scored mean motif duration was similar in both worlds (RW 8.02 ± 0.25; VR $7.33 \pm 0.27, p = 0.03$) and above zero (RW $p = 2.1 \times 10^{-96}$; VR $p = 1.4 \times 10^{-83}$).

2.20d). In fact larger Z-scored values in VR indicate greater propensity for motif generation compared to RW. While for any given cell the motif durations were quite variable in either world, (Figure 2.19b), mean motif durations across all cells displayed small variability (Figure 2.19a). While the variability in motif durations

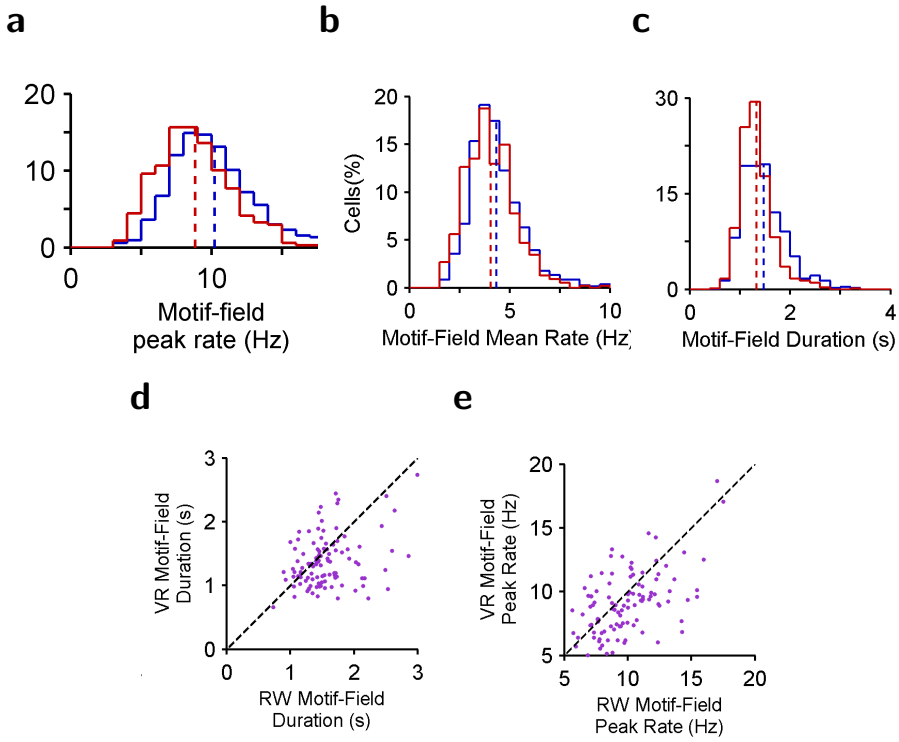

Figure 2.21: Similar hippocampal motif-fields in RW and VR (a) Peak firing rates of motif-fields in VR ($8.85 \pm 0.10Hz$) were only slightly smaller ($13\%, p = 2.1 \times 10^{17}$) than in RW ($10.22 \pm 0.11Hz$). **(b)** Motif-field mean firing rates in VR ($4.12 \pm 0.05Hz$) were only slightly smaller ($5\%, p = 9.2 \times 10^{-3}$) than in RW ($4.34 \pm 0.05Hz$). **(c)** Motif-field durations in VR ($1.33 \pm 0.01s$) were similar but slightly reduced ($10\%, p = 1.1 \times 10^{-12}$) compared to RW ($1.48 \pm 0.01s$). **(d)** For cells active in both worlds on the same day, motif-field duration was correlated between RW and VR ($r = 0.31, p = 1.2 \times 10^{-3}$). **(e)** Motif-field peak firing rate had a similar correlation ($r = 0.54, p = 1.2times10^{-9}$).

in RW could be due to a varying amount of time spent within the place field in each traversal, the motif durations were equally variable in VR (Figure 2.19b) with little spatial selectivity, suggestive of an intrinsic, network-wide mechanism for motif generation. Neurons with a larger fraction of spikes within motifs had greater information content (Figure 2.20b) and mean firing rates (Figure 2.20a), in contrast to the inverse correlation between information content and mean firing rate seen across all cells when all spikes were included (Figure 2.6a). Spiking within

motifs, as opposed to isolated spiking, may therefore serve to group otherwise random and non-informative spikes into more informative clusters. Additionally, the correlation between the percentage of spikes within motifs and mean firing rates (Figure 2.20a) could explain the reduced motif duration and percentage of spikes contained in motifs in VR compared to RW (2.19a–2.19c).

Analysis of motif-fields (Figure 2.18c, 2.18d) showed similar results, with motif-fields having similar durations, mean rates and peak rates in RW and VR (Figure 2.21a, 2.21b, 2.21c), in contrast to the smaller peak rates in spatial ratemaps in VR (Figure 2.4b). Neurons active in RW and VR on the same day also had motif-fields with similar durations and peak firing rates (Figure 2.21d, 2.21e).

In spite of the impaired rate code, do the motifs show a temporal code [14, 17, 32–34, 39]? Due to the absence of clear place fields in VR we quantified the quality of phase precession within motif-fields by computing the circular linear correlation (see Methods) between the time spent within the motif-field and the theta phase of spikes. In RW 80% of neurons showed significant phase precession within motif-fields (Figure 2.22a, 2.22b). This number was reduced to 40% in VR, but was still far greater than expected by chance (Figure 2.22a, 2.22b, see Methods). For cells with significant precession, the quality of precession was comparable in both worlds, although slightly reduced in VR (Figure 2.22b). For all cells, we also computed the difference between the period of theta modulation of spikes and the LFP theta period [6, 32, 34]. A majority of cells in RW (83%) and VR (78%) had longer LFP theta period than spike theta period, indicative of intact temporal coding in VR (Figure 2.22b). This is especially notable because LFP theta had greater peak theta power and reduced theta frequency in VR (Figure 2.23a). The preferred theta phase of neurons was also significantly different and more variable in VR compared to RW (Figure 2.23b), yet neurons showed similar degrees of theta phase locking in both worlds (Figure 2.23b).

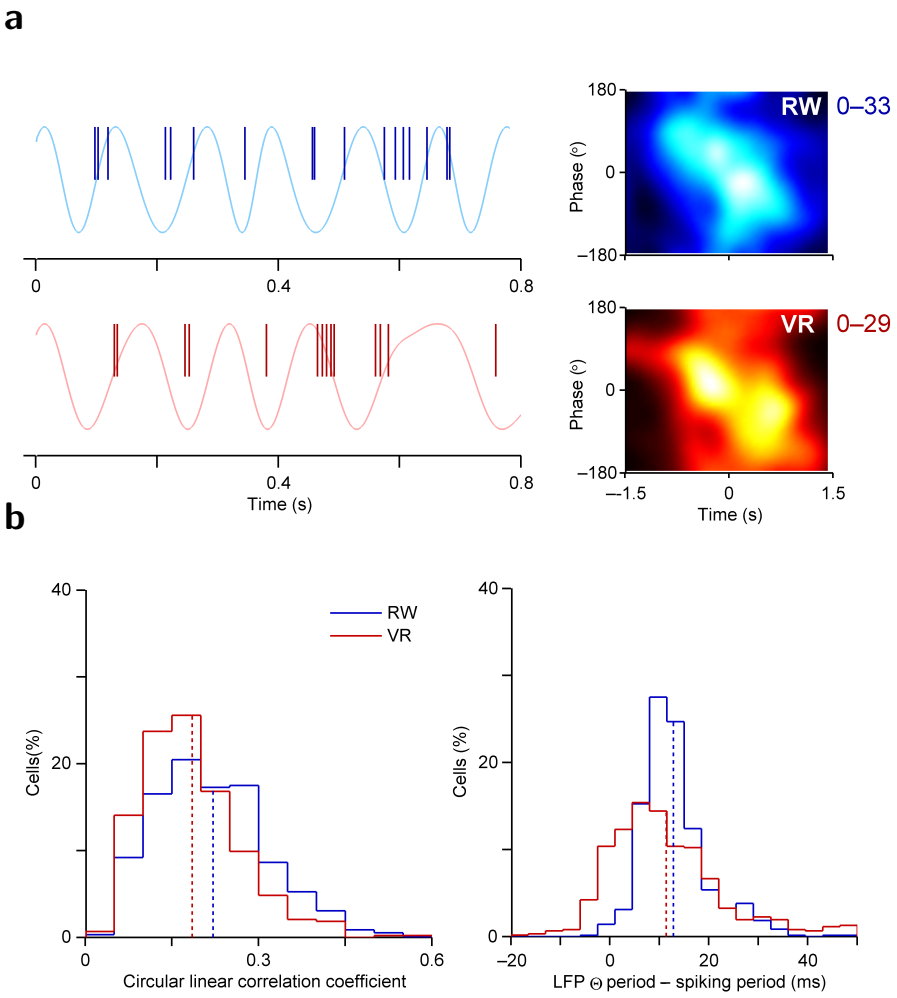

Figure 2.22: Intact phase precession in VR within motif fields. (a) Left) Sample LFP theta traces filtered in theta band $(4-12Hz)$ in RW (top) and VR (bottom) recorded from the same electrode on the same day. Spikes from the same cell (vertical lines) in RW and VR occur at earlier phases on subsequent theta cycles. Right) Motif-fields in RW and VR show clear phase precession. Lighter shades indicate higher values. **(b)** Left) 80.03% and 40.52% of the cells showed significant phase precession in RW and VR respectively. For these, the quality of phase precession in VR cells $(0.19 \pm 0.00, n = 365$ cells, 4 rats) was slightly reduced $(13\%, p = 1.9 \times 10^{11})$ compared to RW $(0.22 \pm 0.00, n = 852$ cells, 4 rats). Right) Difference in LFP theta period and spiking theta period, computed from the autocorrelation of LFP and of spikes shows comparable but reduced $(11\%, p = 4.6 \times 10^{9})$ and more variable temporal coding in VR $(11.38 \pm 0.46ms, mean \pm STD)$ compared to RW $(12.85 \pm 0.23ms, mean \pm STD)$.

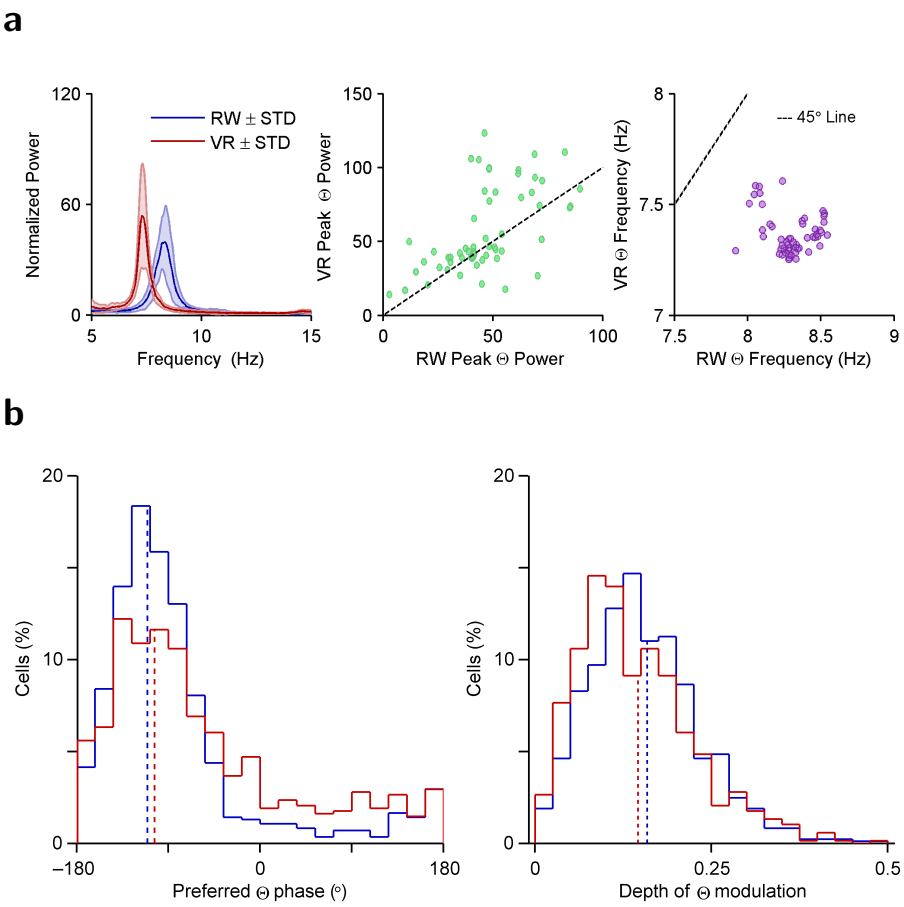

Figure 2.23: Increased Theta Power but Reduced Theta Frequency in VR. (a) Left) , Normalized power between $5 - 15Hz$, averaged over all the LFP ($n = 57$) in RW and VR shows a clear difference in theta power and frequency between the two environments. Center) Peak theta power is significantly increased ($p = 0.002$, paired Wilcoxon signed rank test) in VR (56.95 ± 3.75) compared to RW (46.61 ± 2.51). Right) Theta frequency in VR ($7.21 \pm 0.07Hz$) is significantly lower ($p = 5.1 \times 10^{-11}$) than in RW ($8.32 \pm 0.06Hz$). **(b)** Left) The preferred theta phase of spikes was shifted closer to theta peak ($6\%, p = 0.001$) in VR ($103.70 \pm 2.29°$) and was also more variable ($SD = 61.40°$) compared to RW ($110.58 \pm 1.72°, SD = 56.15°$). Right) The degree of phase locking (depth of modulation) was similar in VR (0.15 ± 0.09) and RW (0.16 ± 0.09), though slightly reduced ($8\%, p = 8.5 \times 10^5$) in VR.

2.5 Discussion

These results provide the first measurements of rodent hippocampal CA1 neuronal activity during random foraging in a two-dimensional body-fixed VR environment where only distal visual cues provide reliable spatial information. We found five key results: a profound loss of spatial selectivity during random foraging in VR; intact spatial selectivity when both location-specific locomotion cues and distal visual cues were repeatedly experienced together during the systematic-pillar tasks; weak but significant selectivity to distance traveled in the random-pillar task and strong distance selectivity in the systematic-pillar tasks; comparable motif dynamics in RW and VR; and intact temporal code within motif-fields in VR.

We speculate that the motif generation mechanisms are intrinsic to the entorhinal-hippocampal network because, unlike most afferent sensory cortices showing punctate neural responses, hippocampal neurons showed approximately 2s long sustained responses in both RW and VR, despite the absence of spatial selectivity in the latter. These sustained responses could enable the entorhinal-hippocampal system to predict the rat's future location based on recent experience [46] by exploiting the continuity of space and locomotion, thus reducing computational load.

The motif generation mechanism is likely network-wide rather than cell-specific since: the variability in motif durations on a population level is small compared to the individual neuronal level; motif-field properties are correlated between RW and VR; and theta-scale dynamics are intact in VR motif-fields. While previous studies have shown intact phase precession without a change in position-defining cues in a working memory task [16], our results demonstrate instead that phase precession can exist without a rate code when spatially informative cues are changing with minimal memory demand. Increased preferred theta phase variability could arise via a rate-phase transformation [33] and reduced excitatory drive in VR due to

a lack of repeatedly paired sensory and motor cues as described below. The underlying network mechanism could thus generate motif-like activity under a variety of conditions including hippocampal place cells in normal subjects [14, 17, 39] and in transgenic mice with taupathy [47], entorhinal cortical grid cells [6], episode or time cells during wheel or treadmill running [15, 16], neural activity during REM sleep [48], and neural activity during free recall in humans [49].

Motifs could originate from several parts of the entorhinal-hippocampal network. The recurrent CA3 network could generate motif-like activity, which might cause the observed approximately 2s delayed responses of the hippocampal ensemble activity pattern to sudden changes in visual cues [36]. Alternatively, the motifs could arise in the medial entorhinal cortex where neurons show motif-like activity lasting several seconds and robustly driving CA1, even in anesthetized or sleeping animals [35]. Accordingly, sustained spiking in consecutive theta cycles was reduced, indicative of diminished motifs, in a GluA1 transgenic mouse with diminished distal dendritic inputs which typically originate in the entorhinal cortex [50]. Motif-field durations could also be modulated by the temporal integration properties of the h-current [51] to generate a dorso-ventral gradient of field sizes.

Though intact motifs and phase precession are present in VR with distal visual cues alone, we found a large reduction in spatial selectivity during two-dimensional random foraging and random-pillar tasks in a body-fixed VR. This demonstrates that distal visual cues alone are not sufficient to generate spatially localized place fields [9, 19]. In contrast, spatial selectivity was present in the systematic-pillar tasks but not in the random-pillar task. While diminished vestibular cues during random foraging in VR might account for reduced spatial selectivity compared to during random foraging in RW, it is inconsistent with the presence of spatial selectivity in the systematic-pillar tasks where the nature of paths and resulting vestibular cues are similar to the random-pillar task. Further, vestibular lesions

caused significant behavioral deficits, reduction in theta power and unaltered peak firing rates [26, 52] all of which are in contrast to our data. These results suggest that the repeated pairing of cues, or lack thereof, as the key reason for the difference in two-dimensional spatial selectivity. The difference in spatial selectivity between the random-pillar and systematic-pillar tasks is also consistent with previous studies demonstrating that the precise nature of paths (random or systematic) can strongly impact the hippocampal spatial representation [11, 53].

While two-dimensional spatial selectivity was equally poor in the VR random foraging and random-pillar tasks, the beginning and end of trials were well defined for the rats in the latter, thus allowing the analysis of selectivity to distance traveled. Neurons in the random-pillar task showed a small but significant degree of selectivity to the beginning and end of trials. In the systematic-pillar task, when locomotion and visual cues were repeatedly paired, this selectivity was strengthened and extended to the middle of the paths. Restricting the analysis to cells that fired on at least two non-overlapping arms on the three-pillar task revealed that these cells exhibited a disto-code [14], which is a specific case of the more general distance selectivity observed in the goal-directed tasks.

We conjecture that repeated pairing of different streams of input could generate robust associations between them via rapid Hebbian synaptic plasticity resulting in stable spatial representations [54] and increased firing rates [33, 54, 55]. Under this model, during RW random foraging, distal visual cues are repeatedly paired with the same constellation of proximal cues at each location resulting in a place code. In contrast, in two-dimensional random foraging in VR with or without pillars, the distal visual cues are not repeatedly paired with any other cue, leading to a lack of spatial selectivity. In the systematic-pillar tasks or one-dimensional VR tracks, distal visual cues are repeatedly paired with locomotion cues to generate spatial selectivity. Neurons with stronger inputs from distal visual cues would exhibit a place code, while those with stronger inputs from locomotion cues would

exhibit a disto-code [14]. Further, the overall reduction in the number of sensory and motor cues that are systematically paired could contribute to the large reduction in neural activity in VR [14]. Alternatively, instead of pairing across multiple modalities, pairing in linear paths could potentially occur between adjacent elements within a repeated sequence of cues from a single modality. Consistently, systematic acceleration and deceleration at the beginning and end of the linearized paths in the random-pillar task could give rise to selectivity in those regions.

Although we characterized distance selectivity as a function of position along the path, neural firing might also be influenced by other factors. Selectivity near the end of the path could be driven by reward-expectancy or the pillar; selectivity near the beginning of the path might be modulated by the recent delivery of reward [56]. These salient episodes associated with entering or leaving a reward zone are present and repeated in all goal-directed tasks, which could result in selectivity to the beginning and ends of paths even in the random-pillar task. We speculate that these episodes might become linked together via Hebbian synaptic plasticity in the systematic-pillar task by the same mechanism discussed above, thus extending selectivity to the entire length of the path. Further studies are needed to fully determine the role of episodic memory in these tasks.

Our results may raise the concern that spatial selectivity is impaired during VR random foraging because the rats are not paying attention to the visual cues present in the VR. We find this unlikely for a number of reasons. First, rats in VR avoid the edges of the virtual table, which is only defined visually. Second, many neurons in the systematic-pillar tasks fire in only a small portion of one segment of the path, which is only differentiated from the other segments by the direction-specific constellation of distal visual cues. Further, in the same virtual maze apparatus with qualitatively similar visual cues the rats were able to navigate to a hidden reward zone from multiple starting locations, analogous to the water maze navigation task [43], showing that rats could see the stimuli and navigate

based on them. Further studies are needed to determine if the nature of spatial selectivity is altered in this task.

The repeated pairing model is compatible with many findings including: place cell remapping after a change in the relationship between locomotion cues and distal visual cues [11]; altered spatial selectivity after changes in distal [8, 9] or proximal cues [8,10,12,13,21,22]; and instability of place fields after maze cleaning between sessions [13]. In each of these cases place cells remap, but spatial selectivity remains intact, presumably because new associations are formed as cues are repeatedly paired in new configurations. It will be important in future studies to determine if different pairings are equally viable or if there is a hierarchy such that certain inputs are more or less effective at contributing to spatial selectivity.

In summary, internally generated and temporally coded motifs represent activity patterns on behavioral timescales, and are localized by the repeated experience of multiple location-specific sensory and motor cues. Some selectivity to distance traveled exists near the beginnings and ends of paths even in the absence of spatial selectivity, but repeated pairing strengthens this selectivity and extends it to the entire length of the path. The impaired spatial selectivity in rats in two-dimensional VR is similar to the weak spatial selectivity seen in human studies, where such pairings are absent as well. Recent studies show that a sufficiently large pool of hippocampal neurons can provide accurate spatial information despite impaired spatial selectivity in one-dimensional environments [50]; such a distributed coding mechanism might also allow rodents and humans to solve spatial tasks in two-dimensional VR. Our results suggest that in human and primate studies in VR repeated pairing of a rich variety of stimuli, especially between motor and visual cues, could enhance neural activity and spatial selectivity. These results bridge the gap between rodent and human studies by showing that distal visual cues alone are insufficient to generate robust spatial selectivity but even with an impaired rate code, temporally coded motifs are intact, likely generated

by intrinsic, network mechanisms.

CHAPTER 3

Visual cues determine hippocampal directional selectivity

3.1 Abstract

Hippocampal neurons show selectivity with respect to visual cues in primates, including humans, but this has never been found in rodents. To address this long-standing discrepancy, we measured hippocampal activity from rodents during two-dimensional random foraging in real world (RW). We found 25% of neurons exhibited significant directional modulation with respect to visual cues, contrary to long-held beliefs. To dissociate the contributions of visual and vestibular cues to directionality, we made similar measurements in virtual reality (VR) where only visual cues are informative. Here, we found significant directional modulation despite the severe loss of vestibular information, thus challenging prevailing theories of directionality. Changes in the amount of angular information in visual cues induced corresponding changes in head-directional modulation at the neuronal and population levels. Thus robust visual cues are sufficient for—and play a causal role in—generating directionally selective hippocampal responses. These results dissociate hippocampal directional and spatial selectivity and bridge the gap between primate and rodent studies.

3.2 Introduction

The hippocampus has been implicated in navigation, for which both spatial and directional information are necessary. Hippocampal spatial selectivity has been well established and the underlying mechanisms extensively studied [4, 19, 57]. However, rodent hippocampal neurons are commonly believed to have no directional selectivity in two-dimensional mazes [57, 58]. This has led to a perplexing hypothesis that directional information is not available in the hippocampus but is instead provided by other parts of the brain, such as the head-direction nuclei. Further, the sensory mechanisms underlying directionality are debated, though vestibular and visual cues are thought to be crucial [11, 14, 59]. In addition, internal mechanisms also contribute to hippocampal activity [15, 16, 60, 61].

Visual cues strongly influence the spatial firing properties of hippocampal neurons [9,12]. For example, changes [12] and rotations [9] of visual cues cause remapping or rotation respectively of some place fields. Further, unlike two-dimensional mazes, on one-dimensional mazes hippocampal neurons exhibit strong directional selectivity [10,11,14,62]. The reasons for this disparity are unknown. Comparable levels of directionality exist on linear tracks in RW and in VR [14]—where the range of rotational vestibular inputs is minimal and visual cues are the only directionally informative cues—suggesting that visual cues also support directionality in one dimension. In addition, selectivity to the visual cue towards which the animal's head is facing, referred to as spatial-view, has been reported in humans [29], primates [37, 63] and bats [64]. However, response to specific features of visual cues has not been observed in rodents, and spatial selectivity persists in darkness, leading to the notion that in these animals visual cues merely provide a context for hippocampal activity.

In parallel, vestibular inputs are crucial to the head-direction system, which is thought to provide directional information to the hippocampus. Consistently,

vestibular lesions disrupt hippocampal spatial selectivity [26], although lesions in the head-direction system do not [27]. Some studies have attributed directionality in two dimensions to vestibular-derived self-motion information [59], [11], [65], but no study has directly measured hippocampal head-directional modulation when vestibular-based signals are impaired.

Thus, the mechanisms governing hippocampal directional activity in rodents are unclear. We hypothesize that visual cues directly influence the activity of rodent hippocampal neurons to generate angular tuning whereas vestibular cues are not required for directionality. This hypothesis is consistent with primate studies and thus bridges a long standing gap between the rodent [57], [58] and primate literature [63], [37].

3.3 Methods

Methods Summary Materials and methods were similar to those formerly described (Section 2.3).

3.3.1 Subjects

Data were obtained from five adult male Long-Evans rats (350–400 g at the time of surgery) that were singly housed on a 12-hour light/dark cycle. The animals were water restricted (minimum of 30 mL/day) in order to increase motivation to perform the task, but allowed an unrestricted amount of sugar water reward during the task. Further, they were food restricted (minimum of 15 g/day) to maintain a stable body-weight. All experimental procedures were approved by the UCLA Chancellor's Animal Research Committee and in accordance with NIH approved protocols.

3.3.2 Surgery, electrophysiology and spike sorting

All the methods were analogous to procedures described previously (Section 2.3) [14, 60]. Rats with satisfactory behavioral performance were anesthetized using isoflurane and implanted with custom-made hyperdrives with approximately 22 independently adjustable tetrodes. Both left and right dorsal CA1 were targeted. After recovery from surgery, tetrodes were gradually lowered to area CA1, which was identified by the presence of sharpwave ripple complexes. Signals were recorded using a Neuralynx data acquisition system at a sampling rate of 40kHz. Spike extraction, spike sorting and single unit classification were done offline using custom software and according to methods described previously [14].

3.3.3 Random foraging tasks in visually rich RW and VR

These tasks were the same as previously described (Section 2.3.3.1) [60]. Briefly, in both RW and VR, a 100 cm radius elevated (50 cm above the floor) platform was located at the center of a $300cm \times 300cm$ room whose walls had distinct visual cues as depicted in Figure 3.1a (referred to as RW_{rich} and VR_{rich}). As commonly done, in RW, rats foraged for food rewards scattered randomly on the platform. In a visually similar VR environment, rats foraged for randomly located but hidden reward zones. Upon entry into reward zones, a white dot (20–30 cm radius) appeared and sugar water was dispensed through reward tubes. Data were collected from four rats in both RW_{rich} and VR_{rich}.

3.3.4 Random foraging in VR tasks with visual cue manipulations

Three rats ran in four visually different VR environments, all of which had the same platform as described above. The reward zone was marked by a small ($12.5cm$ radius) white disc only visible from a very short distance. Upon delivery of a reward, the reward zone moved to a new pseudorandom location on the

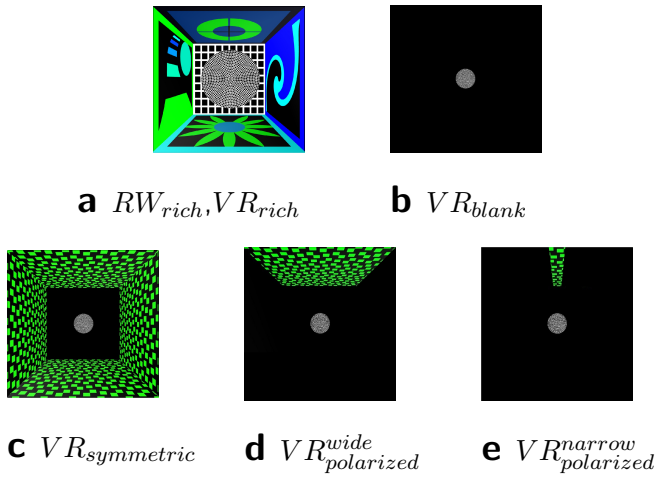

Figure 3.1: Top-view schematics of experimental rooms. The circular structure at the center represents a $200cm$ **diameter platform elevated** $50cm$ **above the ground in all panels. The size of the room in the rich conditions was** $300cm \times 300cm$**, and in all other cases** $900cm \times 900cm$

platform. Visible reward zones were used to ensure uniform coverage on the platform and to avoid any behavioral biases that might be caused by the changes in visual cues.

***VR*$_{blank}$** In the first experiment, all distal visual cues, including the walls and the floor were eliminated (VR_{blank}). The pattern on the platform was the only source of optic flow but provided no spatial or angular information (Figure 3.1b).

***VR*$_{symmetric}$** In the second experiment, four identical and angularly symmetric distal visual cues, positioned along the four virtual walls of the square room, $450cm$ away from the center of the platform were added to the VR_{blank} environment to generate $VR_{symmetric}$. Despite high spatial contrast (to maximize optic flow) the distal visual cues did not provide any angular information due to the angular symmetry and high spatial frequency of the pattern (Figure 3.1c). Further, the four walls were made infinitely tall to eliminate information about the corners.

The large distance of the cues from the center of the table ensured that the cues did not provide any spatial information. Additionally, in order to ensure that the details of the visual cues were visible to the rats, each element of the pattern was made such that at the farthest distance from the wall the size of the element was no smaller than 4° of visual field.

$\boldsymbol{VR^{wide}_{polarized}}$ In the third experiment, only one of the high contrast visual cues used for $VR_{symmetric}$ was placed $450cm$ from the center, creating a single wide polarizing cue which subtended a visual angle of 90° at the center ($VR^{wide}_{polarized}$) (Figure 3.1d). This task had three variations where the visual cue appeared either in the front, right or left of the subject at the beginning of the session. There was no quantitative difference between the data obtained in these variations (data not shown), and hence these data were combined .

$\boldsymbol{VR^{narrow}_{polarized}}$ In the fourth experiment, this visual cue was made narrower (11° visual angle) ($VR^{narrow}_{polarized}$) while maintaining the visual spatial frequency of its pattern, and placed at the same distance from the center as in $VR^{wide}_{polarized}$ (Figure 3.1e).

3.3.5 Statistics

All analyses were done offline using custom codes in MATLAB. Two-sided non-parametric Wilcoxon rank-sum test and Kuiper test were utilized to assess the significance between linear variables and circular variables respectively. For tests of distributions being different from zero, Wilcoxon signed-rank test was used. CircStat toolbox [44] was utilized to compute circular statistics. All values are expressed as $mean \pm s.e.m$ unless stated otherwise. To assess the significance of correlations between variables (reported as the linear correlation coefficient, r) a t-test was utilized.

3.3.6 Quantification of spatial and head-directional modulations using Generalized Linear Model

To quantify the influence of spatial and head-directional covariates on the firing of hippocampal neurons, and to minimize the influence of behavioral bias on spatial and angular selectivity estimates, we used a GLM framework [15, 66–68]. The time-varying spiking activity was modelled as an inhomogeneous Poisson process as a function of space and head-direction:

$$\lambda(t) = \frac{\lambda_{S+HD}(t)}{\tau} \tag{3.1}$$

$$\lambda_{S+HD}(t) = \lambda_{space}(t)\lambda_{headdirection}(t)\lambda_{constant} \tag{3.2}$$

$$\lambda_{space} = e^{H_S\beta_S} \tag{3.3}$$

$$\lambda_{headdirection} = e^{H_{HD}\beta_{HD}} \tag{3.4}$$

$$\lambda_{constant} = e^{\beta_0} \tag{3.5}$$

Where τ is the time bin size, λ is the intensity function, and S and HD denote space and head-direction respectively. H_S and H_{HD} refer to the design matrix associated with spatial and head-directional covariates and β_S and β_{HD} are the parameters associated with these matrices. Here β_0 is a constant and the exponentiation is done element-wise. We expressed basis functions for H_S in terms of the set of orthogonal two-dimensional Zernike polynomials and H_{HD} in terms of sines and cosines. Equation 3.3 and 3.4 can be expressed as follows:

$$\lambda_{space}(t) = exp(\Sigma_{l=0}^{L}\Sigma_{m=-l}^{l}\beta_{l,m}Z_l^m(\rho(t)\psi(t))) \tag{3.6}$$

$$\lambda_{headdirection}(t) = exp(\Sigma_{j=1}^{J}\beta_j sin(j\phi(t)) + \beta_j^{'} cos(j\phi(t))) \tag{3.7}$$

In Equation 3.6, Z_l^m denotes the m^{th} component of the l^{th}-order Zernike polynomial and $\rho(t)$ and $\psi(t)$ denote radial and angular components of position in polar coordinates. In Equation 3.7, $\phi(t)$ is the head-direction of the animal. The parameters of the model (βs) were estimated using the *GLM* function in MATLAB to maximize the likelihood of the model. Further, we used Bayes Information Criterion (BIC) for model selection. The number of the basis functions used for Equations 3.6 and 3.7 was chosen to minimize the following measure:

$$BIC = -2Ln(\widehat{L}) + kLn(n) \tag{3.8}$$

Where $\widehat{L}$ is the maximized value of the likelihood function of the model, k is the total number of parameters to be estimated across both space and head-direction, and n is the number of data points i.e. the length of the intensity function. For a majority of cases BIC chose the fifth order in the angle domain while this order was more variable in space domain. Hence, the number of angular basis functions was fixed at five. The number of spatial basis functions were allowed to vary and ranged from 5 to 32.

We then used the estimated parameters (βs) to reconstruct the modulation of the firing rate of neurons by spatial and head-directional covariates. For the reconstruction process and rendering purposes, we used $5 \times 5cm$ spatial bins and a total of 80 angular bins (although the resulting rates are independent of these parameters). The reconstructed rates can be expressed as follows:

$$\lambda_{space}(x_i, y_j) = exp(\Sigma_{l=0}^{L}\Sigma_{m=-l}^{l}\beta_{l,m} Z_l^m(x_i, y_j)) \tag{3.9}$$

$$\lambda_{headdirection}(\phi_k) = exp(\Sigma_{j=1}^{J}\beta_j sin(j\phi_k) + \beta_j^{'} cos(j\phi_k)) \tag{3.10}$$

where x_i,y_j,refer to the spatial bins and ϕ_k refer to head-direction bins, and βs are the estimated parameters from fitting. Thus, the spatial and angular modulation rates used in all the figures are defined as:

$$F_S = \alpha \times \frac{\lambda_S(x,y)}{\overline{\lambda_S}}, \text{where } \alpha = \frac{\lambda_{constant}\overline{\lambda_S \lambda_{HD}}}{\tau} \tag{3.11}$$

Here $\overline{\lambda_S}$ and $\overline{\lambda_{HD}}$ are the mean values of the spatial and head-directional reconstructed conditional intensity functions. To avoid artifacts, data from periods of immobility (running speed $< 5cms^{-1}$) were discarded. During rate map reconstruction, bins with low occupancy time were excluded.

3.3.7 Measures of selectivity

To quantify the degree of spatial and head-directional modulations we computed spatial and angular sparsity together with the mean vector length of the angular rate map. Sparsity of a rate map given N bins and r_n as the rate in the n^{th} bin is defined as:

$$S = 1 - \frac{1}{N}\frac{(\Sigma_n^N r_n)^2}{\Sigma_n^N r_n^2} \tag{3.12}$$

For firing rates as a function of head-direction, the mean vector length was computed as:

$$MVL = abs(\frac{\Sigma_n^N r_n e^{-i\theta_n}}{\Sigma_n^N r_n}) \tag{3.13}$$

where θ_n and r_n are the angle and rate in the n^{th} circular bin respectively. Both of these measures are invariant to any constant scaling factor in the rates and hence remain unaffected by the normalization used when reconstructing rates using GLM framework.

3.3.8 Generation of surrogate data to validate the GLM method

Non-parametric generation of simulated place fields

To estimate the amount of angular modulation behavioral biases introduce into purely spatially modulated neurons, we generated surrogate data based on the firing rate maps of recorded neurons. Given a behavioral profile $B(t) = (B_{X(t)}, B_{Y(t)})$ and spatial firing rate map $F(X, Y)$, spike times were generated according to an inhomogeneous Poisson process with $F(B(t))$ as the rate parameter. Data generated in this manner were used in Figure 3.2b.

Parametric generation of simulated place fields

To verify the GLM framework accurately estimated the independent contribution of spatial and angular factors in determining spiking, we generated surrogate data with predetermined and variable degrees of spatial and angular modulation. For a surrogate place field centered at $(\overline{x}, \overline{y})$, with spatial variance σ_{XY}, preferred angular orientation $\overline{\phi}$ and angular variance σ_{ϕ}, the relative probability of firing for any (X, Y, ϕ) combination was defined as:

$$p(X, Y, \phi) = P_{XY}(X, Y) \times P_{\phi}(\phi) \tag{3.14}$$

$$P_{XY}(X, Y) = p_{XY}(X, Y) - min(p_{XY}(X, Y)) \tag{3.15}$$

$$p_{XY}(X, Y) = e^{-\frac{D_{XY}}{\sigma_{XY}}}, \qquad D_{XY} = \sqrt{(X - \overline{x})^2 + (Y - \overline{y})^2} \tag{3.16}$$

$$P_{\phi}(\phi) = p_{\phi}(\phi) - min(p_{\phi}(\phi)) \tag{3.17}$$

$$p_\phi(\phi) = e^{-\frac{D_\phi}{\sigma_\phi}}, \qquad D_\phi = angle(e^{i(\phi-\bar{\phi})})^2 \tag{3.18}$$

Where i is the imaginary number $\sqrt{-1}$.

Given a behavioral profile $B(t) = (B_X(t), B_Y(t), B_\phi(t))$ and desired mean firing rate μ, the absolute probability of firing is obtained by scaling the relative probability of firing (Equation 3.12) by a constant factor k:

$$P(X, Y, \phi) = k \times p(X, Y, \phi) \tag{3.19}$$

$$k = \frac{\mu}{E}, \qquad E = \int_{t=t_0}^{T} p(B(t))dt \tag{3.20}$$

Where t_0 indicates the start time of the session, and T indicates the end time of the session. Spike times are then generated according to an inhomogeneous Poisson process with $P(B(t))$ as the rate parameter. Surrogate data generated in this manner were used in Figures 3.2c and 3.2d.

3.3.9 Analysis of statistical significance of spatial and head-directional modulations

To assess the statistical significance of neural modulation by position and head-direction, we used a bootstrapping procedure, which does not assume a Gaussian distribution of the control data. Briefly, for each cell, spike trains were circularly shifted with respect to behavioral data by random amounts (10–100s) to obtain control data. This was repeated 60 times, and the spatial and head-directional modulations of the control data were quantified using spatial and directional sparsity of the resulting rate maps respectively. Sparsity was considered statistically significant at the 0.05 level if the sparsity constructed from the un-shifted spike train was greater than at least 95% (57 of 60) of the control data (one-tailed test).

This method ensured that the degree of angular and spatial modulation was uninfluenced by nonspecific parameters such as the duration of the recording session and the firing rate of a neuron.

To obtain estimates and 95% confidence intervals of the percentage of significantly modulated neurons, and to further characterize the levels of directional modulation across different conditions, we computed the likelihood of the data given a binomial model using the MATLAB function *binofit()*.

3.3.10 Quantification of multimodality of angular rate maps

To detect the number of peaks in angular rate maps, a method similar to detection of place fields [14] was used. First, all of the peaks with a minimum value of 50% of the global maximum were detected. For each peak, the boundaries were defined as the points at which rate drops below 50% of that peak for at least two angular bins.

3.3.11 Analysis of variance (ANOVA) for angular and spatial sparsity

Both angular and spatial sparsity were negatively correlated with the logarithm of the number of spikes a neuron fired in a session, and the mean firing rate (and hence the number of spikes) is different in RW and VR [60]. Therefore, to compare the angular and spatial sparsity of neurons in the RW_{rich} and VR_{rich} conditions, we implemented a Two-way ANOVA in MATLAB with recording condition (RW_{rich} or VR_{rich}) as a categorical predictor, and log_{10}(number of spikes) as a continuous predictor, of the sparsity. The p-values reported in Figures 3.9b and 3.10c are for the main effect of recording condition on sparsity.

3.3.12 Quantification of significance levels of preferred firing direction of neural ensemble

For the head-directionally modulated neurons, preferred direction was defined as the direction of maximum firing obtained from the angular rate maps. To estimate the significance levels of the population bias we used Rayleigh test for uniformity and circular V test to assess polarization towards a certain angle. To test the significance of the mean vector length of the ensemble, random angles between 0° and 360° were added to the preferred direction of the cells and the length of the mean vector was computed. This process was repeated 500 times and data exceeding the 95% of the control (shuffle) data was considered significant.

3.4 Results

3.4.1 Head-directional modulation is present in two-dimensional RW

To test these hypotheses we did a series of experiments and analyses. We first quantified hippocampal spatial and head-directional modulation from 1066 (in 32 recording sessions) active (defined as cells with minimum mean firing rate of 0.2 Hz and with at least a 100 spikes) dorsal CA1 pyramidal neurons (which were part of a previous study of hippocampal spatial selectivity (see 2) [60]). Rats randomly foraged for rewards on a two-dimensional platform in a RW environment which had rich distal visual cues and will henceforth be referred to as RW_{rich} (Figure 3.2a).

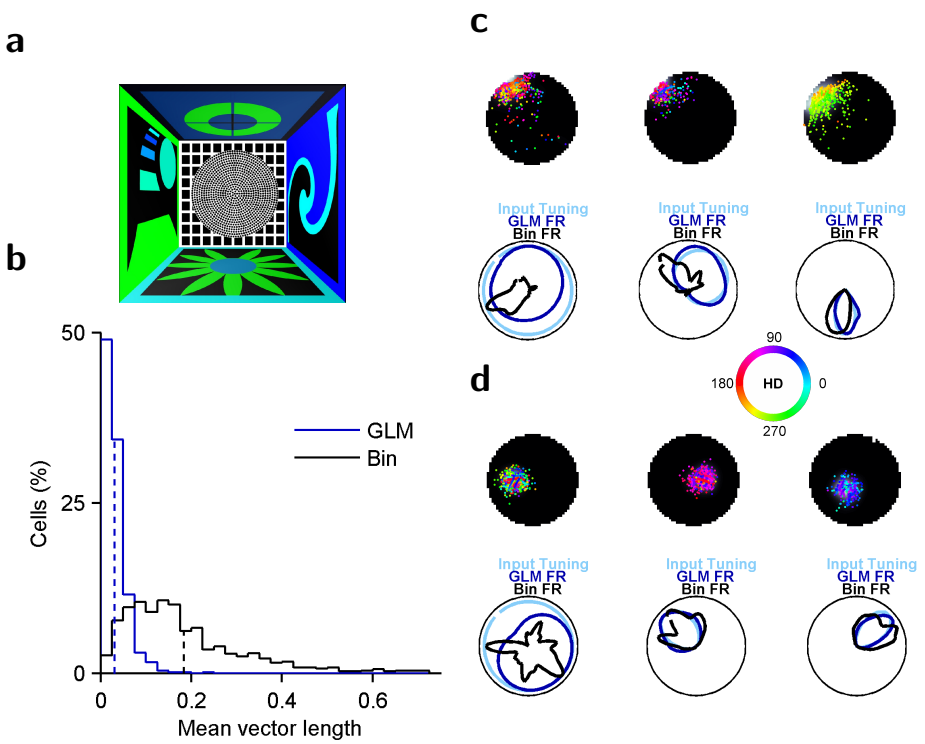

Figure 3.2: Comparison of GLM and binning methods using surrogate data. (a) Top-view schematic of the experiment room. **(b)**Surrogate data generated for each place cell with spatial modulation similar to experimental data but no angular modulation (see Methods) showed mean vector length obtained using the GLM method was close to zero (0.030.00, n=1066) and significantly (p=2.910-278) smaller (six-fold) than that computed using binning method (0.18 0.00). All values reported as $mean \pm s.e.m.$ **(c)**, **(d)** Example cells simulated with different widths and directions of input angular tuning. Top) Spatial firing rate of a simulated place field overlaid with colored dots representing the positions at which spikes occurred (color represents head-direction indicated by color-wheel inset). Bottom) Polar plots depicting the angular input function (light blue), binning method (black) and GLM (dark blue) based head-directional firing rates. Note similarity between input tuning (light blue) and GLM based rate estimate (dark blue) in all cases, unaffected by the behavioral bias, which affects the binning method.

A common technique for quantifying head-directional modulation is to divide the number of spikes in each direction bin by the total time spent in that bin

(Figure 3.2) [3]. However, when neurons have spatially tuned responses, as is the case for hippocampal neurons in RW, this method provides incorrect estimates of angular tuning [58]. For example, for a neuron with a place field at the edge of the maze, this method would yield an erroneous estimate of head-directional tuning due to non-uniform sampling of head angles within the place field (Figure 3.2c) [58]. Various methods have been developed to overcome this confound [11,65,69]. Here, we adopted the well-established generalized linear model (GLM) approach (see Methods) [15, 66–68] which has several advantages. First, it provides an unbiased estimate of the simultaneous and independent contribution of spatial and head-directional modulation. Second, unlike other methods, head-directional modulation obtained with the GLM method is uninfluenced by behavioral biases within the place field as verified using surrogate data with predetermined levels of spatial and angular modulation (see Methods, Figure 3.2b). Finally, this method provides an estimate of the fine structure of the respective tuning curves.

This method revealed a surprising finding: many neurons exhibited clear modulation by the rat's head-direction (independent of the rat's body angle) in RW_{rich} (Figure 3.3, 3.6a, see Methods). Some neurons fired maximally for only one head-direction and minimally elsewhere (Figure 3.3a, 3.3b), while others showed a multimodal response (Figure 3.3c). The degree of head direction selectivity was assessed by computing the angular sparsity of head directional firing rate maps (see Methods). The statistical significance of head-directional modulation was assessed by bootstrapping methods; cells with angular sparsity greater than 95% confidence interval of the control data (for the same cell) were considered significantly modulated (see Methods).

This method showed that 27% of neurons in RW_{rich} exhibited significant head-directional modulation, which is comparable to that in many parts of the head-direction system, although the width of the angular tuning curves (full width at half maximum $101.90 \pm 3.35\,\text{deg}$) was wider [3, 70]. Different place fields of the

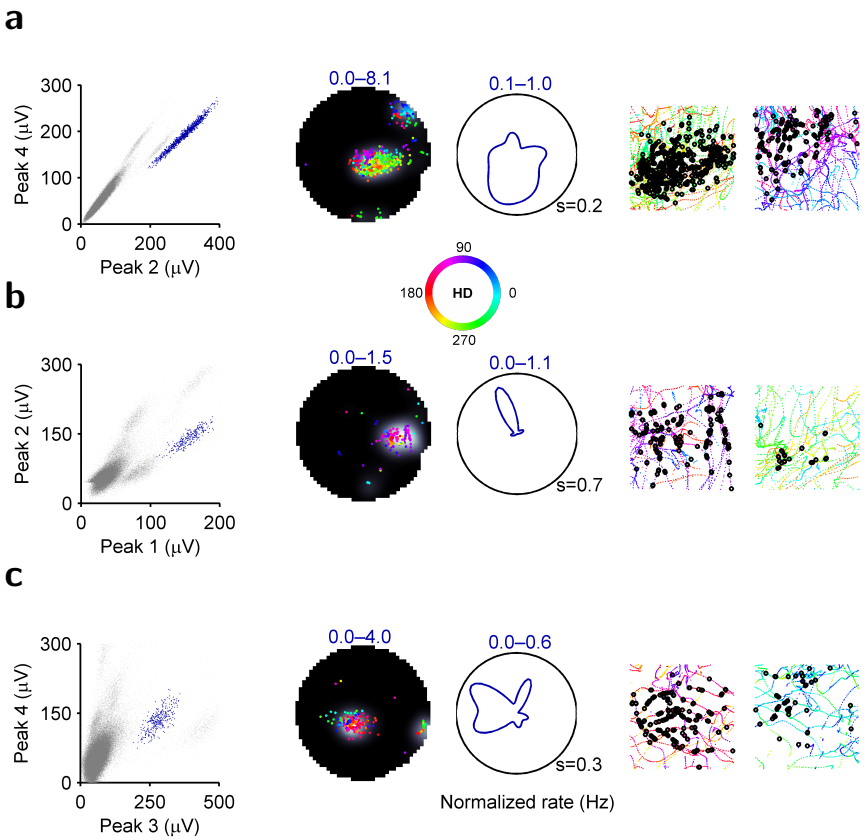

Figure 3.3: Presence of head-directional modulation in hippocampal pyramidal neurons in RW_{rich}. (a) Left) All unclustered (grey dots) and clustered spike amplitudes from an isolated neuron (blue dots) on two different channels of a tetrode in RW_{rich}. Center) Spatial and angular rate maps of a cell. Numbers in color indicate range, here and throughout. Number at the bottom right of the polar plot is the sparsity of the angular rate map. Right) Rats color-coded trajectory and his position at the time of spikes (black circles) for movement in the direction of maximal (left) and minimal (right) firing respectively. **(b)**,**(c)** Same as **(a)** for two other cells in RW_{rich}. All rate maps were computed using the GLM method here and throughout unless otherwise noted. All cells in this figure showed significant angular modulation as verified through bootstrapping methods (see Methods).

same neuron—with multiple fields—exhibited different levels of directional tunings (Figure 3.4) suggesting that directionality was a property of a place field, not

of a neuron. This is also reminiscent of the results observed in double rotation

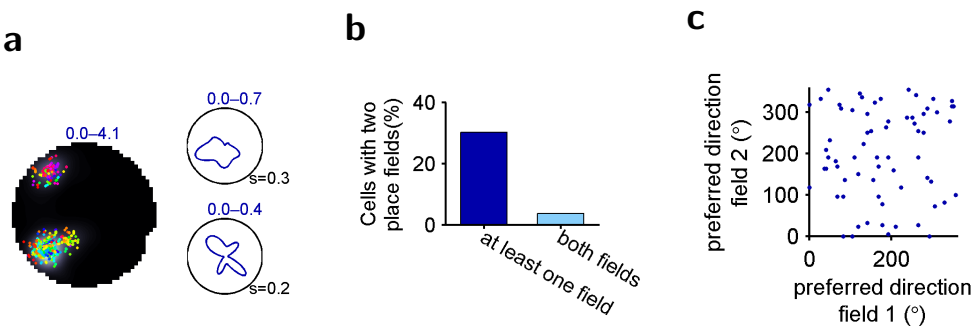

Figure 3.4: Different place fields of the same neurons in RW had uncorrelated directional properties. (**a**) Left) An example cell with two identified place fields. Right) The angular rate map for each field showing one field with significant angular modulation (top) and the other field with no angular modulation (bottom). (**b**) Different place fields of the same neuron (n=138) exhibited different directional properties. For 30, [22, 38]% of cells, at least one field exhibited significant angular modulation, but only for 4, [1, 8]% of neurons, both fields were significantly directionally modulated. (**c**) The preferred firing direction of different place fields of a neuron were not significantly correlated ($r = 0.03$, $p = 0.7$).

experiments where different fields of the same neuron respond differently to the rotation of certain cues [22]. These results show that rodent hippocampal neurons in RW indeed show significant head-directional modulation during two-dimensional random foraging, contrary to previous reports.

3.4.2 Robust vestibular cues are not required for hippocampal directionality

The above results raise an important question: which sensory inputs could generate the head-directional modulation in our data? Two likely candidates are the visual and vestibular modalities. To dissociate the two, we measured the ac-

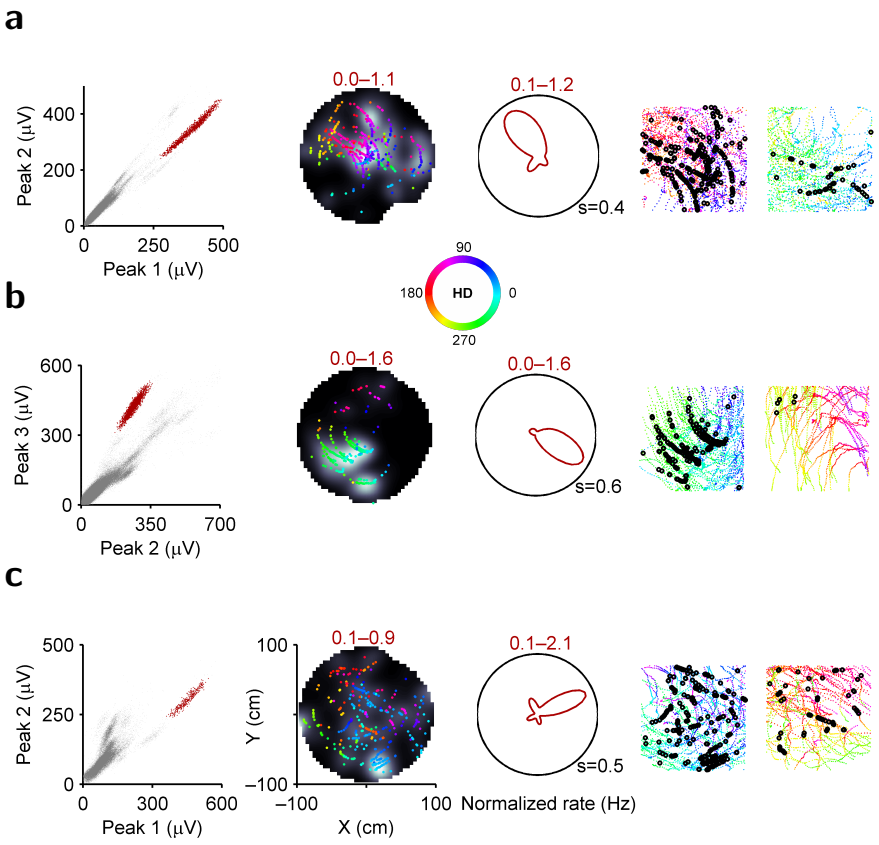

Figure 3.5: Presence of head-directional modulation in hippocampal pyramidal neurons in VR_{rich}. (a)–(c) Three well-isolated neurons showing significant head-directional modulation in VR_{rich} (same conventions as in Figure 3.3). All cells in these three panels showed significant angular modulation as verified through bootstrapping methods (see Methods).

tivity of 719 (37 recording sessions) active dorsal hippocampal CA1 pyramidal neurons [60] during the same random foraging task in a two-dimensional VR environment (VR_{rich}). Here, the distal visual cues were identical to those in RW_{rich}, but the range of vestibular cues was minimized due to body fixation [43]. Despite impaired spatial selectivity [60], many neurons showed clear modulation by the direction of the rat's head with respect to the distal visual cues, which will be henceforth referred to as ***head-direction*** (Figure 3.5, 3.6b).

The observation that head-directional modulation was present in VR—where

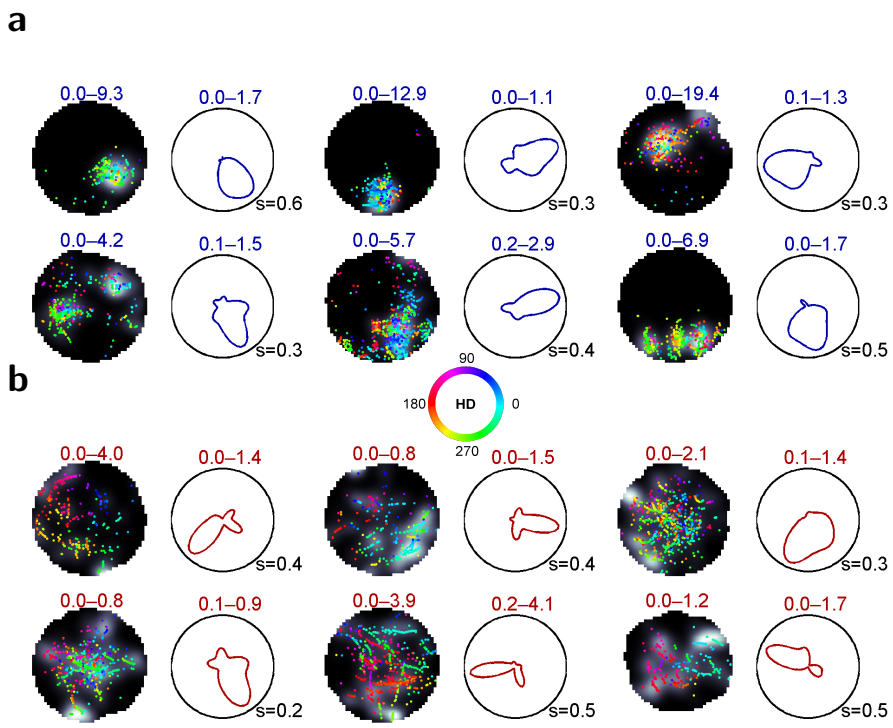

Figure 3.6: Sample cells in RW_{rich} and VR_{rich} with significant head-directional modulation. (a)–(b) Spatial rate maps (grey scale, numbers indicate range) and spike positions (dots color-coded according to the head-directions) and head-directional firing rate (numbers in color indicate range, number at bottom right is angular sparsity of the angular rate map) of nine example cells in RW_{rich} **(a)** and VR_{rich}**(b)**. All cells in these panels showed significant angular modulation as shown by the bootstrapping method (see Methods).

the range of vestibular cues is minimized (Figure 3.7)—suggests that vestibular cues are not required for hippocampal head-directional modulation. In fact, the angular speed—a good measure of the strength of vestibular inputs—at the time of occurrence of spikes had no effect on the fraction of significantly modulated neurons in not only VR but also RW (Figure 3.7).

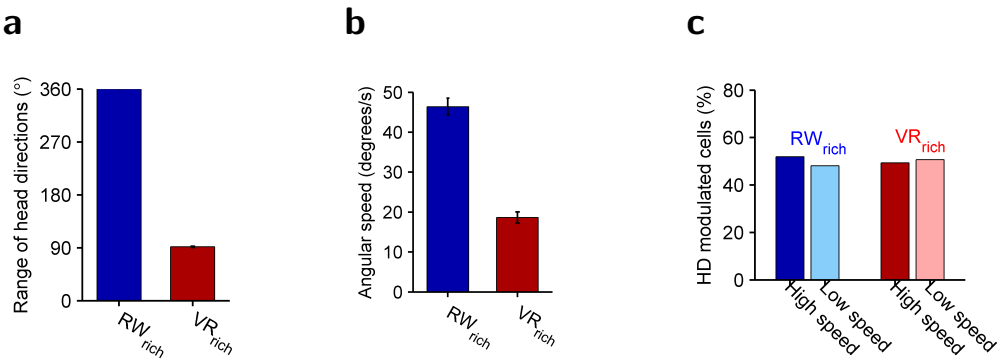

Figure 3.7: Directional modulation was independent of angular speed and range of vestibular inputs. (a) For 32 (37) sessions in RW (VR), the range of head-directions with respect to the experimental room in RW $(359.99 \pm 0.00\,\mathrm{deg})$ was significantly higher than that in VR $(91.67 \pm 0.93\,\mathrm{deg}, p = 2.2 \times 10^{21})$. **(b)** Angular speed in VR $(18.63 \pm 1.37 deg/s, n = 37 sessions)$ was significantly reduced $(60\%, p = 3.6 \times 10^{11})$ compared to RW sessions $(46.40 \pm 2.12 deg/s, n = 32 sessions)$. **(c)** For each neuron, the average angular speed at the time of occurrence of spikes was computed. This value was then used to classify a neuron into either high or low angular speed category, compared to the mean angular speed in RW $(49.60 deg/s)$ and VR $(19.91 deg/s)$. Nearly equal proportions of directionally modulated cells in RW $51.88\%(47.12\%)$ and in VR $49.32\%(50.68\%)$ belonged to the high (low) speed categories respectively.

Indeed, a similar fraction of neurons showed significant head-directional modulation in VR_{rich} (23%) and RW_{rich} (27%, Figure 3.8a).

These results are different from findings in the head-direction nuclei that require robust vestibular cues to generate directional selectivity [3]. Additionally, neurons in VR_{rich} also had multimodal responses like in RW_{rich}, unlike neurons in the head-direction network which have unimodal responses [71].

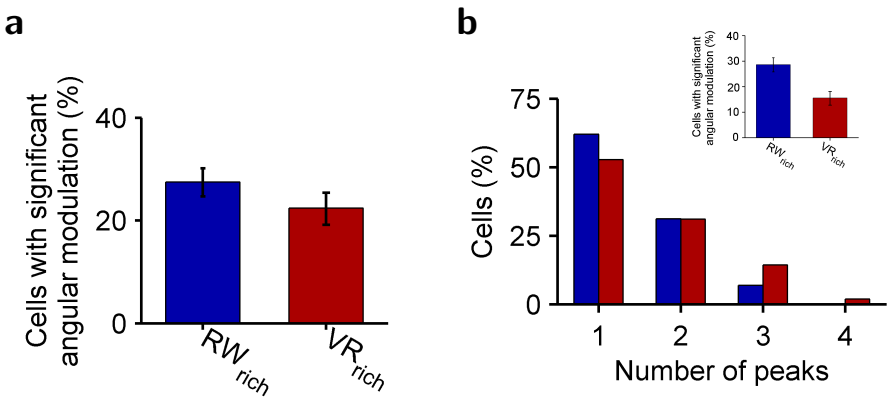

Figure 3.8: (a) The population of neurons in VR_{rich} (red, n=719; 37 sessions) and RW_{rich} (blue, n=1066; 32 sessions) had comparable proportions of cells with statistically significant angular sparsity; 27, [25, 30]% (23, [19, 26]%) of cells in RW_{rich} (VR_{rich}) showed significant head-directional modulation (see Methods). See also Figure S5. **(b)** Head-directionally modulated neurons in VR_{rich} were significantly more multimodal $(1.650.06peaks, p = 1.410 - 2)$ than RW_{rich} cells $(1.450.04peaks)$. **(Inset)** This was reflected at the ensemble level where a smaller proportion of neurons in VR_{rich} (15, [13, 18]%) had significant head-directional modulation using mean vector length compared to angular sparsity (23, [19, 26]%). In RW_{rich} 29, [26, 31]% of neurons showed significant directional modulation using mean vector length.

The multimodality was greater in VR_{rich} than RW_{rich}(Figure 3.8b) which could account for the slightly lower proportion of cells with a significantly large mean vector length in the former (Figure 3.8b inset, Table 3.1). This observation motivates the use of sparsity as a measure for angular selectivity.

HD modulated cells %	**Unimodal** Z_s, Z_{MVL}	**Multimodal** Z_s, Z_{MVL}
RW	40, 44	18, 13
VR	36, 32	20, 7

Table 3.1: **Unreliability of mean vector length in determining directional modulation of multimodal angular rate maps**

Additionally, the width of the angular tuning curves in VR_{rich} (85.41±4.23 deg) was significantly ($16\%, p = 5.13 \times 10^4$) sharper than in RW_{rich}. Further, directionally tuned neurons had greater mean firing rates than the untuned neurons in VR_{rich} (Figure 3.9a) but not in RW_{rich} (103.10 ± 3.50 deg).

Notably, angular sparsity strongly depends on the logarithm of number of spikes generated by a neuron (Figure 3.9b). When accounting for the differences in number of spikes across conditions, there was no significant difference in the angular sparsity of the ensemble of neurons between VR and RW (p=0.09, Two-way ANOVA, see Methods).

We then quantified the spatial modulation of neural responses in both RW_{rich} and VR_{rich} using the rate maps obtained from the GLM method. We found a large proportion of cells with significant spatial selectivity in RW_{rich} but not in VR_{rich} (Figure 3.10a), consistent with previous results obtained using the binning method [60]. Although comparable proportions of cells had significant head-directional modulation, this was not the case for spatial modulation, which suggests a decoupling of the mechanisms of spatial and directional tuning. Consistently, the presence or absence of head-directional modulation had no effect on the percentage of spatially modulated neurons in both RW_{rich} and VR_{rich} (Figure 3.10a). Further, spatial sparsity too depended strongly on the logarithm of number of spikes generated by a neuron (Figure 3.10c). When this was taken into account there was a significant difference between the spatial sparsity of rate

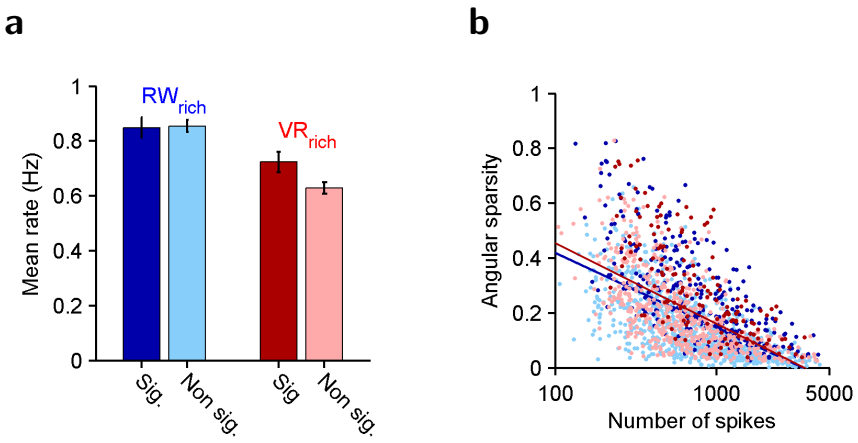

Figure 3.9: Comparison of mean activity of neurons with or without significant directional modulation in RW_{rich} and VR_{rich} conditions. (a) Mean firing rate of head-directionally modulated neurons in RW_{rich} (0.85 ± 0.04 Hz, n=293; dark blue) was similar to that of those with no significant modulation (0.85 ± 0.02 Hz, n=773 p=0.6; light blue). In contrast, in VR_{rich}, significantly head-directionally modulated neurons had higher mean rates (0.72 ± 0.04 Hz, n=162; dark red) compared to those with no modulation (0.63 ± 0.02 Hz, n=557, $p = 5.1 \times 10^{3}$; light red). **(b)** The sparsity of angular ratemaps were significantly negatively correlated with the (logarithm of) number of spikes in both RW_{rich} (r=-0.59, $p = 1.4 \times 10^{100}$) and VR_{rich} (r = -0.58, p=3.91065). However, accounting for the number of spikes, angular sparsity was not significantly different between the two conditions (p=0.09, Two-way ANOVA, see Methods).

maps between VR and RW ($p = 1.7 \times 10^{-6}$, Two-way ANOVA, see Methods)

3.4.3 Visual cues exert a causal influence on hippocampal directional responses

What other mechanism could generate angular modulation? Either it is internally generated [15, 16, 61] or driven by specific visual cues [37, 63]. To disambiguate these possibilities, we generated a virtual world where distal visual cues were entirely eliminated (VR_{blank}) (Figure 3.11a, see Methods). The circular platform in the virtual environment, which was the only visual cue present, provided optic flow information but had no spatial or angular information. The rats' behavior in

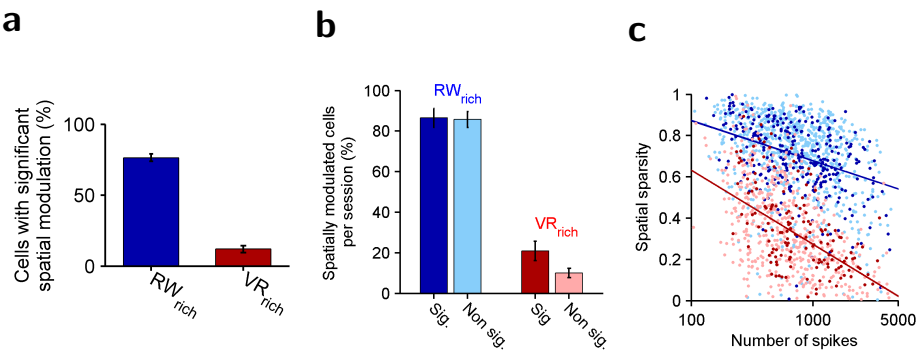

Figure 3.10: Comparison of spatial selectivity RW_{rich} and VR_{rich} conditions. (a) In contrast to angular sparsity, far fewer neurons (12, [10, 15]%) in VR_{rich} had significant spatial sparsity compared to RW_{rich} (76, [74, 79]%, Wilcoxon rank-sum test, numbers in brackets correspond to 95% confidence intervals here and throughout unless otherwise stated). **(b)** In RW_{rich}, the percentage of spatially modulated neurons per recording session (32 sessions) was identical between neurons with or without significant head-directional modulation ($86.53 \pm 4.66\%$ and $85.73 \pm 3.86\%$ respectively, p=0.3). In VR_{rich} (37 sessions), this percentage was slightly but not significantly higher for neurons with significant head-directional modulation ($20.93 \pm 4.80\%$) compared to those without ($9.97 \pm 2.30\%$, p=0.2). Hence, presence or absence of angular selectivity did not influence the degree of spatial selectivity. Numbers are reported as $mean \pm s.e.m.$ and error bars indicate s.e.m. **(c)** Spatial sparsity was also negatively correlated with the number of spikes in both worlds ($RW_{rich} : r = -0.34, p = 9.2 \times 10^{30}; VR_{rich} : r = -0.53, p = 1.3 \times 10^{59}$), but was significantly different between the two conditions ($p = 1.7 \times 10^{6}$, Two-way ANOVA, see Methods). Since all measures of selectivity depend on the number of spikes, to assess significance of tunings, bootstrapping was done for each cell separately.

VR_{blank} was comparable to that in VR_{rich} with visually distinct walls (comparable running speeds and distribution of occupancy across the platform).

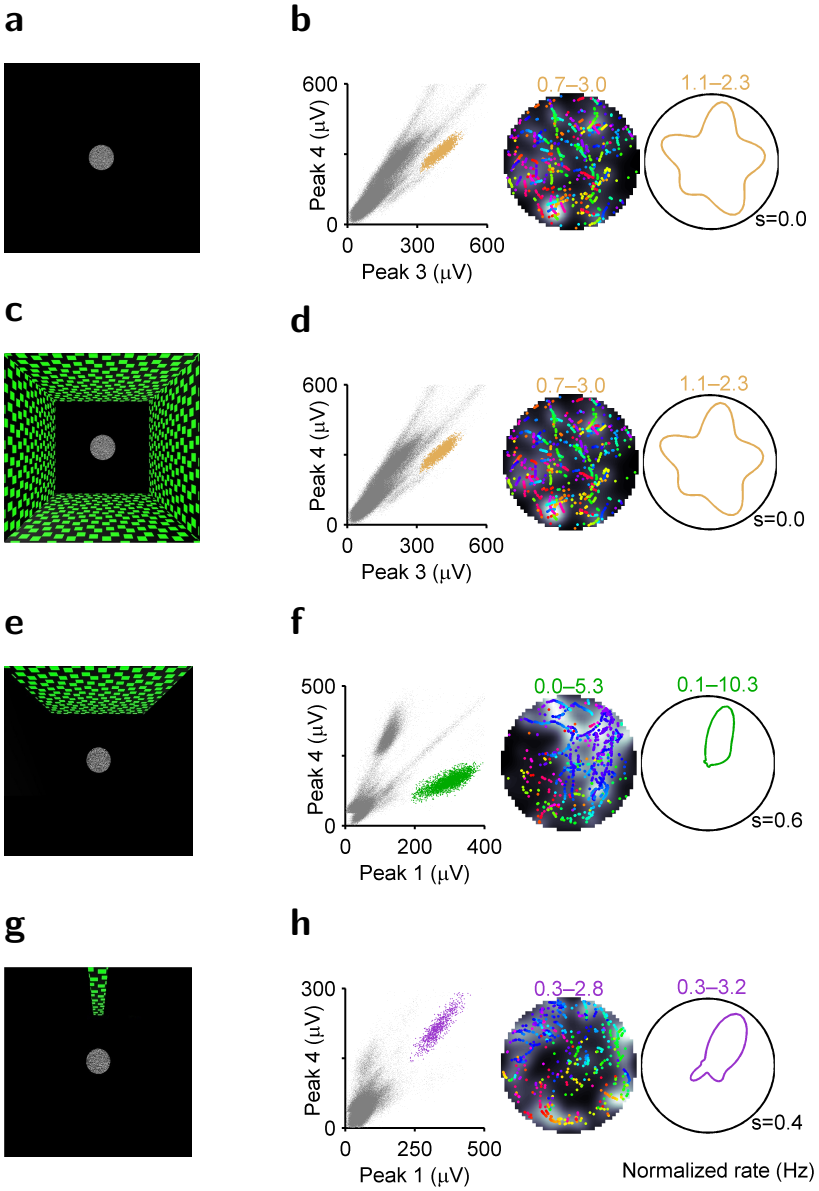

Figure 3.11: Causal influence of visual cues on the degree of directional modulation of neurons. (a) Top-down schematic of $\boldsymbol{VR_{blank}}$. **(b)** Left) Spikes from an isolated neuron (colored dots) in VR_{blank} (same convention as in 3.3). Center, right) Spatial and angular firing rate of this neuron **(c)–(h)** Same as **(a)** and **(b)** but for $\boldsymbol{VR_{symmetric}}$, $\boldsymbol{VR^{wide}_{polarized}}$ and $\boldsymbol{VR^{narrow}_{polarized}}$. Note that the neurons in **(b)** and **(d)** do not show significant angular sparsity, but those in **(f)** and **(h)** show strong head-directional modulation.

Very few hippocampal neurons (6%) showed significant head-directional modulation in this case (Figure 3.11b, 3.12a, 3.13e), close to the chance level of 5%.

The absence of head-directional modulation in VR_{blank} may result from a lack of anchoring visual cues [72] or optic flow created by the distal visual cues which could potentially be integrated to generate directional tuning. To address this, we performed another experiment where all the virtual walls had the same visual texture with high contrast and spatial frequency ($VR_{symmetric}$), thus providing strong optic flow information but no angular information (Figure 3.11c, see Methods). The virtual platform was placed in a larger room where each wall was $450cm$ away from the platform center, which ensured that the distance from the walls provided minimal spatial and angular information. Here too, only a small percentage of neurons (7%) exhibited significant head-directional modulation, similar to VR_{blank} and close to chance level (Figure 3.11d, 3.12a, 3.13f).

While internal mechanisms and optic flow may still modulate the degree of angular tuning, these experiments show that directional modulation is not generated by these mechanisms alone. This leaves open the possibility that head-directional modulation is generated by the angular information contained in the distal visual cues. To confirm this hypothesis we performed another experiment where the virtual world was strongly visually polarized. In this condition, there was just one high contrast wall, $450cm$ from the center of the platform, subtending a 90° angle ($VR^{wide}_{polarized}$)(Figure 3.11e, see Methods). This polarizing cue had no other spatial information and was identical to the walls used in the symmetric world. Here, 31% of hippocampal neurons showed significant head-directional modulation (Figure 3.11f, 3.12a, 3.13g), which is a greater fraction than in all other conditions but comparable to that in RW_{rich} and VR_{rich}. Remarkably, the directional tuning curves of many neurons were much narrower ($77.35 \pm 3.62°$) than the sole, 90° wide polarizing cue.

Is there a lower bound on the width of the angular tuning curves? To address

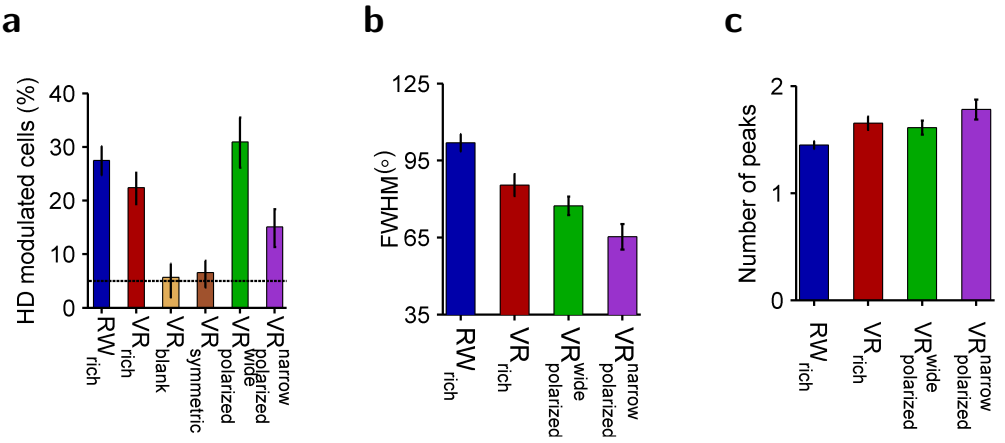

Figure 3.12: Properties of neural activity across experiments. (a) The percentages of cells with significant head-directional modulation was 27, [25, 30]% in RW_{rich} (293 out of 1066 cells; 32 sessions); 23, [19, 26]% in VR_{rich} (162 of 719 cells; 37 sessions); 6, [3, 9]% in VR_{rich} (13 of 230 cells; 8 sessions); 7, [4, 9]% in $VR_{symmetric}$ (28 of 426 cells; 10 sessions); 31, [26, 38]% in $VR^{wide}_{polarized}$ (121 of 391 cells; 14 sessions) and 15, [12, 19]% in $VR^{narrow}_{polarized}$ (64 of 424 cells; 20 sessions). The black horizontal line indicates the chance level of 5%. **(b)** Full width at half max (FWHM) of the angular rate maps for head-directionally modulated neurons in different conditions was as follows: RW_{rich} $(101.90 \pm 3.35°)$, VR_{rich} $(85.41 \pm 4.23°)$, $VR^{wide}_{polarized}$ $(77.35 \pm 3.62°)$ and $VR^{narrow}_{polarized}$ $(65.29 \pm 4.97°)$. The tuning curves in RW_{rich} were significantly wider than all other VR conditions ($p = 5.1 \times 10^4$ versus VR_{rich}, $p = 3.3 \times 10^5$ versus $VR^{wide}_{polarized}$ and $p = 5.3 \times 10^8$ versus $VR^{narrow}_{polarized}$). Within VR conditions, $VR^{narrow}_{polarized}$ had significantly narrower tuning curves with respect to VR_{rich} $(p = 3.7 \times 10^3)$ and $VR^{wide}_{polarized}$ $(p = 6.5 \times 10^3)$. **(c)** Angular rate maps in all VR conditions were significantly more multimodal (1.65 ± 0.07 peaks, $p = 1.4 \times 10^2$ in VR_{rich}; 1.61 ± 0.07, $p = 3.3 \times 10^2$ in $VR^{wide}_{polarized}$; 1.78 ± 0.09, $p = 4.8 \times 10^4$ in $VR^{narrow}_{polarized}$) than RW_{rich} (1.45 ± 0.04 peaks). Values are reported as $mean \pm s.e.m$, the p-values are obtained by Wilcoxon rank-sum test and percentages and numbers in brackets correspond to maximum likelihood estimates and 95% confidence intervals unless noted otherwise.

this we conducted another experiment where the sole polarizing cue was very narrow (11°), thus providing high angular information in the direction of the cue while leaving the majority of the maze blank ($VR^{narrow}_{polarized}$) (Figure 3.11g, see Methods). A large proportion (15%) of neurons had significant head-directional tuning in this condition as well (Figure 3.11h, 3.12a, 3.13h). For neurons with significant

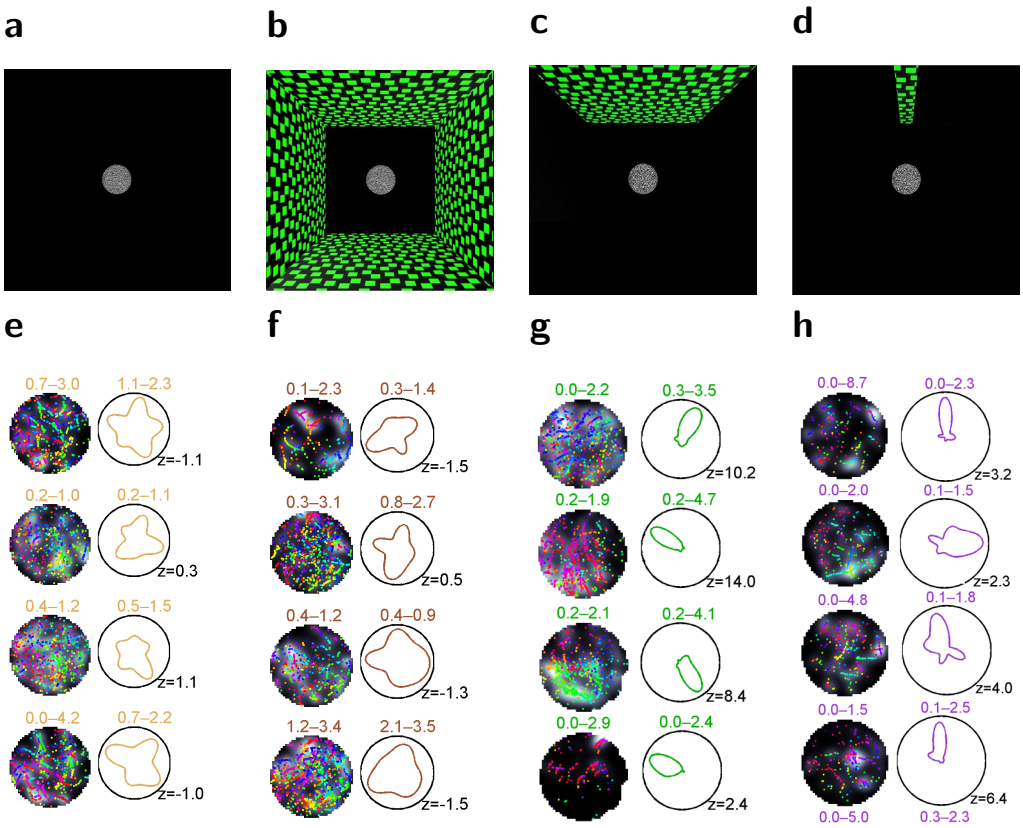

Figure 3.13: Example cells from the corresponding VR task. (a)–(b) Top-view schematics of the four VR enviroments. **(e)–(h)** The left image in each sub-panel shows the position and head-direction of the animal at the time of occurance of spikes. The color of each spike indicates the head-direction according to the colorwheel. The right image depicts the angular firing ratemap of that cell.

head-directional tuning, the width of the tuning curves ($65.29 \pm 4.97°$) was significantly ($p = 6.5 \times 10^{-3}$, Wilcoxon rank-sum test) narrower than in $VR^{wide}_{polarized}$

(Figure 3.12b), however much wider than the 11° polarizing cue, indicating a lower bound on the width of hippocampal angular tuning curves. Further, the fraction of neurons showing significant head-directional modulation (15%) was considerably lower than in $VR^{wide}_{polarized}$ (Figure 3.12a), perhaps because the narrow visual cue is visible to the rat for a smaller fraction of time than the wider polarizing cue, hence modulating a smaller percentage of neurons. Notably, in all RW and VR experiments, several angular rate maps showed multimodal responses, despite considerable differences in the nature of visual cues (Figure 3.12c) suggesting underlying internal mechanisms.

We then asked if the head-directional modulation of hippocampal neurons is stable and whether the stability depends on the experimental condition (Figure 3.14). Tuning curves of neurons with significant head-directional modulation were significantly stable across the experimental session in all four conditions ($RW_{rich}p = 8.71046, VR_{rich}p = 1.11023, VR^{wide}_{polarized}p = 1.11021 and VR^{narrow}_{polarized}p =$ 1.31011, Wilcoxon signed-rank test) (Figure 3.14a–3.14d). The tuning curves were more stable ($p = 9.2 \times 10^7$) in RW_{rich} than in VR_{rich} (Figure 3.14e, 3.14f). This could be due to the presence of other directionally informative multisensory cues in RW, such as distal odors and sounds, and their consistent pairing with visual cues resulting in higher stability. On the other hand, the tuning curves were more stable in the polarized VR experiments than in either of the rich conditions (Figure 3.14e, 3.14f) indicating there may be competing influences of multiple cues within each modality in the rich conditions.

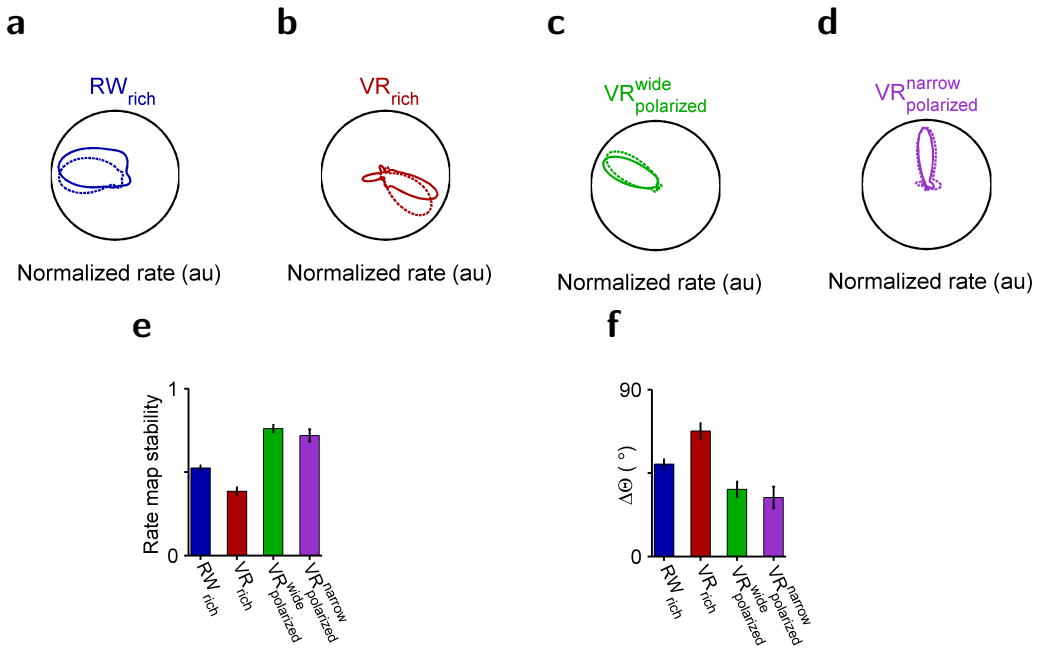

Figure 3.14: Stability of angular rate maps for head-directionally modulated neurons. (a)–(d) Four directionally tuned cells with stable angular firing in the first half (solid colored lines) and second half (dashed colored lines) of the recording session. The peak rates are normalized for ease of comparison. **(e)** Stability of the head-directional modulation (pairwise correlation between the angular rate maps in the two halves) in RW_{rich} (0.52 ± 0.02, n=293) was significantly greater than VR_{rich} (0.39 ± 0.02, n=162, $p = 9.2 \times 10^{7}$, Wilcoxon rank-sum test here and throughout figure legend) but significantly smaller than $VR^{wide}_{polarized}$ (0.76 ± 0.02, n=121, $p = 8.5 \times 10^{19}$) and $VR^{narrow}_{polarized}$ (0.72 ± 0.04, n=64, $p = 2.3 \times 10^{9}$). Stability was not significantly different between $VR^{wide}_{polarized}$ and $VR^{narrow}_{polarized}$ ($p = 0.35$). **(f)** As an alternate stability measure, we computed the absolute value of the circular distance between the preferred directions (defined as the direction of peak firing) in the two session halves. This also resulted in $VR^{wide}_{polarized}$ ($36.23 \pm 4.06°$) and $VR^{narrow}_{polarized}$ ($31.83 \pm 5.82°$) showing identical levels of drift of preferred directions ($p = 0.15$), both smaller than in RW_{rich} ($49.85 \pm 2.83°$,$p = 7.2 \times 10^{5}$ and $p = 7.4 \times 10^{6}$ respectively) and VR_{rich} ($67.65 \pm 4.34°$, $p = 6.3 \times 10^{8}$ and $p = 9.9 \times 10^{8}$ respectively).

3.4.4 Visual cues bias hippocampal ensemble response

These results demonstrate that specific aspects of visual cues modulate the angular tuning of individual neurons; could they also influence the ensemble response? To address this we investigated the activity of the head-directionally modulated neurons on a population level under the four different conditions. For each neuron, the direction of maximum firing was computed from its angular rate map and was designated as its preferred direction (see Methods). We then computed the distribution of these preferred directions and the degree of angular bias of the population for each condition. There was no significant angular bias, as indicated by circular Rayleigh test, in both RW_{rich} (p=0.1) and VR_{rich} (p=0.4), and the two distributions were not significantly different from each other (p=1, circular Kuiper test) (Figure 3.15a, 3.15b,). The lack of population bias in the rich conditions is likely due to the presence of multiple visual cues on all walls, each contributing to tuning towards different directions.

Indeed, in $VR^{wide}_{polarized}$ with only one visual cue, the population was significantly biased (p=0.04, circular V test) towards the prominent visual cue (Figure 3.15c). The directional bias of the population was strongest in $VR^{narrow}_{polarized}$ such that the distribution of preferred orientations was significantly different from a uniform distribution ($p = 3.6 \times 10^3$ Rayleigh test) and in addition was oriented towards the narrow visual cue ($p = 4.3 \times 10^4$, circular V test, Figure 3.15d). There was an apparent reduction in the number of cells with preferred direction directly towards the narrow polarizing cue, and for some cells the preferred direction was opposite to the visual cue, which could arise due to release from potent, feed-forward and lateral inhibition in CA1 [73, 74].

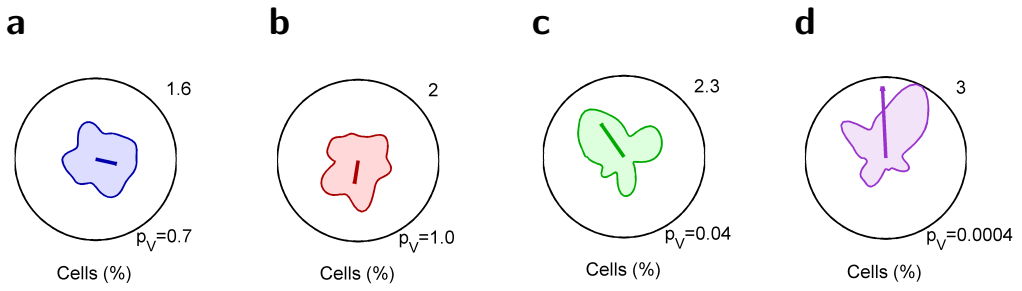

Figure 3.15: Visual cues bias the neural ensemble. (a) Distribution of preferred direction of neurons in RW_{rich} did not show bias ($p = 0.1$, circular Rayleigh test; p_V=0.7, circular V test) and the mean vector length of the ensemble ($MVL_{en} = 0.09$) was smaller than 95% of the shuffles (see Methods) ($347.80 \pm 4.52°, n = 293, circular mean \pm circular s.e.m.$). Number on the top right indicates maximum value of the distribution. The thick blue line originating at the center of the polar plot represents both the direction ($347.80°$)and the magnitude (0.09) of the mean vector length of the preferred directions of the population (scaled by a factor of 5 for clarity). **(b)** Same as in **(a)** but for VR_{rich}. The distribution of preferred directions of neurons in VR_{rich} did not show any significant bias (p=0.4, circular Rayleigh test; $p_V = 1$, circular V test) and $MVL_{en} = 0.1$ was not significantly different from chance ($260.91 \pm 6.07°, n = 162, circular mean \pm circular s.e.m.$). Additionally, this distribution was not significantly different from that in RW_{rich} (p=1, circular Kuiper test). **(c)** The ensemble of head-directionally modulated neurons in $VR^{wide}_{polarized}$ preferentially fired towards the visual cue ($p_V = 0.04$, circular V test) and $MVL_{en} = 0.17$ was greater than chance ($124.99 \pm 8.18°, n = 121, circular mean \pm circular s.e.m.$). Note the direction (124.99 and the longer magnitude (0.17) of the thick green line compared to **(a)**, **(b)**. **(b)** Same as in **(d)** Neurons in $VR^{narrow}_{polarized}$ ($92.68 \pm 8.51°, n = 64, circular mean \pm circular s.e.m.$) were biased towards the narrow cue ($p_V = 0.04$, circular V test; $p = 3.6 \times 10^3$ Rayleigh test), further indicated by the magnitude (0.29, significantly greater than chance) of the MVL_{en} (thick purple line).

3.5 Discussion

These results demonstrate that during two-dimensional random foraging rodent hippocampal CA1 neurons show significant modulation as a function of head-direction with respect to the surrounding distal visual cues in both real and virtual worlds. This directional modulation does not require robust vestibular cues, while angularly informative visual cues are sufficient for its generation. Additionally, the proportion of neurons with significant directional modulation, the direction of their tuning, and the directional tuning curve width are all strongly influenced by the degree of angular information in the distal visual cues, both at the neuronal and ensemble level, thereby demonstrating for the first time the causal influence of visual cues on rodent hippocampal directional responses.

Our demonstration of significant head-directional modulation of hippocampal neurons'activity during random foraging in two dimensions in RW is contrary to the commonly held belief that head-directional modulation is absent in this condition in rodents [57], [58]. There have been a few conflicting reports about hippocampal head-directional selectivity in rats [11, 75] and bats [64, 65] in open fields. Directional selectivity in bats was initially thought to be generated by visual cues [64] but later ascribed to vestibular cues and spatial selectivity [65]. Additionally, a few studies have reported directionally selective responses in the primate hippocampus [37, 63]. Our results about directionally selective responses in RW are consistent with these primate studies. There could be several reasons why we found strong directional selectivity in this condition where previous studies failed to find such responses. Firstly, we used prominent, rich visual cues that could elicit visually evoked responses, unlike most studies. Secondly, we used a large ($200cm$ diameter) open platform placed in a large room ($300 \times 300cm$) where we attempted to eliminate nonspecific cues, in contrast to most studies that use a small enclosure with nearby walls which could provide nonspecific cues that could

interfere with the visual cues. Further, we employed analysis techniques that eliminated the possibility that the directionality we observed was influenced by spatially selective responses or behavioral artifacts. Finally, we estimated angular tuning by computing angular sparsity, which is more robust to estimating the selectivity of multimodal responses than the commonly used mean vector length.

Notably, we found comparable levels of directional responses in both visually rich RW and in VR where the vestibular cues were minimized. This is in contrast to commonly held belief that directional responses in rodent hippocampus and related systems require robust vestibular cues [11, 26, 57, 59] but consistent with visually evoked direction selective responses in primates without vestibular cues [37, 63].

These results demonstrate that visual cues alone are sufficient to generate rodent hippocampal direction selectivity. To determine the causal influence of the nature of visual cues on this selectivity we did a series of experiments in VR. This isolation of visual cues is not possible in RW since nonspecific cues [10] including vestibular cues are invariably present in RW and could confound interpretation. We found that the amount of angular information in the visual cues directly determined the proportion of hippocampal neurons that had significant directional selectivity. Removing angular information in the visual cues eliminated directional selectivity of hippocampal responses. Compared to the visually rich VR, making the visual cues angularly concentrated resulted in sharpening of the head directional tuning curves. In addition, narrowing of the same polarizing visual cue had a predictable effect: fewer neurons were angularly tuned but their directional tuning curves were even sharper. These results show that visual cues play a causal role in determining rodent hippocampal directional responses. While these results are novel for rodents, they are consistent with extensive primate literature showing visually evoked selective responses in the primate hippocampal formation [29, 37, 76, 77]. However, we found that the angular tuning curves were wider

than the visual stimulus. This increased width could arise due to mechanisms of persistent activity [35, 60, 78] and could improve the angular accuracy of the ensemble of neurons by improving signal to noise ratio of the ensemble [79].

In addition, we found that visual cues not only influence the angular responses of individual neurons, but of the hippocampal ensemble response as well. Concentration of visual cues in one part of the wall caused the ensemble to become preferentially biased in that direction, demonstrating that hippocampal responses were visually evoked. This could explain why there was no ensemble bias in the rich conditions where different neurons fire preferentially to different visual features on the walls.

Hence, we hypothesize that while the hippocampal formation receives directional signals from the vestibular cue-dependent head-direction system, it must also be receiving directional information from a pathway that does not require the vestibular signal, but could instead be driven by visual cues, such as the entorhinal cortex [5, 80, 81]. For example, layer 3 of medial entorhinal cortex, which is a primary source of input to the dorsal CA1, and which drives CA1 neurons [35], could contain a subset of the head directionally tuned neurons that are visually driven and maintain significant angular selectivity even in our virtual reality setup, thus contributing to the directional tuning of CA1 neurons. Our findings narrow the gap between the presence of directionality on linear tracks [62], but its apparent absence during random foraging in two dimensions [57, 58], by showing the presence of significant directional tuning in this condition. Further studies are needed to determine if rodent hippocampal responses are distributed in the allocentric [4], egocentric [2, 80, 82], or retinotopic [37] frames of reference. Further, our experiments do not rule out the possibility that other sensory, behavioral and internal cues could also influence hippocampal directionality.

The intact head-directional modulation observed here is in contrast to the large reduction in spatial selectivity in VR [60]. Thus the mechanisms of spatial

and directional selectivity can be dissociated, in that visual cues are sufficient to generate the latter but not the former. Further, these results are also consistent with human and non-human primate studies showing the presence of angular selectivity independent of spatial selectivity [29, 30, 37, 83].

Thus our results bridge the long standing gap between the primate and rodent studies by showing visually evoked, directional responses in the rodents regardless of vestibular cues. These results could potentially resolve the apparent paradox: If the hippocampus is required for navigation [84], how can rats [43], humans, or nonhuman primates navigate with only visual cues and without robust hippocampal spatial selectivity [30, 37, 60]? We hypothesize that angular selectivity of hippocampal neurons reported here, combined with their selectivity to distance traveled [14, 60] and experiential plasticity of hippocampal receptive fields [54, 55, 85] could mediate spatial navigation.

CHAPTER 4

Hippocampus shows no spatial selectivity during navigation in virtual reality

4.1 Abstract

Principal excitatory neurons in area CA1 of the rodent hippocampus show strong selectivity to position in the allocentric frame of reference and are aptly called place cells. Additionally, it has been shown that the hippocampus itself is necessary for solving spatial navigation tasks. Hence, it is commonly believed that the spatially selective activity of place cells are necessary for spatial navigation. However, CA1 neurons have no spatial selectivity during random exploration in two-dimensional virtual reality (VR) where only visual cues are spatially informative. This raises the important question: is spatial selectivity in the form of place fields necessary for navigation at the behavioral level? Hence, we collected electrophysiological data from CA1 of rats trained to solve a spatial navigation task in the same VR setup. At the behavioral level, rats were able to successfully learn how to solve the task which is an analog of the Morris watermaze task in VR. Interestingly, similar to results seen during random foraging, the neurons exhibited no spatial selectivity providing additional evidence that spatial selectivity in hippocampus is not necessary for spatial navigation.

4.2 Introduction

Spatial navigation is a necessity for survival and the hippocampus is a brain area that has been heavily implicated in spatial navigation and memory. Experiments performed in rats by Richard Morris [86] showed that lesions of the hippocampus result in severe deficits in the ability of rodents to learn a spatial navigation task. Prior to this, in 1971, O'Keefe and Dostrovsky [4] had discovered the ***place cell*** in area CA1 of the rodent hippocampus and given birth to the idea of the ***cognitive map***. It has since been believed that the unique ability of place cells to encode the position of the animal in space is necessary in order to solve a spatial navigation task. However, in stark contrast to this idea, experiments performed in virtual reality (VR)—where only visual cues are spatially informative [60]—showed that despite rats being able to easily navigate through the virtual space and forage for randomly distributed rewards, spatial selectivity of neurons in hippocampal CA1 of rats was severely impaired but selectivity to distance traveled was preserved [14, 60]. These data also showed that about a quarter of CA1 neurons encode for the direction that the animal is facing in both RW and VR, despite the loss of position selectivity in VR. This result indicates that selectivity to absolute position is not necessary for spatial navigation and that other forms of coding are sufficient. In order to determine if this is indeed the case, we recorded from area CA1 of rats performing an analog of the spatial navigation task designed by Morris [87] in the same VR setup.

The watermaze task

The spatial navigation task, known as the watermaze task [87], is an experimental tool used widely to measure and quantify the behavioral and physiological correlates of spatial learning and memory. The experimental setup consists of a circular pool of water that has a platform just beneath the surface which is made either

visible or invisible. The walls of the room have distinct visual cues to distinguish them from each other. The rat is placed in the water in a random location near the walls of the pool and the goal of the task is for the rat to locate the platform. When the platform is hidden by making the water opaque, the animal has to learn the location of the platform based on the cues on the walls over several trials. The ability of the animal to solve the task is quantified using measures such as the amount of time it takes for him to find to the platform, the length of the path he takes, the number of trials that are required for him to successfully learn the position of the hidden platform and the quadrant of the circular pool he spends the most time in when the platform is removed.

Spatial navigation in virtual reality

We trained the rats to perform a virtual analog of the watermaze task, henceforth referred to as the ***virtual spatial navigation*** task. Since spatial selectivity was severely impaired [60] during random foraging in virtual reality, we used the same VR setup to determine if spatial selectivity in CA1 is necessary for rats to solve a spatial navigation task. Previously published behavioral experiments [43] in this VR showed that rats are capable of learning to perform the virtual spatial navigation task. Further, other studies done using this VR setup [14, 60] have shown that rats are able to successfully learn how to perform various other kinds of spatial tasks in this virtual environment. Hence, if spatial selectivity is indeed necessary—as commonly held—for spatial navigation, one would expect to see a resuscitation of place fields during the virtual spatial navigation task.

4.3 Methods

Methods Summary Materials and methods were similar to those formerly described (Section 2.3).

4.3.1 Subjects

Data were obtained from four adult male Long-Evans rats (350–400 g at the time of surgery) that were singly housed on a 12-hour light/dark cycle. The animals were water restricted (minimum of 30 mL/day) in order to increase motivation to perform the task, but allowed an unrestricted amount of sugar water reward during the task. Further, they were food restricted (minimum of 15 g/day) to maintain a stable body-weight. All experimental procedures were approved by the UCLA Chancellor's Animal Research Committee and in accordance with NIH approved protocols.

4.3.2 Behavioral Tasks

The task is as previously described [43]. The experimental setup consisted of the VR setup described in Section 2.3.2. The virtual room was $450cm \times 450cm$ wide with four distinct visual cues on the walls. Rats were trained to run on a $200cm$ diameter platform elevated $50cm$ from the virtual floor. Sugar water rewards were dispensed in pulses of 5 at a fixed, unmarked reward zone 20–$25cm$ in radius that will henceforth be referred to as the ***hidden reward zone***. Each trial began with the rat at one of four or eight (depending on the variation of the task) random start locations at the edge of the table and facing outwards towards the wall. The trial ended when the rat had located the reward zone and rewards were dispensed. An intertrial interval of 2–$5s$ separated the trials during which the virtual environment went blank. Rats quickly learnt to locate the hidden reward zone, seemingly using the distalvisual cues since they were the only spatially informative cues in the virtual space [43].

4.3.3 Surgery, electrophysiology and spike sorting

All the methods were analogous to procedures described previously (Section 2.3) [14, 60]. Rats with satisfactory behavioral performance were anesthetized using isoflurane and implanted with custom-made hyperdrives with approximately 22 independently adjustable tetrodes. Both left and right dorsal CA1 were targeted. After recovery from surgery, tetrodes were gradually lowered to area CA1, which was identified by the presence of sharpwave ripple complexes. Signals were recorded using a Neuralynx data acquisition system at a sampling rate of 40kHz. Spike extraction, spike sorting and single unit classification were done offline using custom software and according to methods described previously (Section 2.3.6).

4.3.4 Statistics

Only those data during which the speed of the rat was greater than $5cm/s$ were considered for analyses and all other data were discarded.

Spatial ratemaps

$10cm \times 10cm$ spatial bins were created and only those bins through which the animal traversed more than 5 times were considered for the generation of two-dimensional ratemaps. This was then smoothed by convolving with a Gaussian kernal with a σ of 1 bin.

Confidence intervals

Resampling was done with replacements 10,000 times and the 2.5 and 97.5 quantiles were used for the boundaries of the confidence intervals.

4.4 Results

4.4.1 Rats are able to perform the virtual spatial navigation task

Rats could navigate to the hidden reward zone in the north-east quadrant of the $200cm$ diameter platform (Figure 4.1a). At the beginning of each trial rats found themselves at a start location facing the wall and were required to orient themselves in the virtual room and remember the location of the hidden reward zone in order to navigate to it to obtain rewards in the form of sugar water. The task had two variants: in the first there were four start locations (Figure 4.1b) and in the second, there were eight(Figure 4.1c). The start locations were chosen at random at the start of each trial.

4.4.2 Spatial selectivity is not required for spatial navigation in VR

We recorded from 497 putative pyramidal neurons from hippocampal CA1 of four adult Long-Evans rats. Interestingly, similar to the results obtained during random foraging [60] neurons did not show robust spatial selectivity (Figure 4.2a–4.2d). The distribution of their spatial information content values (Figure 4.2e) was nearly identical to the distribution of those of neurons recorded from the random foraging task in VR (Figure 4.2f, see 2.4.1, Figure 2.4c).

4.5 Discussion

We found that although rats were able to easily perform a spatial navigation task akin to the watermaze task designed by Morris [87] in virtual reality, neurons in hippocampal CA1 did not show the spatially selective activity thought to be necessary for spatial navigation. This indicates that spatial selectivity in hippocampal CA1 is not necessary for spatial navigation.

However, other studies [14,60] (Chapter 2, 3) have shown that the same brain region exhibits strong selectivity to distance and head-direction at a neuronal and population level in the same VR setup. Hence we postulate that in the absence of spatial selectivity, these other forms of encoding space are sufficient to support spatial navigation at the behavioral level.

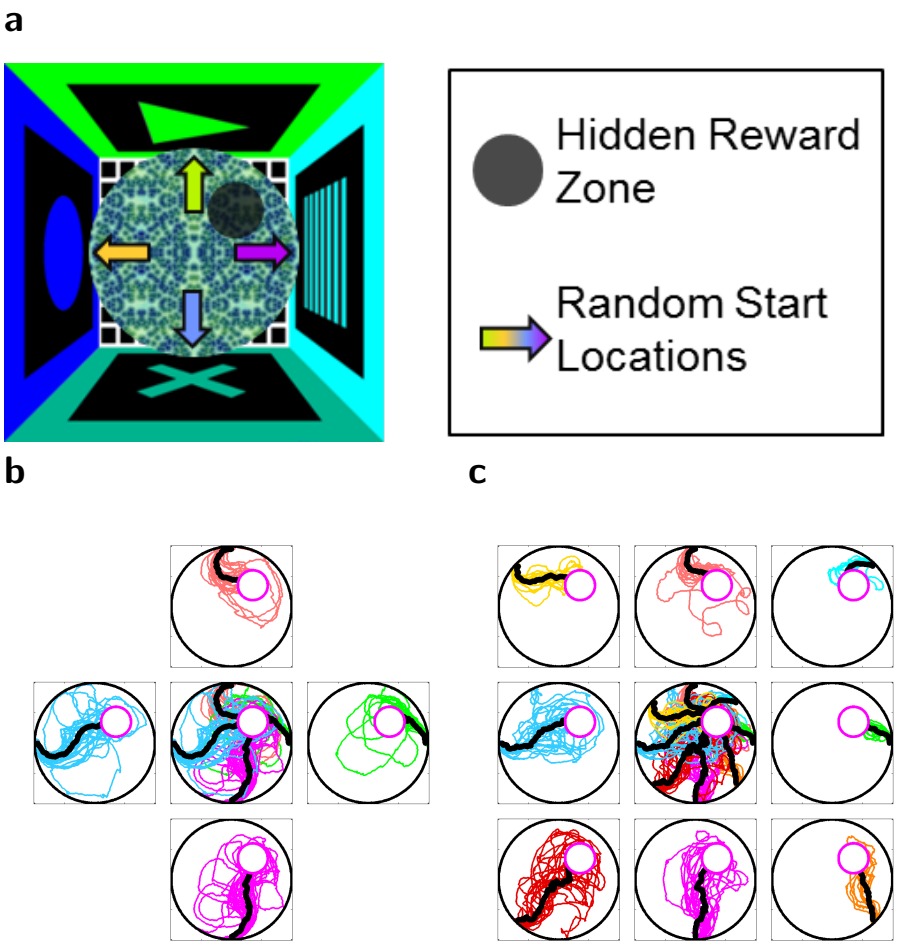

Figure 4.1: Rats can navigate to the hidden reward zone in VR (a) A top-down view schematic of the virtual room. The walls were $450cm$ wide and the platform was $300cm$ in diameter. The hidden reward zone was 40–$50cm$ in diameter. **(b)**, **(c)** The central panel shows the behavior of the rat on the task with the colored lines (color coded by start location) indicating the path taken by the rat from each start location to the reward zone and the solid black lines showing the average path taken by the rat. The surrounding panels show the behavior of the rat for each start location. Note how the rat takes the shortest path to the reward zone for all start locations.

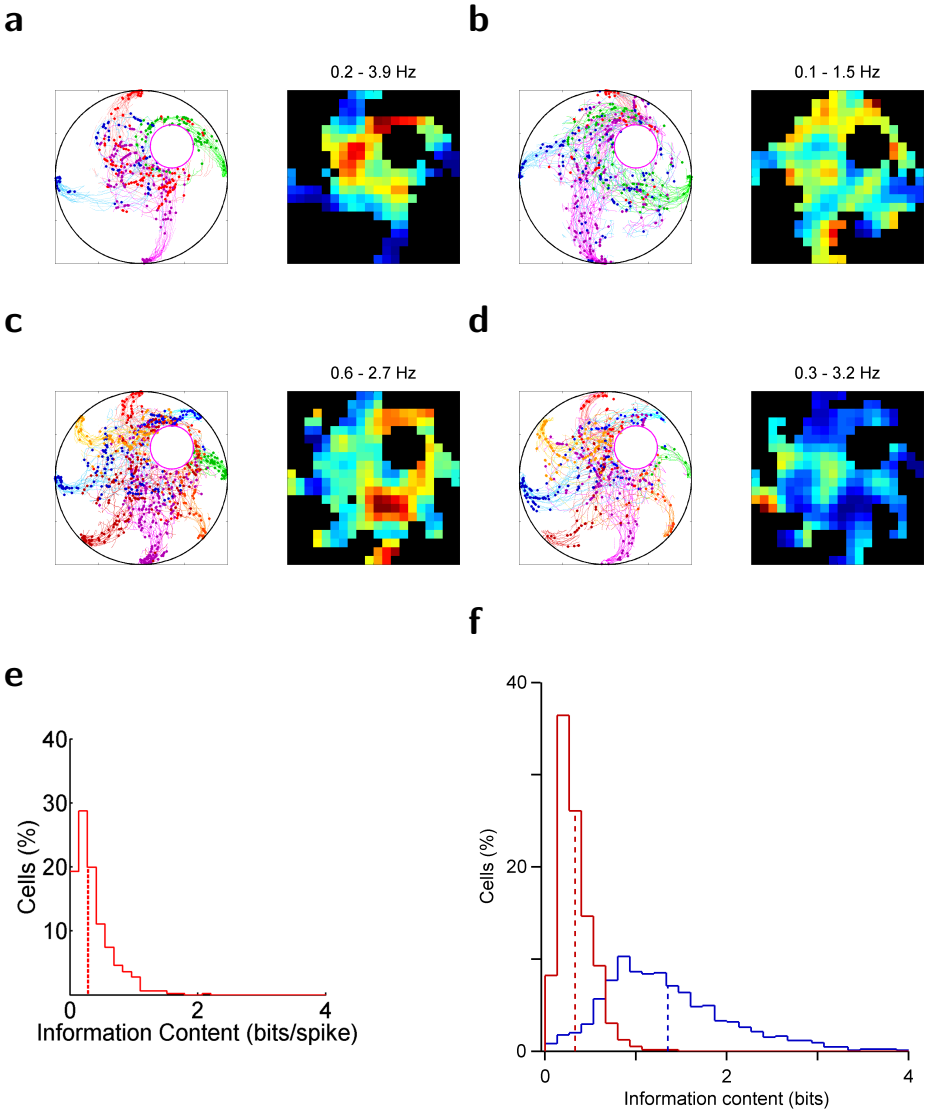

Figure 4.2: Neurons do not show spatial selectivity during spatial navigation in VR **(a)–(d)** Left panels) Spike positions (color coded by start location) and path taken by the rat from start location to the reward zone for four example neurons. Right panels) Firing rate maps for the corresponding neuron. Higher temperature colors indicate higher firing rate. Minimum and maximum firing rate are indicated by the numbers. **(e)** Histogram of information content ($0.29[0.26, 0.32] bits/spike$; median value (indicated by dotted line) and confidence interval) of the neurons shows neurons exhibited very poor spaital selectivity comparable to that seen in virtual reality during two-dimensional random foraging shown in **(f)** **(f)** Spatial information content in VR ($0.33 \pm 0.01 bits$) was 75% ($p = 1.1 \times 10^{183}$) lower than in RW ($1.35 \pm 0.02 bits$).

CHAPTER 5

Conclusion and future directions

The hippocampus has been implicated in a variety of brain functions, and its ability to create a spatial map in rodents was precluded by the discovery that it is an essential part of the circuitry that is responsible for ***declarative memory*** in humans [57]. A large gap currently exists between hippocampal studies in primates and rodents. In primates, the hippocampus is largely studied in the context of episodic memory but in rodents it is considered to function mainly to aid the animal in navigating through space [57]. The results in this thesis narrow this gap considerably and predict that the hippocampus of rodents is more similar than previously believed to that of humans and non-human primates. Additionally, the results shed important light on the mechanisms of multisensory integration and the contributions of the visual, vestibular and proprioceptive inputs to hippocampal activity. Most importantly, this thesis adds to the growing list of studies showing the versatility of this brain region to not only encode the environment the animal is currently situated in and detect the changes that occur, but also to be able to adapt its coding strategy depending on the requisites of the task at hand at the behavioral level. The following paragraphs will summarize each result and describe briefly the potential future studies.

Firstly, studies in humans and non-human primates have shown that hippocampal neurons have very little spatial selectivity [29, 30, 37]. However, these studies were done not in freely moving subjects, but in subjects who were made to navigate in a virtual environment where, as discussed earlier, only visual cues are

spatially informative. We have shown that the rodent hippocampus also shows similar behavior when the only reliable cues are distal visual cues and no other sensory modality provides spatially relevant information. Additionally, our results predict that the hippocampal neurons in humans and non-human primates can also exhibit strong spatial selectivity, albeit in the distance domain, if the experiment is constructed such that internal, self-motion cues provide spatial information more reliably. Future studies are required in order to determine if other combinations of sensory inputs are viable which will provide important insight into the mechanisms of sensory integration in the hippocampal formation.

Second, we have shown that the hippocampus is capable of encoding direction. This in itself is significant not only because it was largely held to be untrue, with any such signal being considered nothing but an artefact, but also because it adds to the growing list of the complex signals the hippocampus can generate. It is not entirely clear if this signal is view-based as observed in primates, or head-direction based like in the rodent thalamus. However, our results strongly point to the possibility that the signal is more similar to the former than the latter especially since the signal is entirely based on visual signals and not dependent on vestibular inputs. Additonally, the differences found between RW and VR indicate that there is competition between elements of the same modality (resulting in neurons having multimodal firing ratemaps), and also between different modalities (affecting stability of the firing ratemaps). Further experiments will determine the contribution of other modalities such as olfactory cues to the directional signal observed in our data.

Third, it is currently unclear whether the firing patterns observed in the hippocampus, which are highly correlated with the behavior of the animal are necessary or even reflected at the behavioral level. Our result showing that rats can navigate in a virtual environment without spatial selectivity indicates that spatial selectivity in the form of place fields is not necessary to accomplish the task

of spatial navigation. The observations made in this thesis, in addition to those of others showing the flexible, versatile nature of hippocampal activity indicates that the ability of hippocampal neurons to encode for distance, head-direction and time, to name a few, is sufficient to solve this complex problem. Further studies are required to determine which of these signals becomes prominent at the population level and how this ensemble activity changes as more sensory inputs are made spatially informative.

While the terms ***place cell*** and ***place field*** are accurate in describing the firing activity of neurons in the hippocampus they are highly limiting in that hippocampal neurons are not restricted to just encoding *cartesian* space. Many studies in the recent years have shown that the very same neurons that produce place fields also have selectivity to other aspects of space. It is important to keep in mind that space does not only consist of the three dimensions but is a complex conglomeration of patterns, and can be expressed and described with more than just the cartesian coordinates. The results in this thesis show that the hippocampus has the incredible ability to encode the same space in more than one way at the same time, speaking for the true complexity of the cognitive map birthed by the discovery of the place cell in 1971.

References

[1] Roberta L Klatzky. Allocentric and egocentric spatial representations: Definitions, distinctions, and interconnections. In *Spatial cognition*, pages 1–17. Springer, 1998.

[2] Jonathan R Whitlock, Gerit Pfuhl, Nenitha Dagslott, May-Britt Moser, and Edvard I Moser. Functional split between parietal and entorhinal cortices in the rat. *Neuron*, 73(4):789–802, 2012.

[3] Jeffrey S Taube. The head direction signal: origins and sensory-motor integration. *Annu. Rev. Neurosci.*, 30:181–207, 2007.

[4] John O'Keefe and Jonathan Dostrovsky. The hippocampus as a spatial map. preliminary evidence from unit activity in the freely-moving rat. *Brain research*, 34(1):171–175, 1971.

[5] Sachin S Deshmukh and James J Knierim. Representation of non-spatial and spatial information in the lateral entorhinal cortex. *Frontiers in behavioral neuroscience*, 5(October):69, January 2011.

[6] T Hafting, M Fyhn, T Bonnevie, M B Moser, and E I Moser. Hippocampus-independent phase precession in entorhinal grid cells. *Nature*, 453(7199):1248–1252, 2008.

[7] James J Knierim, Inah Lee, and Eric L Hargreaves. Hippocampal place cells: parallel input streams, subregional processing, and implications for episodic memory. *HIPPOCAMPUS-NEW YORK-CHURCHILL LIVINGSTONE-*, 16(9):755, 2006.

[8] J O'keefe and DH Conway. Hippocampal place units in the freely moving rat: why they fire where they fire. *Experimental Brain Research*, 31(4):573–590, 1978.

[9] Robert U Muller and John L Kubie. The effects of changes in the environment on the spatial firing of hippocampal complex-spike cells. *J Neurosci*, 7(7):1951–1968, 1987.

[10] F P Battaglia, G R Sutherland, and B L McNaughton. Local sensory cues and place cell directionality: additional evidence of prospective coding in the hippocampus. *J Neurosci*, 24(19):4541–4550, 2004.

[11] Etan J Markus, Yu-Lin Qin, Brian Leonard, William E Skaggs, Bruce L McNaughton, and Carol A Barnes. Interactions between location and task affect the spatial and directional firing of hippocampal neurons. *The Journal of Neuroscience*, 15(11):7079–7094, 1995.

[12] Matthew L Shapiro, Heikki Tanila, and Howard Eichenbaum. Cues that hippocampal place cells encode: dynamic and hierarchical representation of local and distal stimuli. *Hippocampus*, 7(6):624–642, 1997.

[13] Etienne Save, Ludek Nerad, and Bruno Poucet. Contribution of multiple sensory information to place field stability in hippocampal place cells. *Hippocampus*, 10(1):64–76, 2000.

[14] Pascal Ravassard, Ashley Kees, Bernard Willers, David Ho, Daniel Aharoni, Jesse Cushman, Zahra M Aghajan, and Mayank R Mehta. Multisensory control of hippocampal spatiotemporal selectivity. *Science*, 340(6138):1342–1346, 2013.

[15] Christopher J MacDonald, Kyle Q Lepage, Uri T Eden, and Howard Eichenbaum. Hippocampal time cells bridge the gap in memory for discontiguous events. *Neuron*, 71(4):737–749, 2011.

[16] Eva Pastalkova, Vladimir Itskov, Asohan Amarasingham, and György Buzsáki. Internally generated cell assembly sequences in the rat hippocampus. *Science*, 321(5894):1322–1327, 2008.

[17] Guifen Chen, John a King, Neil Burgess, and John O'Keefe. How vision and movement combine in the hippocampal place code. *Proceedings of the National Academy of Sciences of the United States of America*, 110(1):378–83, January 2013.

[18] C Hölscher, A Schnee, H Dahmen, L Setia, H a Mallot, C Holscher, A Schnee, H Dahmen, L Setia, and H a Mallot. Rats are able to navigate in virtual environments. *The Journal of experimental biology*, 208(Pt 3):561–9, February 2005.

[19] John O'keefe and Lynn Nadel. *The hippocampus as a cognitive map*, volume 3. Clarendon Press Oxford, 1978.

[20] Devdeep Aikath, Aldis P Weible, David C Rowland, and Clifford G Kentros. Role of selfgenerated odor cues in contextual representation. *Hippocampus*, 2014.

[21] Michael I Anderson and Kathryn J Jeffery. Heterogeneous modulation of place cell firing by changes in context. *The Journal of neuroscience : the official journal of the Society for Neuroscience*, 23(26):8827–35, October 2003.

[22] James J Knierim. Dynamic interactions between local surface cues, distal landmarks, and intrinsic circuitry in hippocampal place cells. *The Journal of neuroscience : the official journal of the Society for Neuroscience*, 22(14):6254–6264, 2002.

[23] K M Gothard, W E Skaggs, and B L McNaughton. Dynamics of mismatch correction in the hippocampal ensemble code for space: interaction between path integration and environmental cues. *J Neurosci*, 16(24):8027–40., 1996.

[24] Alejandro Terrazas, Michael Krause, Peter Lipa, Katalin M Gothard, Carol A Barnes, and Bruce L McNaughton. Self-motion and the hippocampal spatial metric. *The Journal of neuroscience*, 25(35):8085–8096, 2005.

[25] Robert W Stackman and Jeffrey S Taube. Firing properties of head direction cells in the rat anterior thalamic nucleus: dependence on vestibular input. *The Journal of neuroscience*, 17(11):4349–4358, 1997.

[26] Robert W Stackman, Ann S Clark, and Jeffrey S Taube. Hippocampal spatial representations require vestibular input. *Hippocampus*, 12(3):291–303, 2002.

[27] J L Calton, R W Stackman, J P Goodridge, W B Archey, P A Dudchenko, and J S Taube. Hippocampal place cell instability after lesions of the head direction cell network. *J Neurosci*, 23(30):9719–9731, 2003.

[28] Dora E Angelaki and Kathleen E Cullen. Vestibular system: the many facets of a multimodal sense. *Annu. Rev. Neurosci.*, 31:125–150, 2008.

[29] A D Ekstrom, M J Kahana, J B Caplan, T A Fields, E A Isham, E L Newman, and I Fried. Cellular networks underlying human spatial navigation. *Nature*, 425(6954):184–188, 2003.

[30] Joshua Jacobs, Michael J Kahana, Arne D Ekstrom, Matthew V Mollison, and Itzhak Fried. A sense of direction in human entorhinal cortex. *Proceedings of the National Academy of Sciences of the United States of America*, 107(14):6487–92, April 2010.

[31] Jonathan F Miller, Markus Neufang, Alec Solway, Armin Brandt, Michael Trippel, Irina Mader, Stefan Hefft, Max Merkow, Sean M Polyn, Joshua Jacobs, et al. Neural activity in human hippocampal formation reveals the spatial context of retrieved memories. *Science*, 342(6162):1111–1114, 2013.

[32] John R Huxter, Timothy J Senior, Kevin Allen, and Jozsef Csicsvari. Theta phase-specific codes for two-dimensional position, trajectory and heading in the hippocampus. *Nature neuroscience*, 11(5):587–94, May 2008.

[33] MR Mehta, AK Lee, and MA Wilson. Role of experience and oscillations in transforming a rate code into a temporal code. *Nature*, 417(6890):741–746, 2002.

[34] John O'Keefe and Michael L Recce. Phase relationship between hippocampal place units and the eeg theta rhythm. *Hippocampus*, 3(3):317–330, 1993.

[35] Thomas T G Hahn, James M McFarland, Sven Berberich, Bert Sakmann, and Mayank R Mehta. Spontaneous persistent activity in entorhinal cortex modulates cortico-hippocampal interaction in vivo. *Nature Neuroscience*, 15(11):1531–1538, 2012.

[36] Karel Jezek, Espen J Henriksen, Alessandro Treves, Edvard I Moser, and May-Britt Moser. Theta-paced flickering between place-cell maps in the hippocampus. *Nature*, 478(7368):246–249, 2011.

[37] Edmund T Rolls et al. Spatial view cells and the representation of place in the primate hippocampus. *Hippocampus*, 9(4):467–480, 1999.

[38] Daniel A Dombeck, Christopher D Harvey, Lin Tian, Loren L Looger, and David W Tank. Functional imaging of hippocampal place cells at cellular resolution during virtual navigation. *Nature neuroscience*, 13(11):1433–1440, 2010.

[39] Christopher D Harvey, Forrest Collman, Daniel a Dombeck, and David W Tank. Intracellular dynamics of hippocampal place cells during virtual navigation. *Nature*, 461(7266):941–6, October 2009.

[40] Christoph Schmidt-Hieber and Michael Häusser. Cellular mechanisms of spatial navigation in the medial entorhinal cortex. *Nature neuroscience*, 16(3):325–331, 2013.

[41] Anne Cei, Gabrielle Girardeau, Céline Drieu, Karim El Kanbi, and Michaël Zugaro. Reversed theta sequences of hippocampal cell assemblies during backward travel. *Nature neuroscience*, 2014.

[42] Case H Vanderwolf. Hippocampal electrical activity and voluntary movement in the rat. *Electroencephalography and clinical neurophysiology*, 26(4):407–418, 1969.

[43] Jesse D. Cushman, Daniel B. Aharoni, Bernard Willers, Pascal Ravassard, Ashley Kees, Cliff Vuong, Briana Popeney, Katsushi Arisaka, and Mayank R. Mehta. Multisensory Control of Multimodal Behavior: Do the Legs Know What the Tongue Is Doing? *PLoS ONE*, 8(11):e80465, November 2013.

[44] Philipp Berens. CircStat: A MATLAB Toolbox for Circular Statistics. *Journal of Statistical Software*, 31(10):1–21, 2009.

[45] Tora Bonnevie, Benjamin Dunn, Marianne Fyhn, Torkel Hafting, Dori Derdikman, John L Kubie, Yasser Roudi, Edvard I Moser, and May-Britt Moser. Grid cells require excitatory drive from the hippocampus. *Nature neuroscience*, 16(3):309–317, 2013.

[46] Mayank R Mehta. Neuronal dynamics of predictive coding. *The Neuroscientist*, 7(6):490–495, 2001.

[47] Jingheng Cheng and Daoyun Ji. Rigid firing sequences undermine spatial memory codes in a neurodegenerative mouse model. *eLife*, 2:e00647, January 2013.

[48] Kenway Louie and Matthew A Wilson. Temporally structured replay of awake hippocampal ensemble activity during rapid eye movement sleep. *Neuron*, 29(1):145–156, 2001.

[49] Hagar Gelbard-Sagiv, Roy Mukamel, Michal Harel, Rafael Malach, and Itzhak Fried. Internally generated reactivation of single neurons in human hippocampus during free recall. *Science (New York, N.Y.)*, 322(5898):96–101, October 2008.

[50] Evgeny Resnik, James M McFarland, Rolf Sprengel, Bert Sakmann, and Mayank R Mehta. The effects of glua1 deletion on the hippocampal population code for position. *The Journal of Neuroscience*, 32(26):8952–8968, 2012.

[51] Mayank R Mehta. Contribution of i h to ltp, place cells, and grid cells. *Cell*, 147(5):968–970, 2011.

[52] Noah A Russell, Arata Horii, Paul F Smith, Cynthia L Darlington, and David K Bilkey. Lesions of the vestibular system disrupt hippocampal theta rhythm in the rat. *Journal of neurophysiology*, 96(1):4–14, 2006.

[53] Douglas A Nitz. Path shape impacts the extent of ca1 pattern recurrence both within and across environments. *Journal of neurophysiology*, 105(4):1815–1824, 2011.

[54] Mayank R Mehta, Michael C Quirk, and Matthew A Wilson. Experience-dependent asymmetric shape of hippocampal receptive fields. *Neuron*, 25(3):707–715, 2000.

[55] Mayank R Mehta, Carol A Barnes, and Bruce L McNaughton. Experience-dependent, asymmetric expansion of hippocampal place fields. *Proceedings of the National Academy of Sciences*, 94(16):8918–8921, 1997.

[56] T Kobayashi, H Nishijo, M Fukuda, J Bures, and T Ono. Task-dependent representations in rat hippocampal place neurons. *J Neurophysiol*, 78(2):597–613, 1997.

[57] Per Andersen, Richard Morris, David Amaral, Tim Bliss, and John O'Keefe. *The hippocampus book*. Oxford University Press, 2006.

[58] Robert U Muller, Elizabeth Bostock, Jeffrey S Taube, and John L Kubie. On the directional firing properties of hippocampal place cells. *Journal of Neuroscience*, 14(12):7235–7251, 1994.

[59] JJ Knierim, HS Kudrimoti, and BL McNaughton. Place cells, head direction cells, and the learning of landmark stability. *J. Neurosci.*, 15(3):1648–1659, March 1995.

[60] Zahra M Aghajan, Lavanya Acharya, Jason J Moore, Jesse D Cushman, Cliff Vuong, and Mayank R Mehta. Impaired spatial selectivity and intact phase precession in two-dimensional virtual reality. *Nature neuroscience*, 2014.

[61] Adrien Peyrache, Marie M Lacroix, Peter C Petersen, and György Buzsáki. Internally organized mechanisms of the head direction sense. *Nature neuroscience*, 18(4):569–575, 2015.

[62] BL McNaughton, CA Barnes, and J O'keefe. The contributions of position, direction, and velocity to single unit activity in the hippocampus of freely-moving rats. *Experimental Brain Research*, 52(1):41–49, 1983.

[63] Edmund T Rolls and Shane M O'Mara. View-responsive neurons in the primate hippocampal complex. *Hippocampus*, 5(5):409–424, 1995.

[64] Nachum Ulanovsky and Cynthia F Moss. Dynamics of hippocampal spatial representation in echolocating bats. *Hippocampus*, 21(2):150–161, 2011.

[65] Alon Rubin, Michael M Yartsev, and Nachum Ulanovsky. Encoding of head direction by hippocampal place cells in bats. *The Journal of Neuroscience*, 34(3):1067–1080, 2014.

[66] Kyle Q Lepage, Christopher J MacDonald, Howard Eichenbaum, and Uri T Eden. The statistical analysis of partially confounded covariates important to neural spiking. *Journal of neuroscience methods*, 205(2):295–304, 2012.

[67] Douglas A Nitz. Spaces within spaces: rat parietal cortex neurons register position across three reference frames. *Nature neuroscience*, 15(10):1365–1367, 2012.

[68] Wilson Truccolo, Uri T Eden, Matthew R Fellows, John P Donoghue, and Emery N Brown. A point process framework for relating neural spiking activity to spiking history, neural ensemble, and extrinsic covariate effects. *Journal of neurophysiology*, 93(2):1074–1089, 2005.

[69] N Burgess, F Cacucci, C Lever, and J O'Keefe. Characterizing multiple independent behavioral correlates of cell firing in freely moving animals. *Hippocampus*, 15(2):149–153, 2005.

[70] Charlotte N Boccara, Francesca Sargolini, Veslemøy Hult Thoresen, Trygve Solstad, Menno P Witter, Edvard I Moser, and May-Britt Moser. Grid cells in pre- and parasubiculum. *Nature neuroscience*, 13(8):987–94, August 2010.

[71] Jeffrey S Taube, Robert U Muller, and James B Ranck. Head-direction cells recorded from the postsubiculum in freely moving rats. i. description and quantitative analysis. *The Journal of Neuroscience*, 10(2):420–435, 1990.

[72] Hugh T Blair and Patricia E Sharp. Visual and vestibular influences on head-direction cells in the anterior thalamus of the rat. *Behavioral neuroscience*, 110(4):643, 1996.

[73] T T Hahn, B Sakmann, and M R Mehta. Phase-locking of hippocampal interneurons' membrane potential to neocortical up-down states. *Nat Neurosci*, 9(11):1359–1361, 2006.

[74] Thomas T G Hahn, Bert Sakmann, and Mayank R Mehta. Differential responses of hippocampal subfields to cortical up-down states. *Proceedings of the National Academy of Sciences of the United States of America*, 104(12):5169–74, March 2007.

[75] SI Wiener, CA Paul, and H Eichenbaum. Spatial and behavioral correlates of hippocampal neuronal activity. *The Journal of neuroscience*, 9(8):2737–2763, 1989.

[76] Nathaniel J Killian, Michael J Jutras, and Elizabeth a Buffalo. A map of visual space in the primate entorhinal cortex. *Nature*, 491(7426):761–4, November 2012.

[77] Wendy A Suzuki, Earl K Miller, and Robert Desimone. Object and place memory in the macaque entorhinal cortex. *Journal of neurophysiology*, 78(2):1062–1081, 1997.

[78] Motoharu Yoshida and Michael E Hasselmo. Persistent firing supported by an intrinsic cellular mechanism in a component of the head direction system. *The Journal of neuroscience*, 29(15):4945–4952, 2009.

[79] Kechen Zhang and Terrence J Sejnowski. Neuronal tuning: To sharpen or broaden? *Neural Computation*, 11(1):75–84, 1999.

[80] Andrew S Alexander and Douglas A Nitz. Retrosplenial cortex maps the conjunction of internal and external spaces. *Nature neuroscience*, advance on, July 2015.

[81] Shawn S Winter, Benjamin J Clark, and Jeffrey S Taube. Disruption of the head direction cell network impairs the parahippocampal grid cell signal. *Science*, 347(6224):870–874, 2015.

[82] Douglas A Nitz. Tracking route progression in the posterior parietal cortex. *Neuron*, 49(5):747–756, 2006.

[83] TAKETOSHI Ono, KIYOMI Nakamura, HISAO Nishijo, and SATOSHI Eifuku. Monkey hippocampal neurons related to spatial and nonspatial functions. *Journal of Neurophysiology*, 70(4):1516–1529, 1993.

[84] Richard Morris. Developments of a water-maze procedure for studying spatial learning in the rat. *Journal of neuroscience methods*, 11(1):47–60, 1984.

[85] Mayank R Mehta. From synaptic plasticity to spatial maps and sequence learning. *Hippocampus*, 25(6):756–762, 2015.

[86] RGM Morris, Paul Garrud, JNP Rawlins, and John O'Keefe. Place navigation impaired in rats with hippocampal lesions. *Nature*, 297(5868):681–683, 1982.

[87] Richard GM Morris. Spatial localization does not require the presence of local cues. *Learning and motivation*, 12(2):239–260, 1981.